NAVAL POSTGRADUATE SCHOOL

MONTEREY, CALIFORNIA

THESIS

A STUDY OF THE VERTICAL COMPONENT OF OCEAN FLOOR VIBRATIONS IN TWO GEOGRAPHICAL CHOKEPOINTS

by

Jeremy R. Hankins

March 2017

Thesis Advisor: Daphne Kapolka
Second Reader: Steve Libby

Approved for public release. Distribution is unlimited.

Reissued 30 May 2017 with Second Reader's non-NPS affiliation added to title page.

THIS PAGE INTENTIONALLY LEFT BLANK

REPORT DOCUMENTATION PAGE			Form Approved OMB No. 0704–0188
Public reporting burden for this collection of information is estimated to average 1 hour per response, including the time for reviewing instruction, searching existing data sources, gathering and maintaining the data needed, and completing and reviewing the collection of information. Send comments regarding this burden estimate or any other aspect of this collection of information, including suggestions for reducing this burden, to Washington headquarters Services, Directorate for Information Operations and Reports, 1215 Jefferson Davis Highway, Suite 1204, Arlington, VA 22202-4302, and to the Office of Management and Budget, Paperwork Reduction Project (0704-0188) Washington, DC 20503.			
1. AGENCY USE ONLY ***(Leave blank)***	**2. REPORT DATE** March 2017	**3. REPORT TYPE AND DATES COVERED** Master's thesis	
4. TITLE AND SUBTITLE A STUDY OF THE VERTICAL COMPONENT OF OCEAN FLOOR VIBRATIONS IN TWO GEOGRAPHICAL CHOKEPOINTS			**5. FUNDING NUMBERS**
6. AUTHOR(S) Jeremy R. Hankins			
7. PERFORMING ORGANIZATION NAME(S) AND ADDRESS(ES) Naval Postgraduate School Monterey, CA 93943-5000			**8. PERFORMING ORGANIZATION REPORT NUMBER**
9. SPONSORING /MONITORING AGENCY NAME(S) AND ADDRESS(ES) N/A			**10. SPONSORING / MONITORING AGENCY REPORT NUMBER**
11. SUPPLEMENTARY NOTES The views expressed in this thesis are those of the author and do not reflect the official policy or position of the Department of Defense or the U.S. Government. IRB number ____N/A____.			
12a. DISTRIBUTION / AVAILABILITY STATEMENT Approved for public release. Distribution is unlimited.			**12b. DISTRIBUTION CODE**

13. ABSTRACT (maximum 200 words)

The purpose of this thesis is to characterize typical levels of vibrational noise on the ocean floor to ascertain the vibration's effect on possible future bottom mounted sensors. The data used for this thesis was obtained from publicly available recorded information from four ocean bottom seismometers (OBS). The OBSs were located in two geographical choke points: the Luzon Strait and west of the Strait of Juan de Fuca. These highly trafficked choke points were considered to be a good representation of where these experimental bottom mounted sensors might be located should they be built. Unix-based seismic processing software available from the Incorporated Research Institutions for Seismology (IRIS) proved essential to obtaining calibrated data, and the methodology used to get the calibrated data is discussed in detail. The results showed that one OBS out of the four was highly variable, with decibel levels varying widely from day to day. The other OBSs remained fairly consistent. In addition, there were no common discrete frequencies between sensors that were in the same geographic area. Recommended future research involves the study of environmental effects on the OBSs, additional research to correlate the results observed in the Luzon Strait, and a look into the electronic noise floors of the OBSs used.

14. SUBJECT TERMS ocean bottom, seismometer, vibrational noise			**15. NUMBER OF PAGES** 127
			16. PRICE CODE
17. SECURITY CLASSIFICATION OF REPORT Unclassified	**18. SECURITY CLASSIFICATION OF THIS PAGE** Unclassified	**19. SECURITY CLASSIFICATION OF ABSTRACT** Unclassified	**20. LIMITATION OF ABSTRACT** UU

NSN 7540–01-280-5500 Standard Form 298 (Rev. 2–89)
Prescribed by ANSI Std. 239–18

THIS PAGE INTENTIONALLY LEFT BLANK

Approved for public release. Distribution is unlimited.

A STUDY OF THE VERTICAL COMPONENT OF OCEAN FLOOR VIBRATIONS IN TWO GEOGRAPHICAL CHOKEPOINTS

Jeremy R. Hankins
Lieutenant Commander, United States Navy
B.S., Tulane University, 1997

Submitted in partial fulfillment of the
requirements for the degree of

MASTER OF SCIENCE IN ENGINEERING ACOUSTICS

from the

NAVAL POSTGRADUATE SCHOOL
March 2017

Approved by: Daphne Kapolka
Thesis Advisor

Steve Libby, Lawrence Livermore National Laboratory
Second Reader

Daphne Kapolka
Chair, Engineering Acoustics Academic Committee

THIS PAGE INTENTIONALLY LEFT BLANK

ABSTRACT

The purpose of this thesis is to characterize typical levels of vibrational noise on the ocean floor to ascertain the vibration's effect on possible future bottom mounted sensors. The data used for this thesis was obtained from publicly available recorded information from four ocean bottom seismometers (OBS). The OBSs were located in two geographical choke points: the Luzon Strait and west of the Strait of Juan de Fuca. These highly trafficked choke points were considered to be a good representation of where these experimental bottom mounted sensors might be located should they be built. Unix-based seismic processing software available from the Incorporated Research Institutions for Seismology (IRIS) proved essential to obtaining calibrated data, and the methodology used to get the calibrated data is discussed in detail. The results showed that one OBS out of the four was highly variable, with decibel levels varying widely from day to day. The other OBSs remained fairly consistent. In addition, there were no common discrete frequencies between sensors that were in the same geographic area. Recommended future research involves the study of environmental effects on the OBSs, additional research to correlate the results observed in the Luzon Strait, and a look into the electronic noise floors of the OBSs used.

THIS PAGE INTENTIONALLY LEFT BLANK

TABLE OF CONTENTS

LIST OF FIGURES

THIS PAGE INTENTIONALLY LEFT BLANK

LIST OF TABLES

THIS PAGE INTENTIONALLY LEFT BLANK

LIST OF ACRONYMS AND ABBREVIATIONS

ABALONES	Autonomous Broad Application Low Obstruction Noise Exempt System
AP	amplitude phase
BREQ_FAST	batch request
CS	complex spectra
DFT	Digital Fourier Transform
DMC	Data Management Center
DPG	differential pressure gauge
EVALRESP	evaluate response (computer program)
FAP	frequency amplitude phase
IRIS	Incorporated Research Institutions for Seismology
LDEO	Lamont-Doherty Earth Observatory
LLNL	Lawrence Livermore National Laboratory
NSF	National Science Foundation
OBS	ocean bottom seismometer
OBSIP	Ocean Bottom Seismograph Instrument Pool
PSD	Power Spectral Density
PZ	poles and zeros file
rdseed	read SEED (computer program)
RESP	response file
SAC	Seismic Analysis Code
SEED	Standard for the exchange of Earthquake Data
SIO	Scripps Institution of Oceanography
TAIGER	Taiwan Integrated Geodynamic Research
TSWS	timeseries webserver

THIS PAGE INTENTIONALLY LEFT BLANK

ACKNOWLEDGMENTS

To my wife, Wendy: throughout my years in the Navy, you have faced every challenge thrown your way with grace and determination, and I am forever grateful. Thank you for keeping the Hankins family running smoothly while I was completing this thesis.

To my thesis advisor, Dr. Daphne Kapolka, I cannot thank you enough for your mentorship, guidance, and patience. I could not have completed this thesis without you.

THIS PAGE INTENTIONALLY LEFT BLANK

I. INTRODUCTION

A. CONCEPT

The purpose of this thesis is to characterize typical levels of vibrational noise on the ocean floor to ascertain the vibration's effect on possible future bottom mounted sensors. Lawrence Livermore National Laboratory (LLNL) is interested in possibly using an experimental sensor on the ocean floor. LLNL characterized the noise response for various terrestrial versions of this particular sensor, and they expressed interest in collaborating in a study of the vibrational noise on the ocean floor, focusing on low frequencies during quiescent periods. The data used for this thesis was obtained from publicly available recorded information from ocean bottom seismometers (OBS). It is beyond the scope of this thesis to characterize all low frequency noise on the ocean floor since noise can differ by area and the seismic events occurring during the measurement. The data was obtained, then, by focusing on two geographical choke points which have co-located OBSs. These highly trafficked choke points were considered to be a good representation of where these experimental bottom mounted sensors might be located should they be built.

Discussions were held with scientists from LLNL to find out sensor information and, specifically, the frequency regimes, amplitudes, and vibration axis that affect the current sensors. The LLNL personnel discussed what an underwater version of this sensor might look like, but they were more interested in the statistics of the vibrational noise of the ocean floor between large amplitude events to determine what to account for in future designs.

B. RELATED WORK

A thesis by Jonathon P. Scobo entitled "Ocean Observing Systems" was used for this research to start obtaining OBS data and the various seismology software to process it [1]. Even though most OBS data is publicly available, OBS data can be difficult to access and cumbersome to analyze. Scobo's thesis

proved essential to find the desired OBSs, which seismology computer programs to use and which to avoid, and how to request specific time periods of data [1].

Most other work that was found with regards to seismic vibrations on the ocean floor concentrated on larger seismic events as against the noise environment between these events. LLNL expressed less interest in large events and more interest in the noise environment during quiescent periods between large amplitude events.

Somewhat related research has been conducted which discusses the shortcomings of different types of OBSs due to the bottom type on which they are mounted. These shortcomings will be discussed, because the data used for this thesis could be affected by these shortcomings.

C. ORGANIZATION

This thesis will start with background information discussing the Incorporated Research Institutions for Seismology (IRIS) website and the Ocean Bottom Seismograph Instrument Pool (OBSIP). The background chapter also discusses specific OBS sensors used for this thesis and OBS fidelity on different bottom types. The next chapter discusses theory (Chapter III) and includes an introduction to seismic waves. Chapter IV, Methodology, discusses the process to obtain, process, and analyze the OBS data. Next, the results chapter (Chapter V) contains a discussion of the low frequency vibrational noise environment in the different areas of interest. Chapter VI discusses the overall conclusions as well as recommendations on future work, and the appendices contain the MATLAB code and data tables.

D. OVERVIEW

Four OBSs in two different geographic locations were chosen and subsequently their vibrational noise environments were investigated. Figure 1 from the IRIS website shows a global view of publicly available OBSs. This global

view allows the user to zoom in on and select the desired OBS, which then opens a link to download the different types of available data.

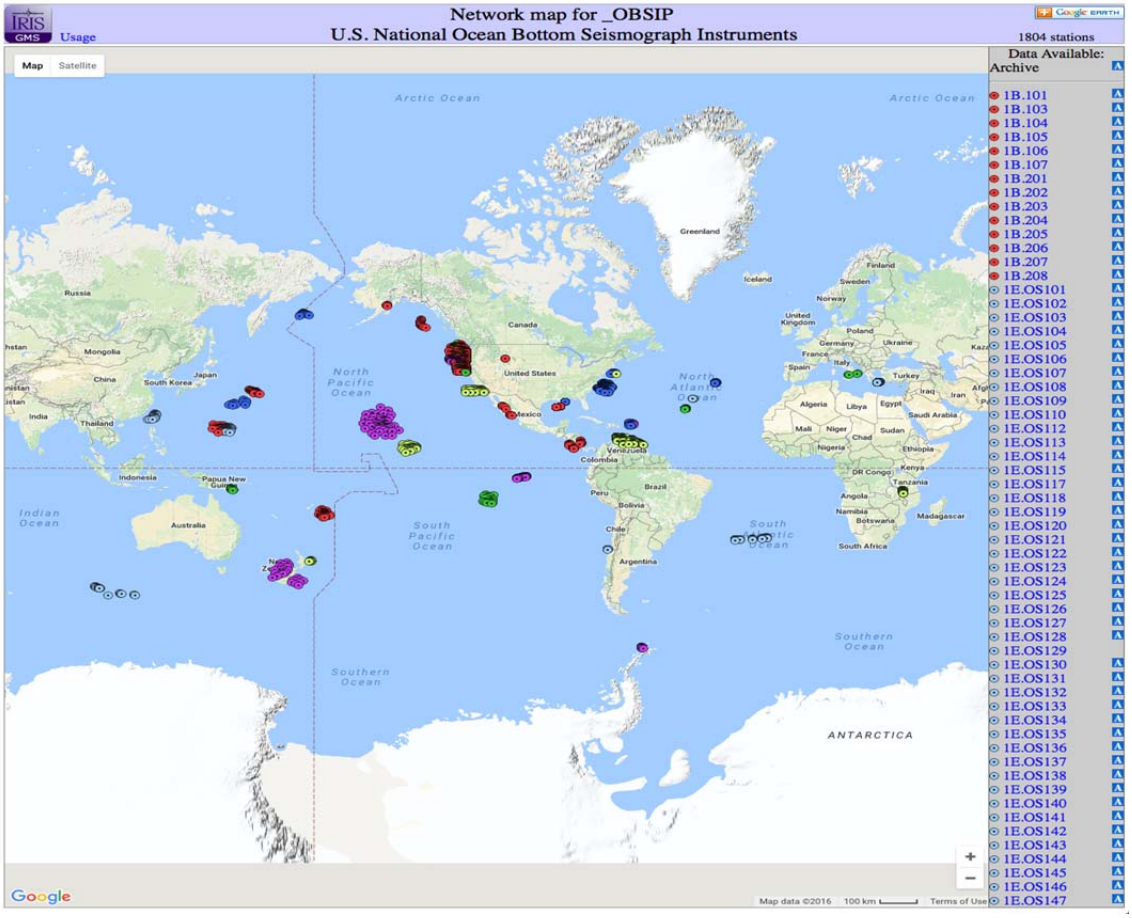

Figure 1. The Global View of Publicly Available OBSs. Source: [2].

Two geographic choke points were chosen: the Luzon Strait and west of the Strait of Juan de Fuca. IRIS publicly available software, specifically a program to read information in the form of Standard for the Exchange of Earthquake Data (SEED), called “rdseed,” a program used to evaluate response files called “EVALRESP,” and Seismic Analysis Code (SAC) were used to transfer downloaded data into a usable format and then calibrate the data. The analysis conducted on the calibrated data was accomplished with MATLAB. Figure 2 and Figure 3 display the available OBSs at the chosen choke points.

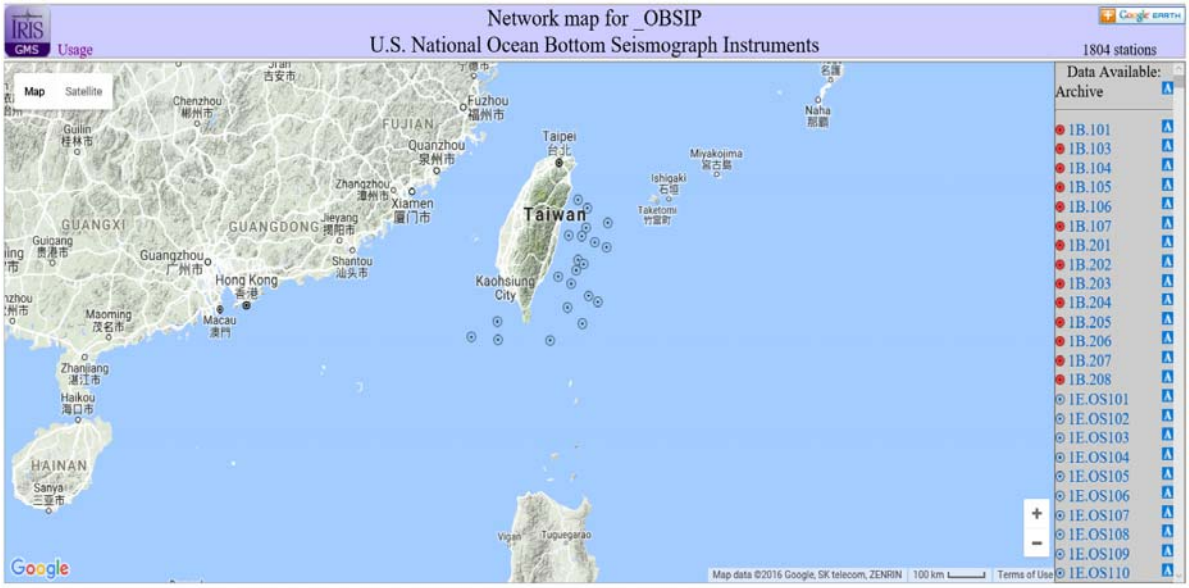

Figure 2. Available OBSs in the Luzon Strait. Source: [2].

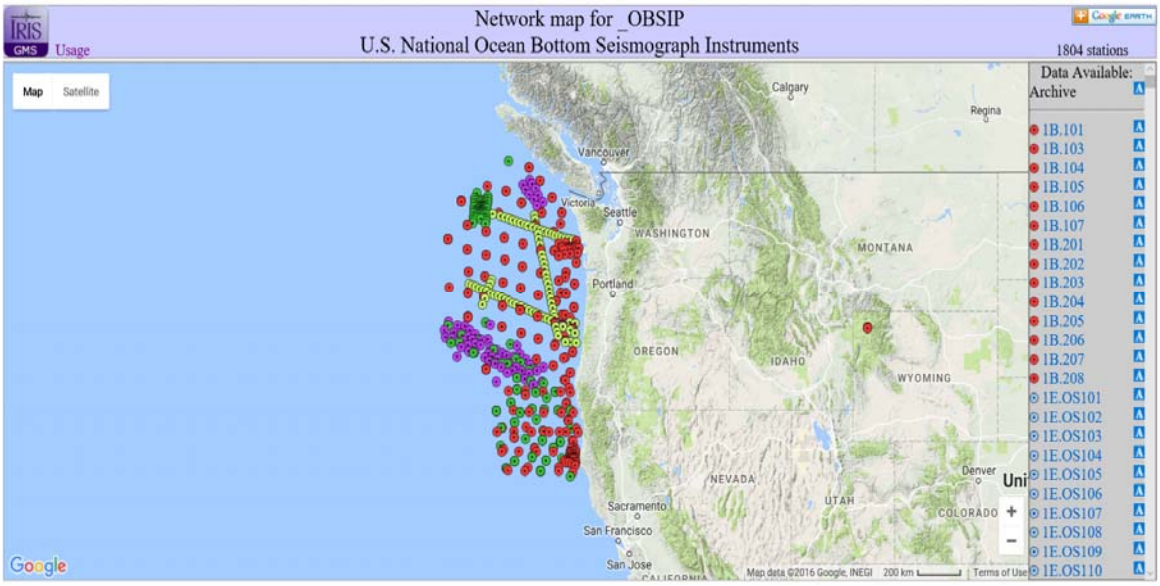

Figure 3. Available OBSs West of Strait of Juan de Fuca. Source: [2].

The data was obtained, then, by focusing on known geographical choke points which have co-located OBSs. These highly trafficked geographic choke points were considered to be a good representation of where these experimental

bottom mounted sensors would be located for either testing or operations after they are built. Initially, more geographic choke points with OBSs were inspected in hopes to add additional locations to analyze. One of the OBS locations near a choke point south of the Bering Strait was inspected, but the OBSs were short period OBSs (discussed later) that were used during an active sound transmission test. At this location, there was only a week's worth of noisy data. According to IRIS in Figure 1 there are no OBS locations for the majority of the operationally significant choke points. The OBS locations are understandably chosen for geological significance (e.g., hydrothermal events in the middle of the Atlantic Ocean).

THIS PAGE INTENTIONALLY LEFT BLANK

II. BACKGROUND

A. IRIS AND OBSIP

All of the OBS data obtained for this thesis was from the IRIS and OBSIP websites. IRIS is a non-profit organization, created in 1984 by the National Science Foundation (NSF). According to their website, IRIS involves over 100 universities in the United States. Their programs "contribute to scholarly research, education, earthquake hazard mitigation, and verification of the Comprehensive Nuclear-Test-Ban Treaty" [3]. One of IRIS's mission statements is to promote seismic data availability, and they allow access to data by using a simple request format, which will be addressed later in this thesis.

IRIS oversees and coordinates multiple seismic networks, which includes the network used for this thesis, the OBSIP. OBSIP focuses on marine seismology, geology, and geodynamics. The OBSIP website [4] also contains links describing current OBS instrumentation, links to access OBS data, and information for researchers to request OBSIP instrument usage. The OBSIP allows their OBS equipment to be available to NSF-sponsored investigators and to other government research or educational institutions [4].

B. OBS

Ocean Bottom Seismometers can be broken into two fundamental types: long period and short period. According to OBSIP's website [4], the long period OBSs have a 3-component broadband seismometer (one vertical component and two horizontal) and a low-frequency differential pressure gauge (DPG)/hydrophone. These long period OBSs are primarily designed for passive recording and are normally capable of a greater than 12-month deployment. The short period OBSs consist of either a vertical seismometer or, like the long period OBS, three orthogonal seismometers and a hydrophone [4]. The OBSIP website [4] also states that the sampling rates for the short period OBSs are typically much higher (200–250Hz), and these instruments are normally deployed from 1

to 6 months. The short period OBSs are typically used for active-source experiments [4].

The OBSs used in this thesis are long period. Because of how OBSs are placed on the ocean floor, the orientation of the horizontal channels are usually unknown. Methods to orientate the horizontal channels can involve analyzing data from the known location of an active source (e.g., air gun) or using P or Rayleigh waves from a known earthquake [5]. The orientation of the horizontal channels used in this thesis were unknown.

1. LDEO OBS Sensor MK2

Figure 4 from the IRIS website displays the highlights from the Lamont-Doherty Earth Observatory (LDEO) Standard Ocean Bottom Seismometer. The LDEO OBSs used for this thesis are located in the Luzon Strait and were used in the Taiwan Integrated Geodynamic Research (TAIGER) project. The TAIGER project is a joint USA-Taiwan program that studies the tectonic development of Taiwan [6]. The network identifier “YM” designates the OBSs in the TAIGER project. The two OBS stations that were used to provide data were YM 38 and YM 39, displayed in Figure 5.

LDEO Standard Ocean-Bottom Seismometer

Ocean-Bottom Seismology Laboratory
Lamont-Doherty Earth Observatory
Columbia University | Earth Institute

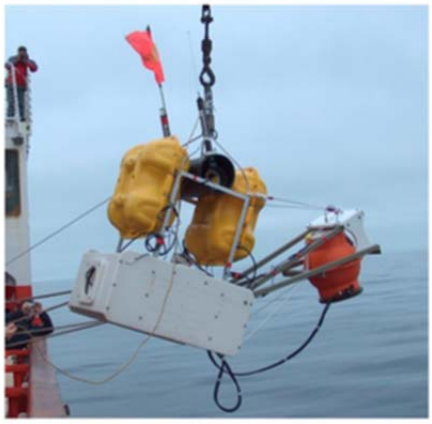

The LDEO standard seismometer design has been in use for nearly 10 years. The LDEO OBS lab has built and operates 25 standard OBSs as part of the NSF OBS Instrumentation Pool. The seismometer sensor is an L4C 1 Hz geophone, with a low-noise amplifier, giving useful response down to 100 s, and a differential pressure gauge. This instrument has been used in both year-long passive-source and shorter-term active-source experiments. The design includes dual redundancy with two transponders and two dropweights.

Specifications

Max. Depth	5000 m
Max. Duration	400 days @ 125 sps
Channels	4, 24-bit recording
Sensors	L4C 3-component geophones; differential pressure gauge
Response	100 s - 60 Hz (seismometer) 0-20 Hz (DPG)
Leveling system	Active 360°,motor-driven
Weight	750 lb in air
Footprint	3'X4'
Flotation	9X12" glass spheres
Sampling	40-100-125 sps
Release	Dual dropweights
Acoustics	Two ORE 12 kHz transponders
Power	Lithium battery pack, +/- 7.5 V
Oscillator	Seascan 10 MHz clock
Sensor housing	17" glass sphere
Burnwires	LDEO design
Recovery aids	Radio, strobe, flag
Recording	2 X 32 Gb CompactFlash cards
Dropweights	Two steel weights (75 lb in air)
Datalogger	LDEO ultra-low power OBS datalogger (300 mW @ 125 sps)

Variants and add-ons

Trawl-resistant OBS
Moored DPG/hydrophone
Ocean-bottom magnetometer
Diffuse flowmeter
Trillium Compact sensor
Absolute pressure gauge
Hydrophone

Deployment History

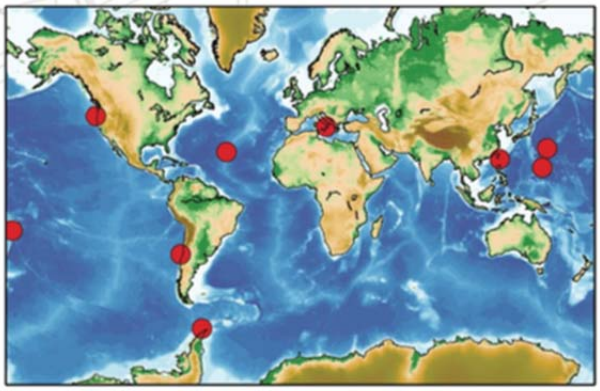

Figure 4. Highlights of the LDEO OBS, Which Includes a Useful Instrument Response Down to a Period of 100 Seconds. Source: [7].

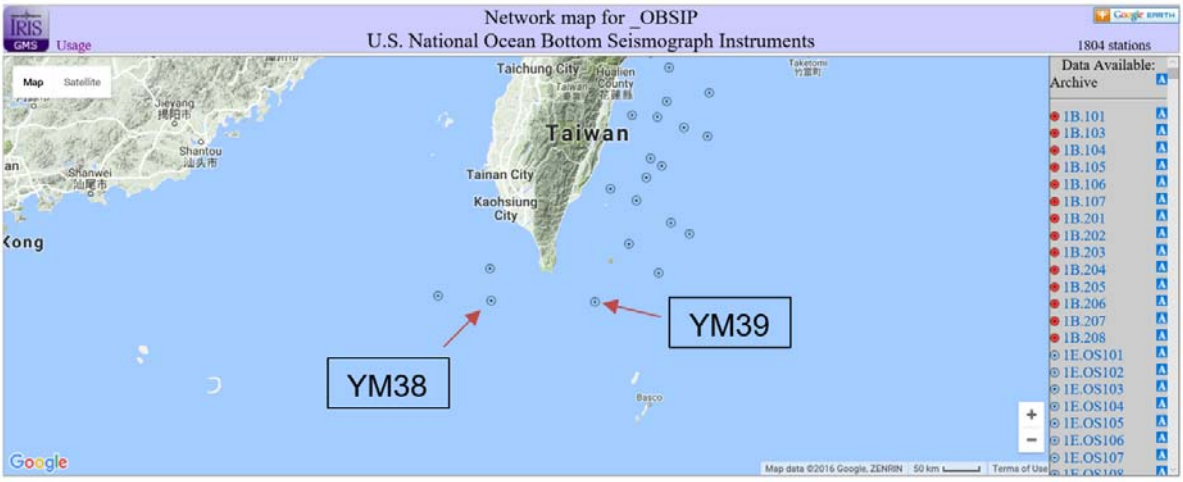

Figure 5. Location of YM38 and YM39, the Two OBS Locations in the Luzon Strait. Source: [2].

The LDEO OBS uses an L4C 1 Hz geophone as the seismometer sensor [8], which is displayed in a drawing in Figure 6. As discussed in [9], the vertical L4C geophone produces a voltage which is proportional to the difference in velocity between the mass, M, and the ground ($\dot{x} - \dot{x}_g$). The mass, *M*, is suspended with a spring with stiffness *k* and a dashpot, *b*, for damping. The voltage is produced by the motion sensing coil with inductance, L_c, and coil resistance, R_c. The L4C 1 Hz geophone has a harmonic frequency of 1 Hz, and the resistor, R_s, is an external resistor to shunt the output and critically damp the system at that frequency, as explained in the paper by Bowden [9].

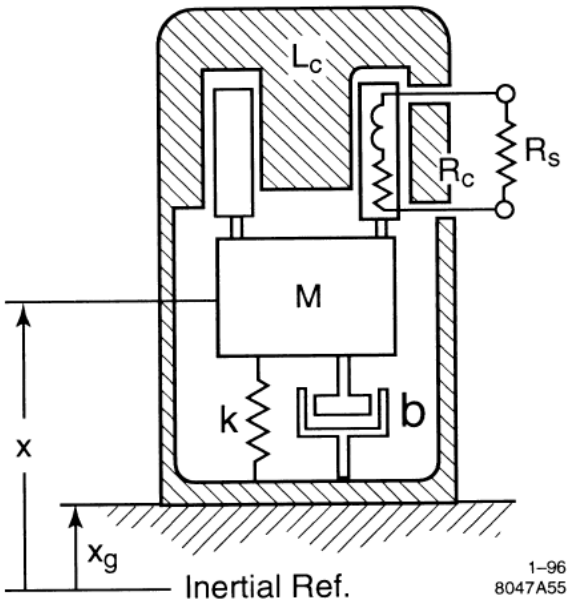

Figure 6. Drawing of Vertical L4C 1 Hz Geophone, Which Is Used as the Seismometer Sensor of the LDEO OBS. Source: [9].

2. SIO ABALONES OBS System

The Scripps Institution of Oceanography (SIO) Autonomous Broad Application Low Obstruction Noise Exempt System (ABALONES) OBS system can have a variety of configurations. The particular OBSs used for this thesis, located to the west of the Strait of Juan de Fuca as displayed in Figure 7, are considered an intermediate-period sensor because of their large frequency range. In this configuration they concentrate on long-period vibrations with a Nyquist frequency of 25 Hz. Table 1 displays the specification for the SIO ABALONES system, and Figure 8 displays a 3D-CAD drawing of the ABALONES OBS design. The yellow shell of the ABALONES design is a trawl and current resistant enclosure, allowing these OBSs to be set in shallow, continental shelf areas to as deep as 6000m [10]. It is equipped with a Nanometrics Trillium Compact Seismometer, which has the advantage of a nearly flat response curve from 120 seconds to 100 Hz [10], [11].

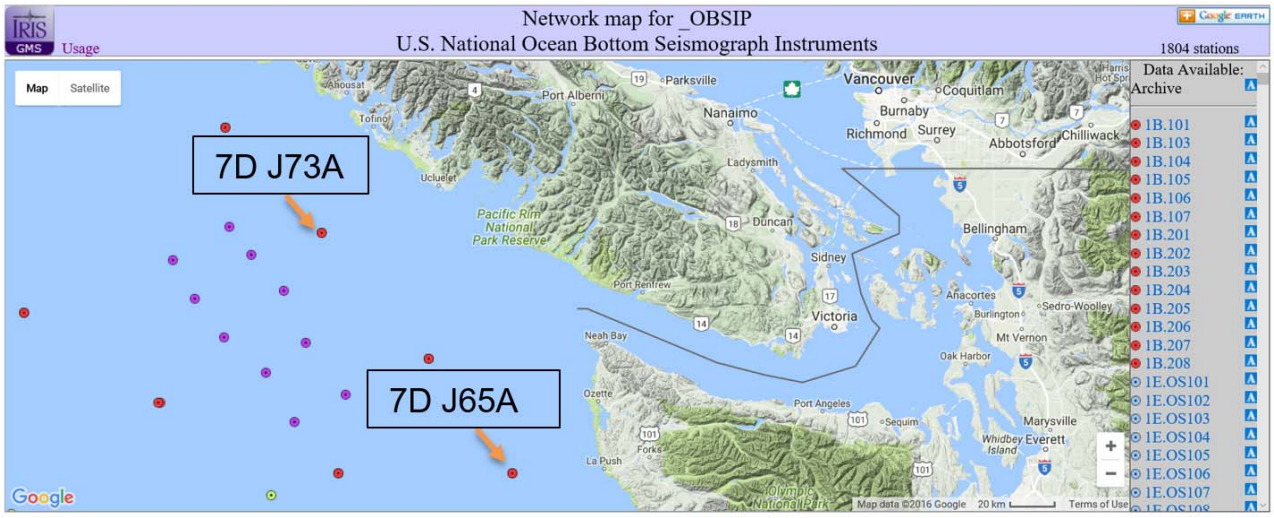

Figure 7. 7D J73A and 7D M02A, the Two OBS Locations West of the Strait of Juan de Fuca Used for this Thesis. Source: [2].

Table 1. SIO ABALONES OBS Specifications. Source: [11].

Seismometer/ Accelerometer	**Intermediate-Period:** Nanometrics Trillium-Compact seismometer, which has a flat velocity response from 120s to 100 Hz. The seismometer is housed within an 8" Inside Diameter (ID) Titanium cylinder and a custom-designed active leveling system which can be leveled from ±180° to vertical with ~0.3° accuracy.
Pressure Sensor	**Short-period:** Customized HiTech hydrophone with internal preamp. Bandwidth (-3 dB) is 50 mHz - 15 kHz. **Long-period:** Differential Pressure Gauge (DPG) with response from 10 mHz - 10 Hz.
Digitizer	24-bit A/D with solid-state recording (CompactFlash). The dynamic range is ~126 dB (3-bit self-noise). The ABALONES design includes the latest seismic A/D chip with programmable sample rates from 1 Hz to 4 kHz.
Clock	Low-power, digitally-temperature-compensated (DTCXO), precision time base. The drift rate is 1:3-5 x 10^{-8} (<5 ms/day before correction and <1.5 s/yr)
Recording Capacity	Single CompactFlash card slot → 64 Gb CF cards currently available. Capable of recording 1-year deployment on 4-channels @ 100 Hz.
Data Offload	USB2 through the end cap without opening the pressure case. Offload rates are CF card dependent, currently up to 400 Mb/s.
Battery Pack	Batteries are mounted in the main data logger pressure case and optionally in an additional battery case. Alkaline batteries power the acoustic release.
Recording duration	**IPA:** Lithium battery pack can provide power for 12 months, Alkaline packs can provide power for 4+ months. SPA: Lithium battery pack can provide power for 18+ months.
Weight	850/550 lbs with/without anchor (in air)
Pressure Case	5" diameter Al cylinder – 6 km depth rating
Release	Double burn wire operated acoustically
Dimensions	29" high x 42" x 42" (w/ bail)
Power (Total)	**Intermediate:** <300 mW (4 chan), plus ~160 mW w/ Trillium-Compact

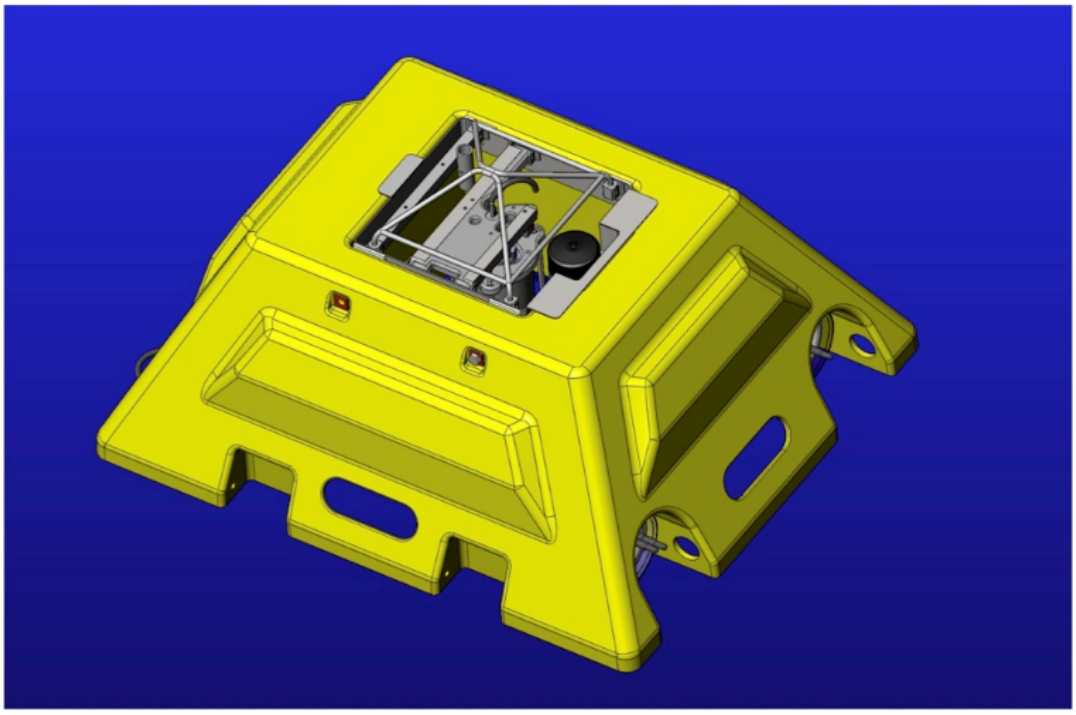

Figure 8. 3D-CAD Drawing of ABALONES Ocean Bottom Seismometer Design. Source: [11].

C. OBS FIDELITY

As mentioned by Sutton et al., “The usual reason for placing a seismometer anywhere is to measure free-field particle motion in response to some seismic source” [12]. The complication presented by soft sediment of the ocean floor is that the coupling between the seismometer and the sediment may be unknown [12]. Vertical vibration, channel Z in this thesis, is of more concern than any horizontal motion, channels 1 and 2. Duennebier and Sutton maintain that vertical motion across the water-sediment boundary is reasonably represented by an OBS due to particle motion continuity across the interface [12], [13]. The fidelity of horizontal motion captured by an OBS is also less accurate because of the shear discontinuity between the sediment and the water [14]. Problems with OBS horizontal fidelity are compounded by bottom ocean currents in addition to the soft sediment.

In [14], Duennebier and Sutton point out that horizontal motion is discontinuous across the boundary of the ocean floor. This differential motion generates torque on the instrument which in turn causes both horizontal and vertical motion to be captured by the seismometer channels. In addition, if the sensor is not completely level, components of vertical and horizontal motions will couple into the wrong channels. Consequently, cross-correlation between the horizontal and vertical channels is common on bottom mounted OBSs [14]. The horizontal channels are considered to be more susceptible to noise from this source. Duennebier and Sutton collected data in a study proving increased OBS fidelity when the OBS is buried beneath the sediment on the ocean floor [13].

Any sensor placed on the ocean floor will be subject to the same vibrations as the OBS. Therefore, these issues relating to the fidelity of the seismic measurements may be of concern to LLNL for their potential to affect the performance of the proposed sensor as well as for possible limitations in the accuracy of the seismic measurements provided in this thesis. If a bottom-mounted sensor is used, [14] explains that the effects of unwanted vertical motion can be minimized by increasing the footprint of a sensor package relative to its height. The tradeoff is a decreased sensitivity to certain types of waves when the sensor base approaches too high a fraction of the seismic wavelength, particularly in higher frequency shear waves.

III. THEORY

Seismic waves can be divided into two categories: body waves and surface waves. The body waves travel through the interior of the earth and are the first waves to arrive after a seismic event [15]. The surface waves cause the most damage associated with an earthquake, and they travel along the earth's crust [15]. The mathematical theory behind both types of waves is discussed in this chapter. Figure 9 is the coordinate system used in the equations. All of the equations in this chapter are from Bullen and Bolt [16].

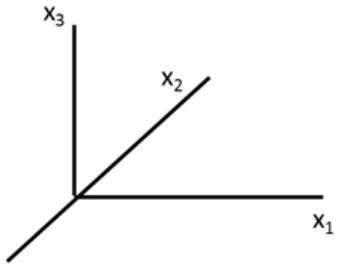

Figure 9. Coordinate System Used in Equations 1 through 20.

A. BODY WAVES

1. P Wave

The P wave is the primary or "push wave." Bullen and Bolt [16] describe the P wave in terms of the dilatation, θ. The dilatation, or irrotational disturbance, is the fractional change in volume of a point in the medium as the wave passes. It is given by the divergence of the vector u_i, which gives the displacement of a point with respect to its equilibrium position in direction x_i as shown in Equation 1. Equation 2 is the scalar wave equation for the dilatational disturbance. The P wave is transmitted through a substance at speed α, given in Equation 3.

$$\theta = \frac{\partial u_1}{\partial x_1} + \frac{\partial u_2}{\partial x_2} + \frac{\partial u_3}{\partial x_3} \tag{1}$$

$$\frac{\partial^2 \theta}{\partial t^2} = \alpha^2 \nabla^2 \theta \tag{2}$$

$$\alpha = \left(\frac{\lambda + 2\mu}{\rho} \right)^{1/2} \tag{3}$$

λ is Lamé's first parameter, which is an elastic modulus defined by Equation 4. μ is Lamé's second parameter, which is also known as the shear modulus, and ρ is the volume density of the material. The Lamé parameters together characterize the linear elasticity for homogeneous isotropic media [17]. The relationship between Lamé's first parameter and the shear modulus, μ, is given by [16]

$$\lambda = K - \frac{2}{3}\mu = \rho(\alpha^2 - 2\beta^2), \tag{4}$$

where K is the bulk modulus of the material.

Figure 10 illustrates how a P wave travels. It is a longitudinal wave consisting of changes in the density of the material.

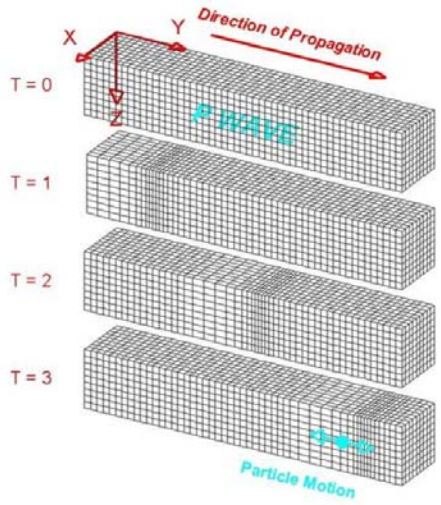

Figure 10. Illustration of P Wave. Source: [15].

2. S Wave

S waves are a type of shear wave and are described by the vector wave equation

$$\frac{\partial^2}{\partial t^2} curl(u_i) = \beta^2 \nabla^2 curl(u_i) \tag{5}$$

where β is the speed of the rotational disturbance [16] and given by

$$\beta = \left(\frac{\mu}{\rho} \right)^{\frac{1}{2}} \tag{6}$$

Since the speed depends on the shear modulus, S waves will not propagate through fluids which cannot support shear stress. The S wave in the far field can be plane polarized [16]. If an S wave is traveling horizontally and the particle motion is also horizontal, it is denoted SH. If the particle motion is vertical only, the S wave is denoted SV [16]. Figure 11 illustrates an SV wave assuming that z is vertical and x and y are horizontal.

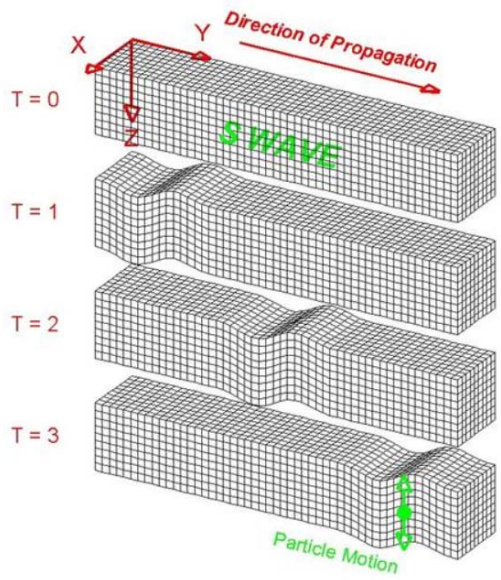

Figure 11. Illustration of an S Wave. Source: [15].

B. SURFACE WAVES

In Figure 12, which is adapted from an illustration in Bullen and Bolt [16], *M* is an elastic, homogeneous half-space below the plane denoted by the x_1 and x_2 axes. *M* is bordered above the x_1 / x_2 plane by another homogeneous elastic half-space, *M'*.

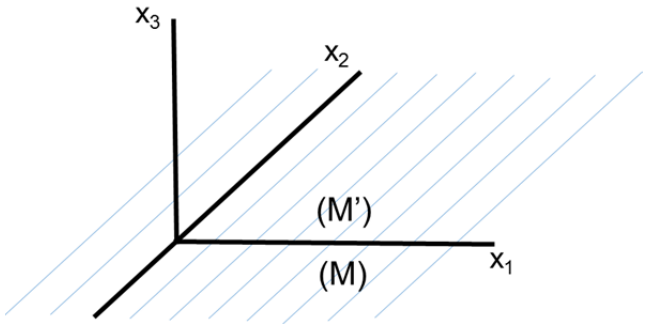

Figure 12. Two Isotropic Homogeneous Elastic Media M' and M. Adapted from [16].

Waves can travel along the boundary between these two half spaces. To be trapped along the boundary, the amplitude of these waves must decrease exponentially as the distance from the boundary increases. Consider such a plane wave traveling in the x_1 direction. Since it is a plane wave, the particle displacement along any line parallel to x_2 is equal. As a result, any partial derivative taken with respect to x_2 will be zero [16]. Letting ϕ and ψ be functions which can be used to express the displacement components u_1 and u_3 as given by

$$u_1 = \frac{\partial \phi}{\partial x_1} + \frac{\partial \psi}{\partial x_3}, u_3 = \frac{\partial \phi}{\partial x_3} - \frac{\partial \psi}{\partial x_1}, \tag{7}$$

it can be shown that

$$\nabla^2 \phi = \theta \tag{8}$$

$$\nabla^2 \psi = \frac{\partial u_1}{\partial x_3} - \frac{\partial u_3}{\partial x_1} \ . \tag{9}$$

This suggests that ϕ is linked with P waves since they are described by the dilatation. ψ is linked with SV waves since it is associated with a differential displacement between the direction of propagation and the vertical. Any displacement, u_2, would be linked with SH waves.

The wave equations associated with ϕ, ψ, and u_2 are given by

$$\frac{\partial^2 \phi}{\partial t^2} = \alpha^2 \nabla^2 \phi \tag{10}$$

$$\frac{\partial^2 \psi}{\partial t^2} = \beta^2 \nabla^2 \psi \tag{11}$$

$$\frac{\partial^2 u_2}{\partial t^2} = \beta^2 \nabla^2 u_2 \tag{12}$$

where the speeds in M' are replaced with α' and β'.

To find solutions for ϕ, ψ, and u_2 [16] sets r and s to the following, where c is the speed of a set of simple harmonic waves with wavelength $2\pi/k$. Again, for *M'*, the variables are r' and s'. The variables r, r', s, and s' designated in Equations 13 and 14 are imaginary.

$$r = \left(\frac{c^2}{\alpha^2} - 1\right)^{\frac{1}{2}}, s = \left(\frac{c^2}{\beta^2} - 1\right)^{\frac{1}{2}} \tag{13}$$

$$r' = \left(\frac{c^2}{\alpha'^2} - 1\right)^{\frac{1}{2}}, s' = \left(\frac{c^2}{\beta'^2} - 1\right)^{\frac{1}{2}} \tag{14}$$

Solutions in M and M' are sought in the form:

$$\phi = Ae^{ik(-rx_3 + x_1 - ct)} \tag{15}$$

$$\psi = Be^{ik(-sx_3 + x_1 - ct)} \tag{16}$$

$$u_2 = Ce^{ik(-sx_3 + x_1 - ct)} \tag{17}$$

$$\phi = D'e^{ik(-r'x_3 + x_1 - ct)} \tag{18}$$

$$\psi = E'e^{ik(-s'x_3 + x_1 - ct)} \tag{19}$$

$$u_2 = F'e^{ik(-s'x_3 + x_1 - ct)} \tag{20}$$

Since both r and s are imaginary, the positive or negative square root is taken as needed to ensure that all solutions consist of waves that exponentially decrease as the distance away from the boundary is increased. Expressions for the displacements u_1 and u_3 as a function of time and position can be found from these solutions by applying the relationships which implicitly define ϕ and ψ in Equation 7.

The boundary conditions dictate which solutions propagate. For example, if *M* is not homogeneous elastic half space, but is instead a vacuum (or air) the

resulting wave is a Rayleigh wave, where there are no SH waves. The particle motion is retrograde, and displayed in Figure 13.

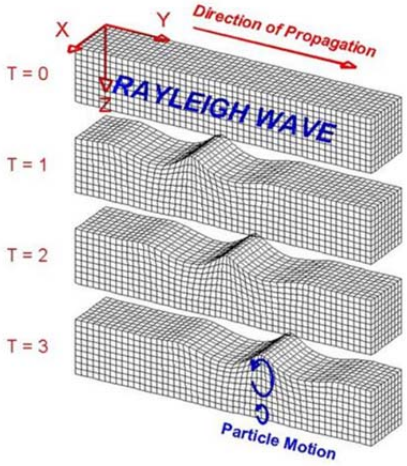

Figure 13. Illustration of Rayleigh Wave. Source: [15].

If *M* is not a homogeneous elastic half space, but is instead an incompressible fluid (water) the resulting wave is a Scholte wave [18]. The particle motion again is retrograde, and the amplitude decays exponentially with distance from the boundary. An illustration of a Scholte wave is displayed in Figure 14.

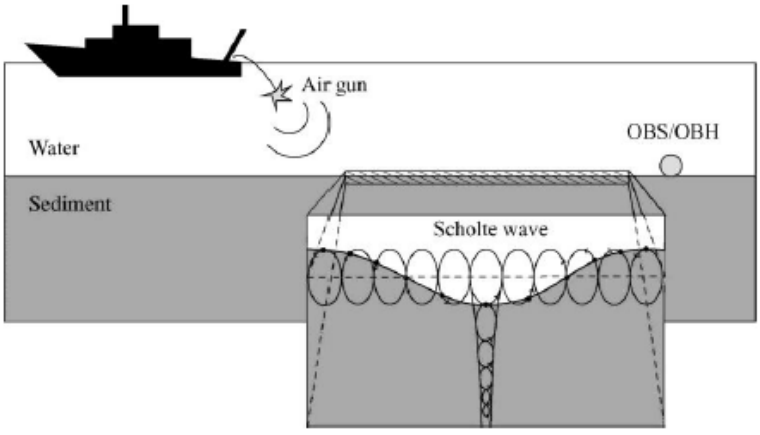

Figure 14. Illustration of Scholte Wave. Source: [19].

THIS PAGE INTENTIONALLY LEFT BLANK

IV. METHODOLOGY

A. OVERVIEW

This chapter explains the methods chosen to calibrate the data using IRIS software, why these methods were chosen, and the data analysis conducted with MATLAB. Multiple routes to calibration were available, and picking the most effective way forward proved challenging. Many different software calibrations methods are available from IRIS, and a few different methods to get calibrated data on MATLAB (manually) were attempted before the steps were decided upon. The steps laid out in this chapter should allow follow-on study with somewhat less of a learning curve for non-seismologists.

B. CHOOSING THE OBS

The global view on the IRIS website, displayed in Figure 1, of the available OBSs proved a convenient place to start the OBS selection process. This global view allows the user to focus on the desired area and select individual sensors. Once selected, a window, which is shown in Figure 15, is opened that displays to the user the dates of available data and a link to more information. It becomes readily apparent if the selected OBS is a short period vice long period. In most cases, the short period OBS dates available will be for days and weeks versus multiple months.

Figure 15. Convenient Use of Global View for OBS Selection.
Source: [1].

Once the user clicks on the “more information” link, the specific OBS page opens and allows the user to view the network and station information with the channels available. Figure 16 shows this page. The user can select any of the channels and view the response curve, the depth, sensor location in latitude and longitude, and the response (RESP) and poles and zeroes (PZ) files.

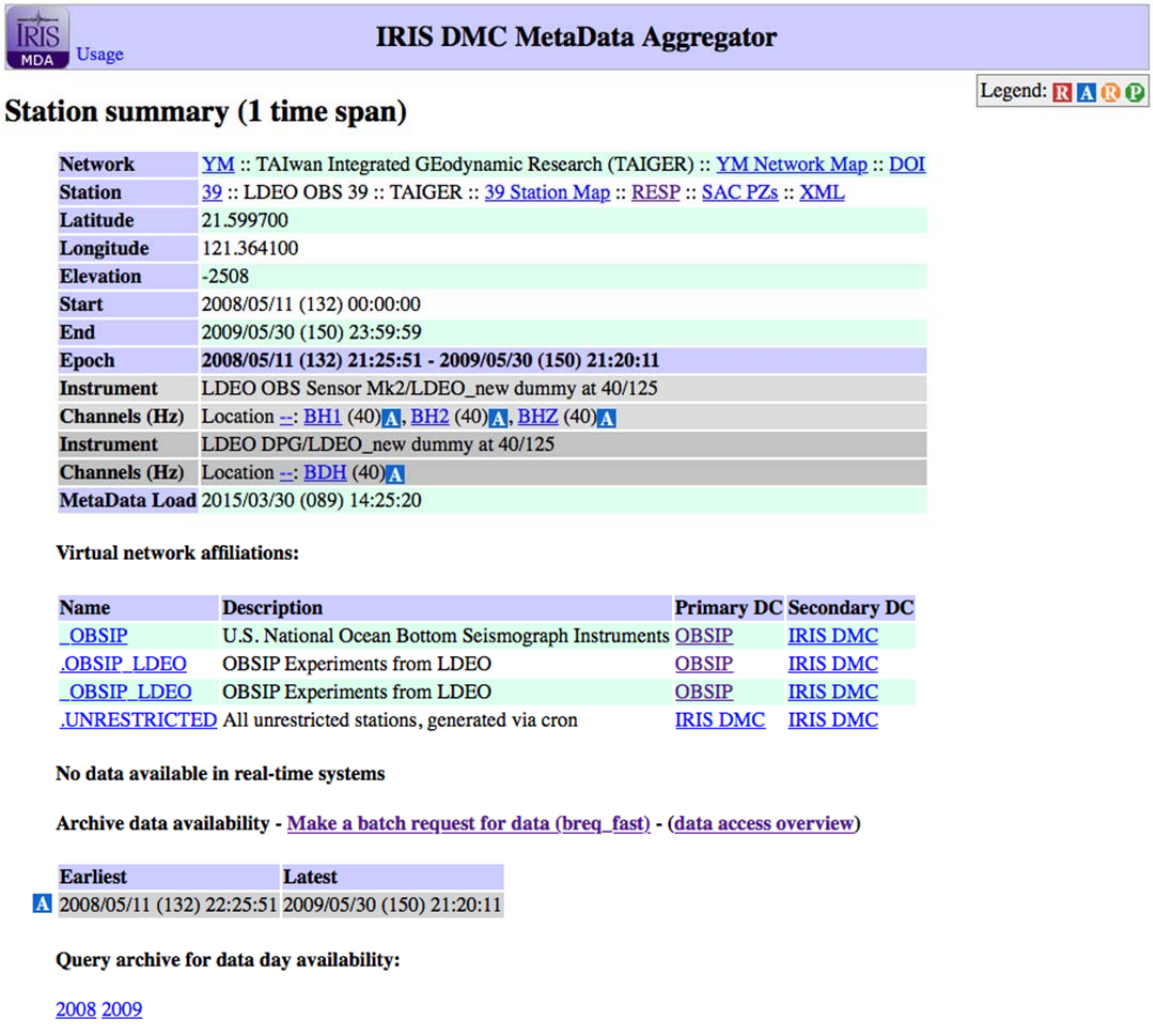

IRIS MDA Usage

IRIS DMC MetaData Aggregator

Legend: R A R P

Station summary (1 time span)

Network	YM :: TAIwan Integrated GEodynamic Research (TAIGER) :: YM Network Map :: DOI
Station	39 :: LDEO OBS 39 :: TAIGER :: 39 Station Map :: RESP :: SAC PZs :: XML
Latitude	21.599700
Longitude	121.364100
Elevation	-2508
Start	2008/05/11 (132) 00:00:00
End	2009/05/30 (150) 23:59:59
Epoch	**2008/05/11 (132) 21:25:51 - 2009/05/30 (150) 21:20:11**
Instrument	LDEO OBS Sensor Mk2/LDEO_new dummy at 40/125
Channels (Hz)	Location --: BH1 (40) A, BH2 (40) A, BHZ (40) A
Instrument	LDEO DPG/LDEO_new dummy at 40/125
Channels (Hz)	Location --: BDH (40) A
MetaData Load	2015/03/30 (089) 14:25:20

Virtual network affiliations:

Name	Description	Primary DC	Secondary DC
_OBSIP	U.S. National Ocean Bottom Seismograph Instruments	OBSIP	IRIS DMC
.OBSIP_LDEO	OBSIP Experiments from LDEO	OBSIP	IRIS DMC
_OBSIP_LDEO	OBSIP Experiments from LDEO	OBSIP	IRIS DMC
.UNRESTRICTED	All unrestricted stations, generated via cron	IRIS DMC	IRIS DMC

No data available in real-time systems

Archive data availability - Make a batch request for data (breq_fast) - (data access overview)

	Earliest	Latest
A	2008/05/11 (132) 22:25:51	2009/05/30 (150) 21:20:11

Query archive for data day availability:

2008 2009

Figure 16. Detailed Information on OBS Selected from Global Map. Source: [20].

C. REQUESTING DATA FROM IRIS

There are multiple ways to request data from IRIS. The method used in this thesis made use of the link in Figure 16, “Make a batch request for data (breq_fast).” The breq_fast request form, displayed in Figure 17, is self-explanatory with required items that must be entered starred. The “label” can be anything the user wants, which is the name of the file sent by the Data Management Center (DMC) to the entered email. The DMC is the part of IRIS that stores and makes available the seismic data [21]. After the “Start Query”

button is pressed, Figure 18 depicts the final webpage opened. For this thesis, “Full SEED” was the format used. After the form is submitted, IRIS sends an email with a link to download the requested SEED file directly. The link is available for 24 hours. “Full SEED” is used because of the various calibration files that Full SEED makes available with IRIS software.

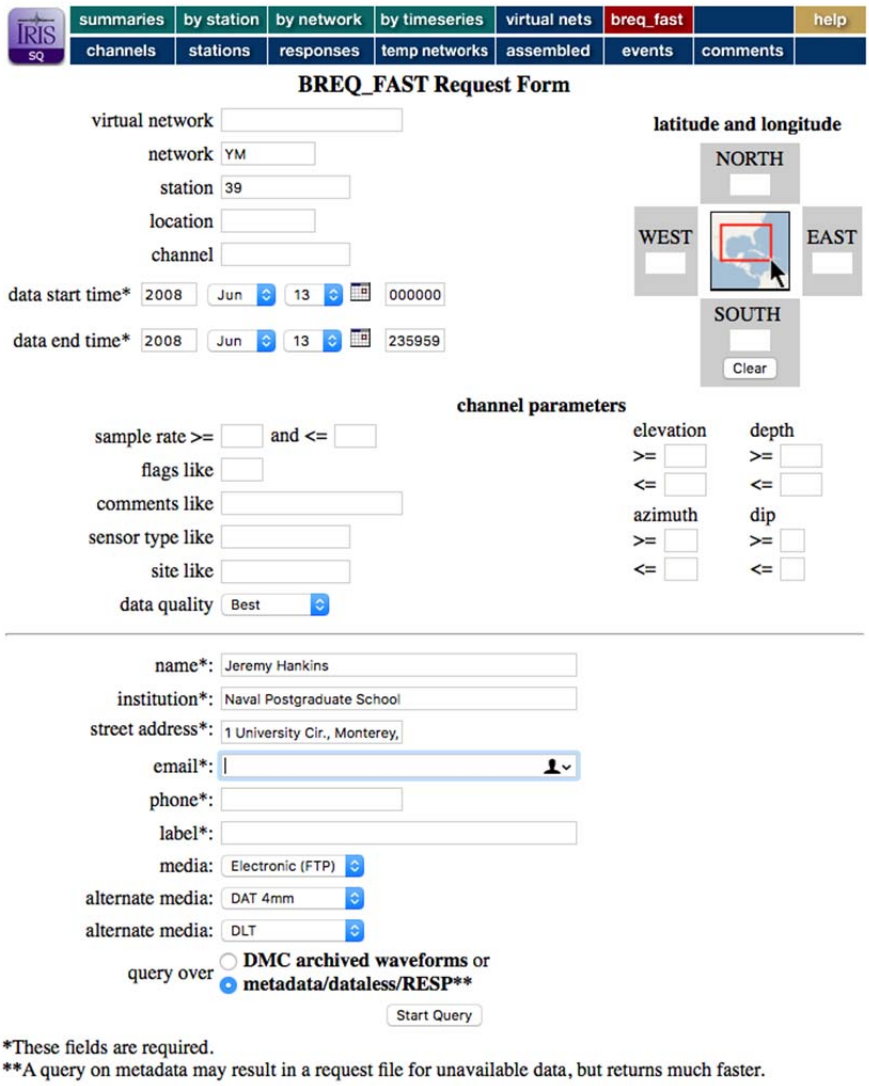

Figure 17. The BREQ_FAST Request Form Used to Get SEED Data from IRIS. Source: [22].

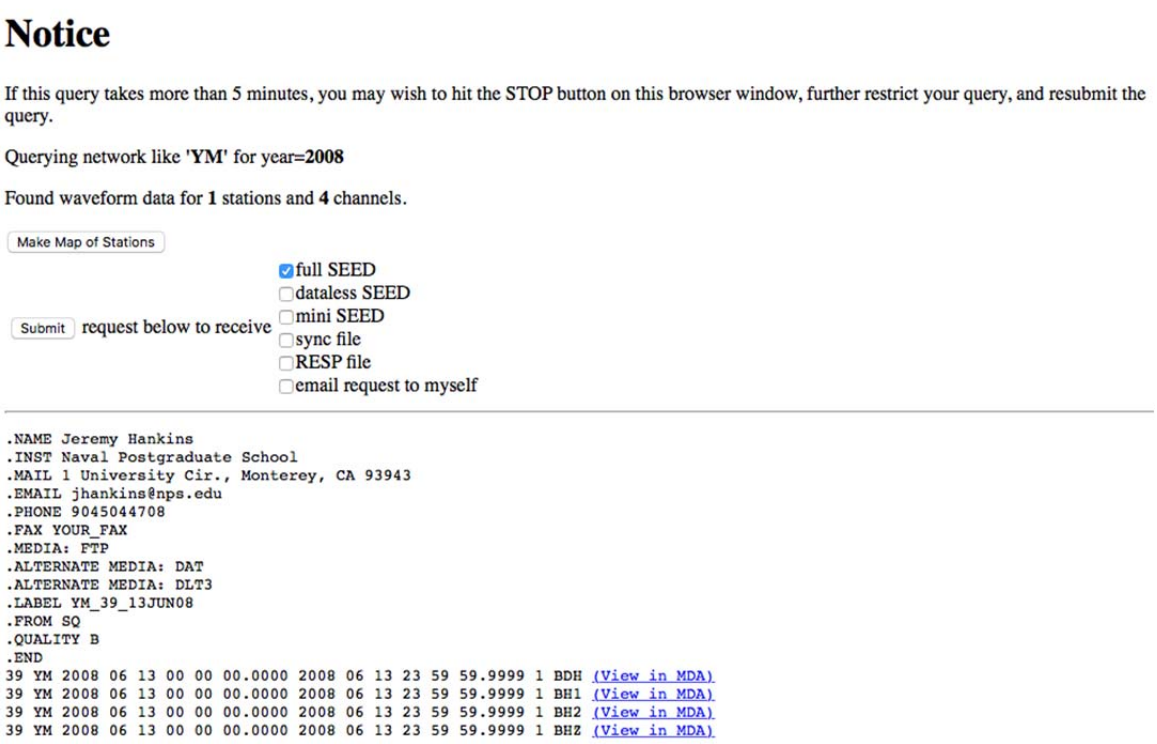

Notice

If this query takes more than 5 minutes, you may wish to hit the STOP button on this browser window, further restrict your query, and resubmit the query.

Querying network like **'YM'** for year=**2008**

Found waveform data for **1** stations and **4** channels.

Make Map of Stations

Submit request below to receive

- [x] full SEED
- [ ] dataless SEED
- [ ] mini SEED
- [ ] sync file
- [ ] RESP file
- [ ] email request to myself

```
.NAME Jeremy Hankins
.INST Naval Postgraduate School
.MAIL 1 University Cir., Monterey, CA 93943
.EMAIL jhankins@nps.edu
.PHONE 9045044708
.FAX YOUR_FAX
.MEDIA: FTP
.ALTERNATE MEDIA: DAT
.ALTERNATE MEDIA: DLT3
.LABEL YM_39_13JUN08
.FROM SQ
.QUALITY B
.END
39 YM 2008 06 13 00 00 00.0000 2008 06 13 23 59 59.9999 1 BDH (View in MDA)
39 YM 2008 06 13 00 00 00.0000 2008 06 13 23 59 59.9999 1 BH1 (View in MDA)
39 YM 2008 06 13 00 00 00.0000 2008 06 13 23 59 59.9999 1 BH2 (View in MDA)
39 YM 2008 06 13 00 00 00.0000 2008 06 13 23 59 59.9999 1 BHZ (View in MDA)
```

Figure 18. Final Submission Page to Get SEED Data from IRIS. Source: [23].

D. DATA ANALYSIS

It is at this point where a Mac computer (or another Unix-based machine) is required to process the data. As pointed out in Scobo's thesis [1], Unix is required to run IRIS's available software. A Mac computer proves useful because of the UNIX availability in the "Terminal" application. With an Internet search of Unix commands combined with the manuals that are available on IRIS's website, a novice Unix user can at least use the installed programs from IRIS with practice. Installing and compiling Unix code, though, is not a trivial endeavor without previous Unix experience, and it is recommended to get assistance installing and compiling from someone with skills in Unix before proceeding with the data analysis portion. The IRIS website conveniently has instruction manuals for all of its software with examples that greatly assist novice operators.

1. Rdseed v5.3.1

Rdseed reads the SEED files and outputs the raw data in SAC format, which is a binary format that can be read by the SAC software or MATLAB. In addition, RESP files and PZ files for all available channels can be output by rdseed for use in the calibration process. Rdseed proved effective and somewhat user-friendly after installed. Figure 19 displays a terminal window with typical rdseed commands. It is recommended to have an interactive manual open during the first few times using this software. The user can choose the dates and times to limit the SAC file's size. A user could also download a multiple-day SEED file and then use rdseed to chop the SEED file into the desired times for SAC file output. The rdseed depicted in Figure 19 is in the prompt mode, which walks the user through the inputs to get a SAC file, a RESP file, and a PZ file (if desired).

```
phs-imac:rdseedv5.3.1 phimac7$ ./rdseed
<< IRIS SEED Reader, Release 5.3.1 >>
Input  File (/dev/nrst0) or 'Quit' to Exit: /users/phimac7/desktop/YM_39/YM_39_DEC_08/YM_39_DE
C_13_14.104940.seed
Output File (stdout)    :
Volume #  [(1)-N]       :
Options [acCsSpRtde]    : d
Summary file (None)     :
Station List (ALL)      :
Channel List (ALL)      :
Network List (ALL)      :
Loc Ids (ALL ["--" for spaces]) :
Output Format [(1=SAC), 2=AH, 3=CSS, 4=mini seed, 5=seed, 6=SAC ASCII, 7=SEGY, 8=Simple ASCII(
SLIST), 9=Simple ASCII(TSPAIR)] : 1
Output file names include endtime? [Y/(N)]Y
Output poles & zeroes ? [Y/(N)]N
Check Reversal [(0=No), 1=Dip.Azimuth, 2=Gain, 3=Both]: 0
Select Data Type [(E=Everything), D=Data of Undetermined State, M=Merged data, R=Raw waveform
Data, Q=QC'd data] :E
Start Time(s) YYYY,DDD,HH:MM:SS.FFFF : 2008,348,00:00:00
End Time(s)   YYYY,DDD,HH:MM:SS.FFFF : 2008,348,23:59:59.9999
Sample Buffer Length [20000000]:
Extract Responses [Y/(N)]     : Y
Output data format will be sac.binary.
INFO: sac variable EVDP will be in KILOMETERS
Writing YM.39..BDH, 3456000 samples (binary), starting 2008,348 00:00:00.0080 UT
Writing YM.39..BH1, 3456000 samples (binary), starting 2008,348 00:00:00.0080 UT
Writing YM.39..BH2, 3456000 samples (binary), starting 2008,348 00:00:00.0080 UT
Warning... Azimuth/Dip Reversal found 39.BHZ, Data inversion was not selected
Writing YM.39..BHZ, 3456000 samples (binary), starting 2008,348 00:00:00.0080 UT
Writing RESPONSE file: RESP.YM.39..BDH
Writing RESPONSE file: RESP.YM.39..BH1
Writing RESPONSE file: RESP.YM.39..BH2
Writing RESPONSE file: RESP.YM.39..BHZ
Input  File (/dev/nrst0) or 'Quit' to Exit:
```

Figure 19. Example Rdseed Usage in Prompt Mode.

2. EVALRESP

For this thesis, EVALRESP was used to produce frequency amplitude phase (FAP) files. The FAP file is an ASCII file with three columns (frequency, amplitude, and phase) which can be used to apply the sensor response and obtain calibrated data. EVALRESP is built into the SAC program's "transfer" command, but if the user wants to obtain a FAP file, the EVALRESP software must be run separately. According to the SAC Manual [24], the advantage of using a FAP with the "transfer" function "is that one can include additional stages of the instrument response and/or control more explicitly the frequency range over which the correction is applied." A frequency range is chosen when building a FAP file within EVALRESP.

Figure 20 depicts a sample EVALRESP command to generate a FAP file from the YM 39 OBS used in this thesis. Because channels 1, 2, and Z were used in data analysis, a FAP file for all three channels had to be generated in the method shown in Figure 20 for channel Z. The EVALRESP manual [25] provides detailed information on the commands in Figure 20. In this figure, "39" is the station, "BHZ" is the channel, 2008 is the year, 348 is the Julian date, "0 20' lists the frequency range sought after, "2049" is the requested number of samples in the given frequency range, and "-f" precedes the file location. The RESP file called, in this case "RESP.YM.39..BHZ," is the response file generated by the rdseed program, "-s" is the type of spacing requested ("lin" for linear spacing is chosen here), and "-r" is the response type which is set to "FAP" [25].

```
phs-imac:src phimac7$ ./evalresp 39 BHZ 2008 348 0 20 2049 -f /Users/phimac7/desktop/YM_39/YM_39
_DEC_08/RESP.YM.39..BHZ -s lin -r 'fap'
phs-imac:src phimac7$
```

Figure 20. Sample EVALRESP Input for FAP File.

In addition to a FAP file, EVALRESP can also output a complex spectra (CS) file and an amplitude phase (AP) file. The CS file is a three column file

containing the frequency, real part of the amplitude, and imaginary part of the amplitude, whereas the AP file is similar to the FAP file except that frequency is not included.

3. SAC

SAC software, with the built-in transfer function, produced the calibrated data for this thesis. Figure 21 demonstrates the commands used for this thesis. Again, it is recommended to open an interactive software manual, available on the IRIS website, when using SAC. After reading-in the SAC data file with the read (r) command, any linear trends and offsets were removed with a remove trend command (rtr). The digital Fourier transform (DFT) that is used with a transfer function can pad the beginning and end of a time series with zeros so that SAC can achieve a power of 2 number of points. The “taper” command was applied to the data sequence after removing the trend to reduce sidelobes in the spectral data. The default setting for the taper command is a Hanning taper with a width of .05 times the entire length of data used [24]. Therefore, the amplitude of 10% of the data sequence is reduced by the taper and was discarded from analysis.

The SAC program has multiple built-in seismic analysis tools. Unfortunately, the SAC manual does not go into much detail discussing the theory behind how these analysis tools operate. The “transfer” command built into the SAC program “performs deconvolution to remove an instrument response and convolution to apply another instrument response.” [24] The transfer command can be achieved using either a RESP file, a FAP file, or a PZ file. During a transfer with FAP file option, if a frequency is encountered below the lowest frequency in the FAP file, the algorithm uses the lowest frequency given for the correction. Similarly, if the frequency encountered is above the max FAP file frequency, the algorithm uses the highest frequency given. The rdseed program produces the PZ and RESP files. The EVALRESP program, as discussed earlier, produces the FAP file. The four numbers following “freq” in

Figure 21 are the frequency limits, *f1* through *f4.* According to the SAC Manual [24], the frequency limits should be such that *f1 < f2 < f3 < f4.* A high-pass taper is applied between *f1* and *f2,* no taper (unity) is applied between *f2* and *f3*, and a low-pass taper is applied between *f3* and *f4.* To avoid ringing, [24] recommends that *f2=2*f1* and *f4>=2*f3.* When using SAC, the file that is read-in will remain there unless the program is commanded to do otherwise. The INICM command deletes any data in memory and was used prior to any new file to be read in [24].

```
 SEISMIC ANALYSIS CODE [11/11/2013 (Version 101.6a)]
 Copyright 1995 Regents of the University of California

SAC> r /users/phimac7/desktop/7D_J65A/NOV2011/NOV15/2011.319.00.00.00.0195_2011.319.2
[3.59.59.0195.7D.J65A..BHZ.M.SAC                                                    ]
SAC> rtr
[SAC> taper                                                                         ]
SAC> trans from fap s /users/phimac7/desktop/FAP.7D.J65A..BHZ to vel freq .01 .02 10
20
[ Extrapolating below lowest FAPFILE frequency                                      ]
[ Extrapolating above highest FAPFILE frequency                                     ]
 Station (J65A    ), Channel (BHZ     )
SAC> write NOV15_2011_7D_J65A_BHZ_fap01_to_25_calibrated_01_02_10_20.sac
SAC> INICM
```

Figure 21. SAC Example of Transfer Command Using FAP File to Calibrate Data.

4. RSAC.m

The rsac.m program is a publicly available MATLAB program that reads a SAC file and outputs a three column MATLAB file that is easily useable for analysis. The first rsac.m column in the output is time, the second column is amplitude, and the third column contains the SAC header information and was not used in this thesis.

5. MATLAB Data Analysis

MATLAB was used for data analysis on the calibrated SAC files after the data was read using rsac.m. Three functions (see Appendix A) were written that take as inputs a maximum desired amplitude, the sampling frequency of the OBS, and the data from the three orthogonal seismometer channels from an OBS. The first function entitled “vibration_analysis.m” finds the peaks of the

signal above the maximum amplitude and checks the times between these peaks. It then looks for the longest period of time between peaks. If a quiescent period (a period of time during which the signal remains below the maximum amplitude) is found in the vertical channel that is at least an hour long, a power spectral density (PSD) using the pwelch function in MATLAB is conducted on the quiescent period. The PSD displays all three orthogonal channels. The data within the taper at the beginning and end of the input time series is not included in the quiescent period and is removed prior to a PSD being conducted. If there is not at least an hour of quiescent time, a different MATLAB function was used. If the signal was too high and no hour-long quiescent periods exist, the function high_amp_vibration_analysis.m was used. This program finds the three-hour time period with the lowest mean amplitude and outputs the same information as the vibration_analysis.m program. If the 24-hour sample was low amplitude and did not cross the maximum amplitude line, the low_amp_vibration_analysis.m was conducted, which outputs a PSD for the entire sample.

There are also three different types of histograms produced by these programs. The first is a histogram of the amplitudes throughout a 24-hour period. Both non-logarithmic and logarithmic y-axes were required to adequately display all of the occurrences. The next two histograms involved the desired maximum amplitude threshold which is entered into the functions. The first is a histogram of width of pulses that exceed the maximum amplitude threshold, and the second is a histogram of lengths of time between these pulses that exceed the maximum amplitude threshold. Both of these histograms are completed logarithmically and non-logarithmically to ensure that outliers are displayed.

The maximum amplitude threshold histograms were completed because vibration amplitudes above a certain level would likely result in a noise floor too high to obtain satisfactory performance for the bottom mounted sensor. However, since the performance of a future bottom mounted sensor is unknown, the maximum amplitude threshold was chosen somewhat arbitrarily to be 5×10^{-5} m/s based on observations of high amplitude activity. This threshold proved to be a

good indicator of high amplitude, seismic activity (non-quiescent), and the threshold was thus used to compare the velocities measured at all of the OBS locations. Only YM 39 had standard deviations for 24-hour periods that regularly exceeded this threshold, and the other three OBSs, with the exception of a couple of days, remained well below.

E. CHALLENGES FACED WITH CALIBRATION

The largest challenge faced for this thesis was obtaining calibrated data before analysis could be conducted in MATLAB. [8] describes the LDEO OBS as able to effectively measure from .01 to 20 Hz. The LDEO OBS's response curve, illustrated in Figure 22, changes by 2 orders of magnitude from .01 to 1 Hz. Figure 23 exhibits the SIO OBS's response curve that has nearly a flat response from .01 to 20 Hz. Because of the LDEO response curve, getting the calibrated data becomes more complicated than just dividing the raw counts by the sensitivity.

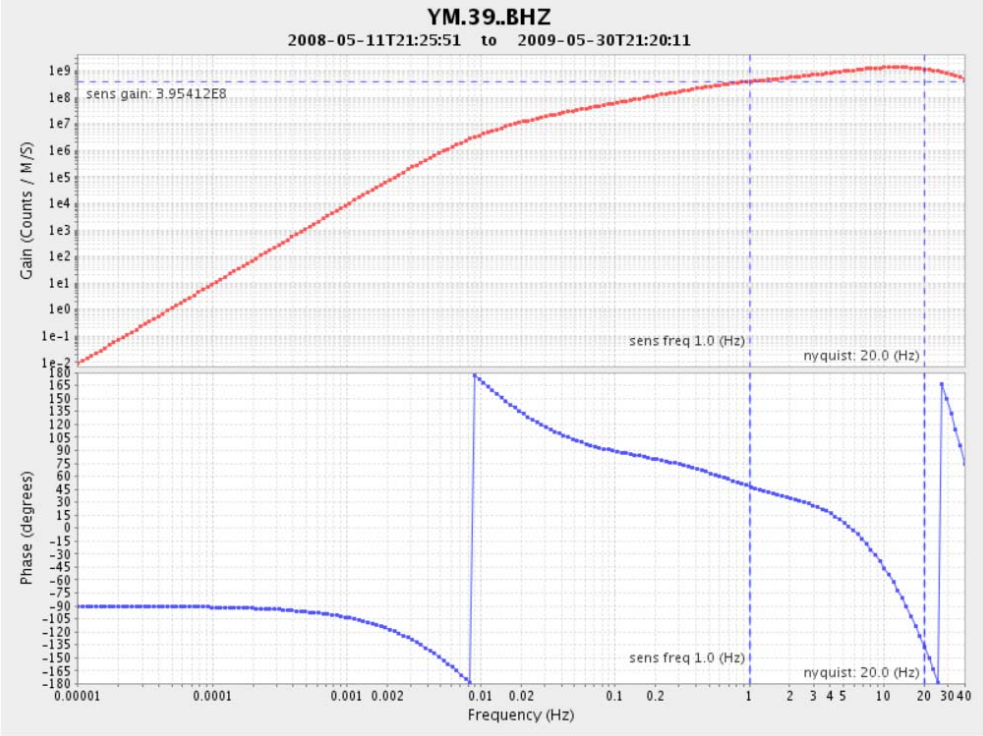

Figure 22. LDEO OBS Response Curve for YM 39 Channel Z. Source: [26].

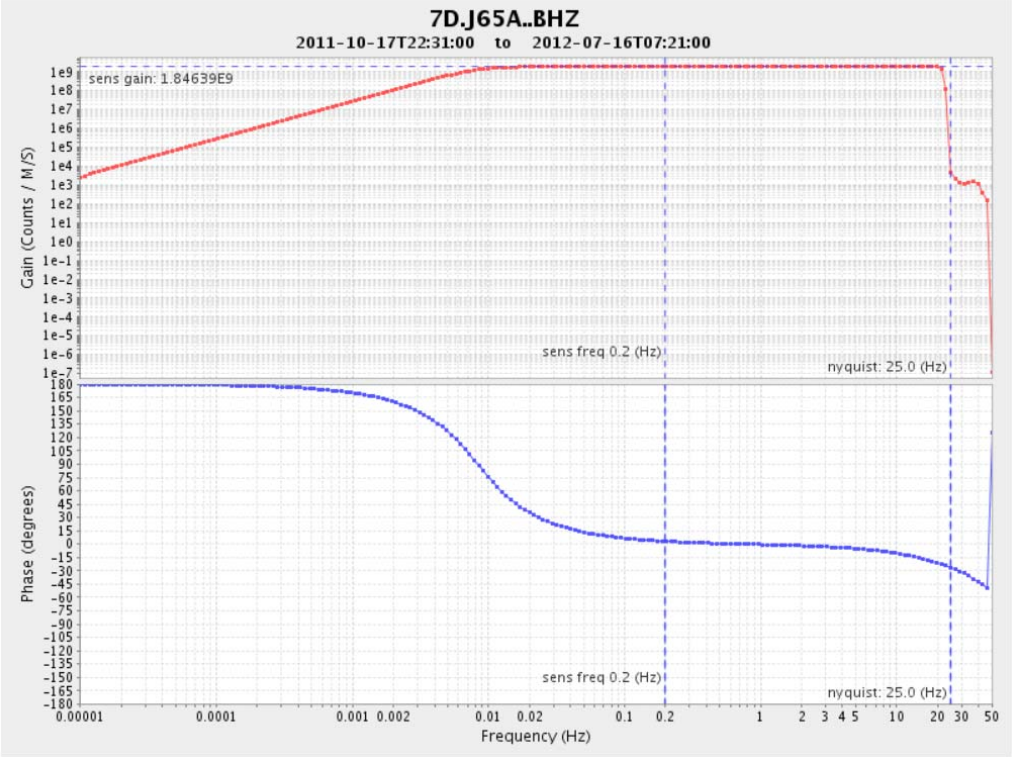

Figure 23. SIO OBS Response Curve from Channel Z of 7D J65A. Source: [27].

Due to lack of familiarity with SAC software, and because the SAC manual does not go into detail about the process behind calibration, calibration was initially conducted with MATLAB using the CS file. This proved to be more complicated than necessary, especially after conversation with a seismologist who stated that the SAC software was quite able to complete the calibration correction sufficiently. There were four ways attempted to complete the calibration that involved the IRIS SAC software and the time series webserver (TSWS).

Figure 24 displays the TSWS webpage. The TSWS allows a user to pick the network, station, channel, date(s), time, and multiple calibration/filtration options. Depending on the selection, it will immediately produce a plot or downloadable data in a user-selected format. For rsac.m to work with the TSWS data, “SAC binary little-endian” must be selected. With the correct settings, the

TSWS provided a convenient way to double check time plots. Without correct settings, the TSWS produced some odd results that could be misleading.

To illustrate, Figure 25 is a TSWS plot of a full day from YM 39, with frequency limits of .01-.02-10-20 Hz, the instrument correction applied, and “remove mean” selected. Figure 26 is a MATLAB plot produced with FAP calibrated data of the same time period and settings. Both plots appear similar.

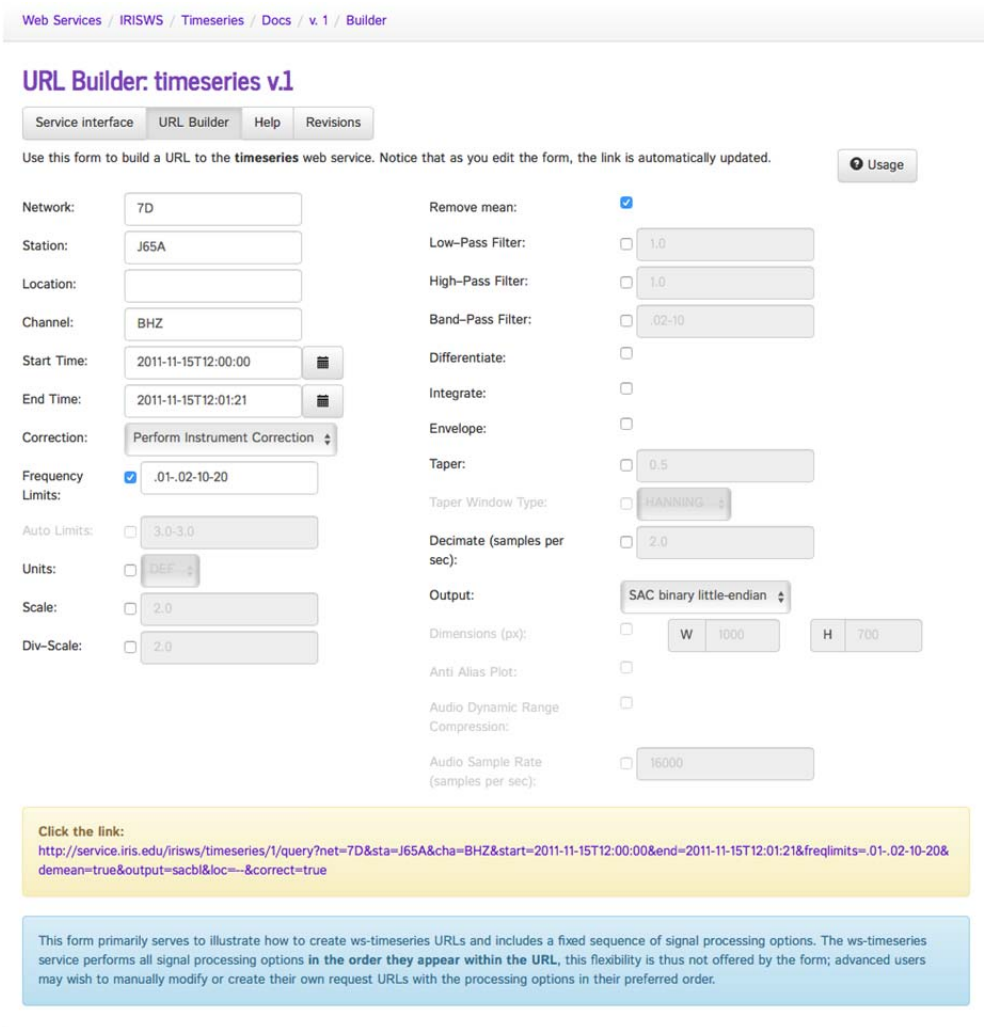

Figure 24. TSWS Webpage. Source: [28].

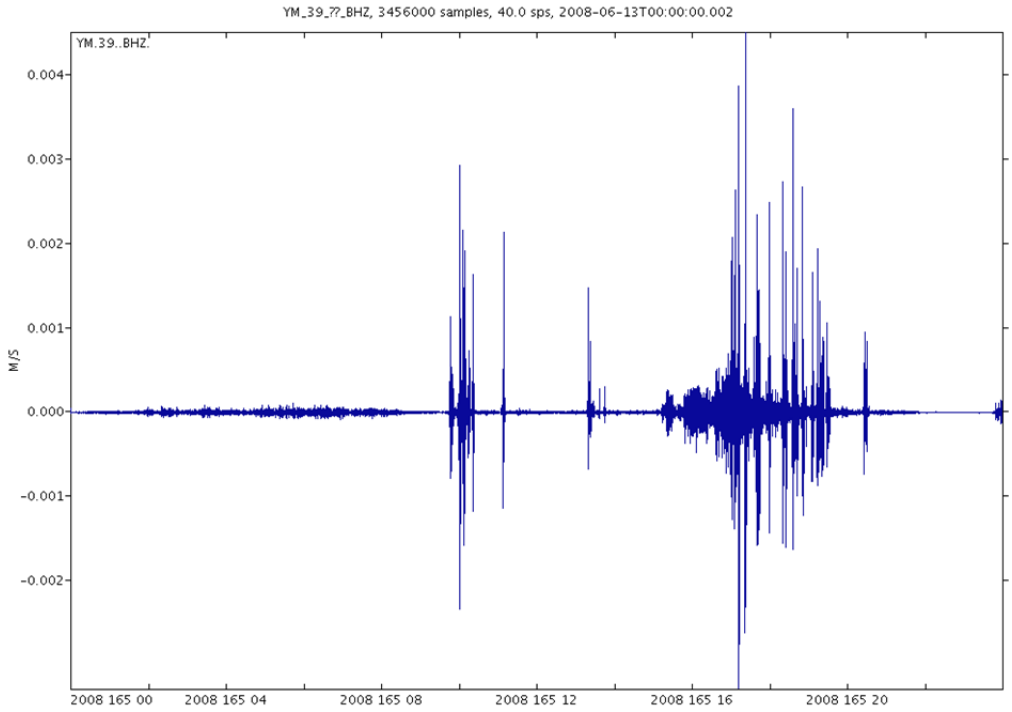

Figure 25. TSWS Plot of YM 39 on June 13, 2008, 24 Hours, Frequency Limits of .01-.02-10-20 Hz. Source: [28].

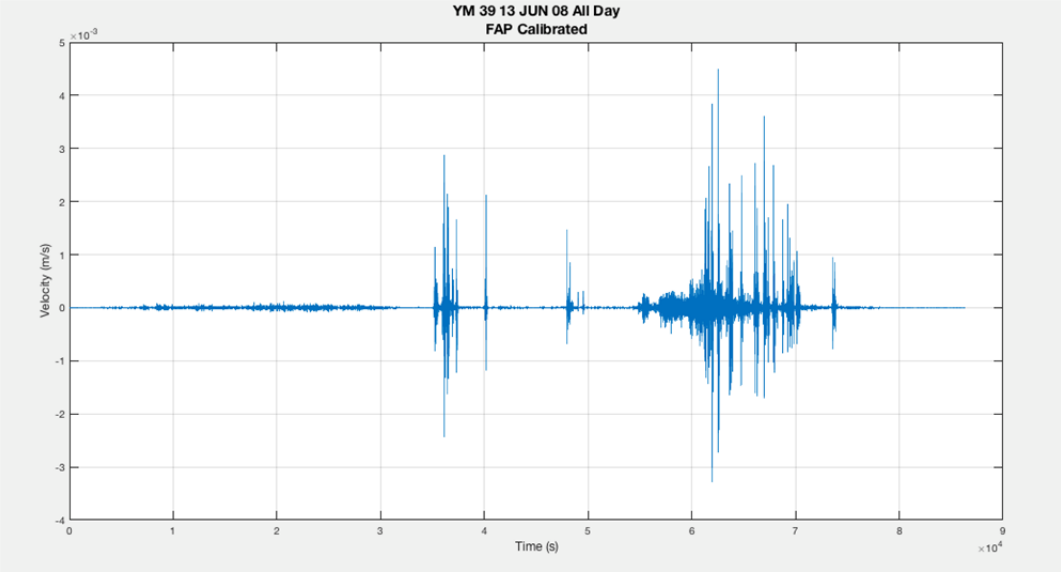

Figure 26. MATLAB Plot of YM 39 on June 13, 2008, 24 Hours, Frequency Limits of .01-.02-10-20 Hz, FAP Calibrated.

However, if the frequency range is changed slightly to 0-.02-10-20 Hz, and all other settings remain unchanged, the TSWS produces the plot in Figure 27. Figure 28 displays the FAP calibrated file with the same settings. Although the plot has changed with apparent ringing, it still is recognizable as a seismogram with close to the same values as the previous FAP plot.

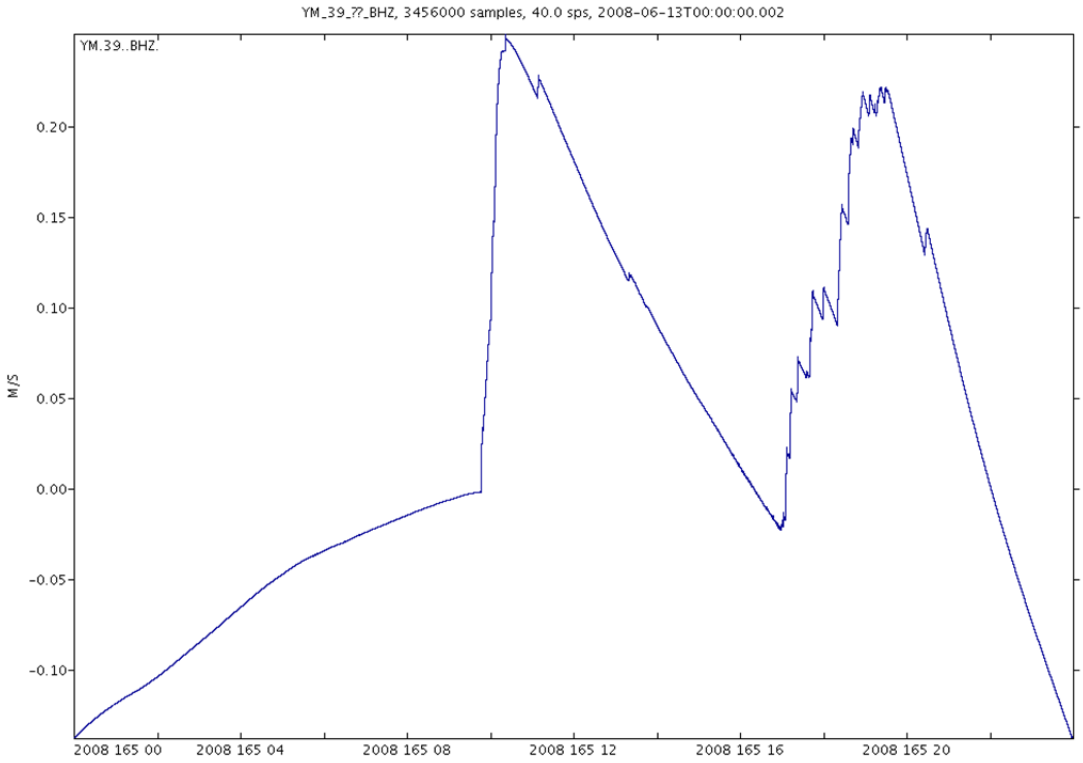

Figure 27. TSWS Plot of YM 39 on June 13, 2008, 24 Hours, Frequency Limits of 0-.02-10-20 Hz. Source: [28].

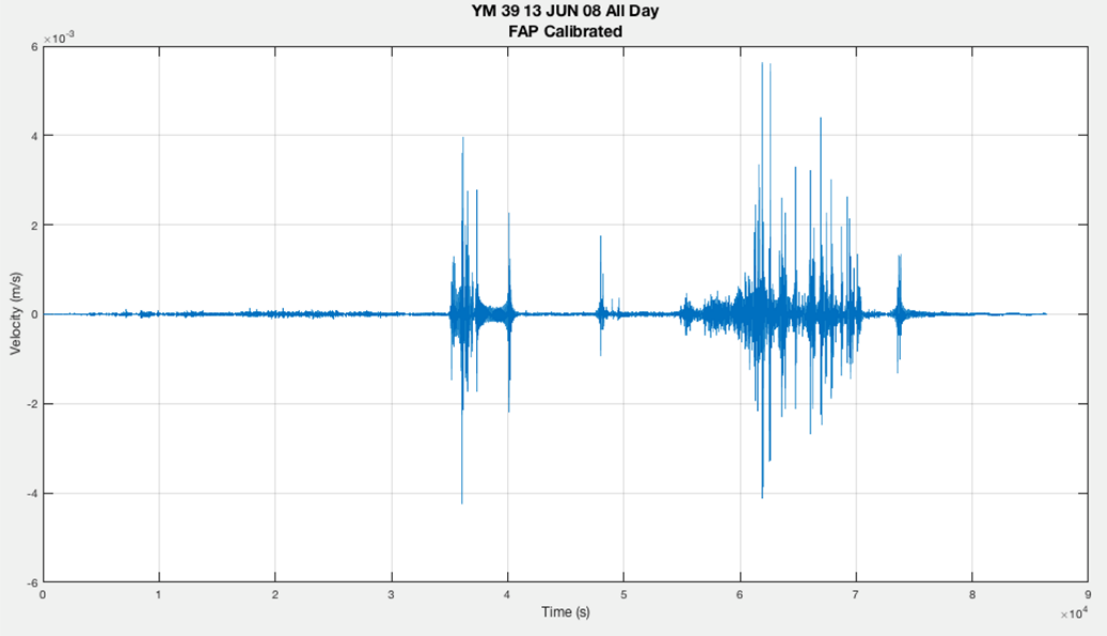

Figure 28. MATLAB Plot of YM 39 on June 13, 2008, 24 Hours, Frequency Limits of 0-.02-10-20 Hz, FAP Calibrated.

Smaller samples of the same day were inspected with similar results. Figure 29 shows a TSWS output of 4080 samples, from 12:00:00 to 12:01:42 on 13 June 2008. The settings were the same as for Figure 25, with frequency limits of .01-.02-10-20 Hz, instrument correction applied, and “remove mean” selected. Figure 30 displays what happens to this smaller data sample when “remove mean” is not selected with all other settings unchanged.

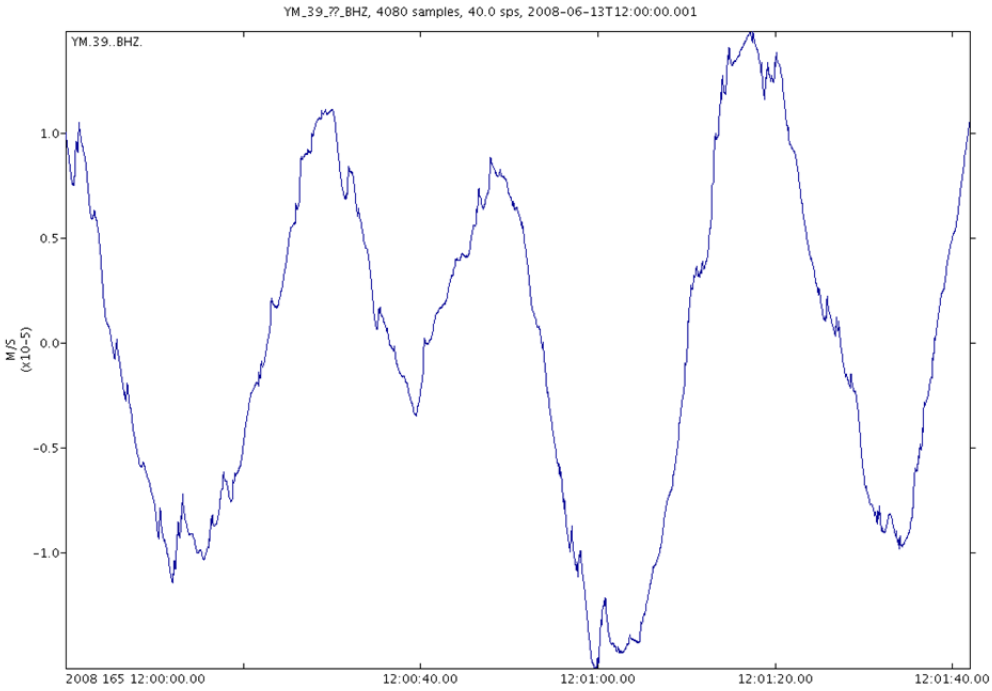

Figure 29. TSWS Plot of YM 39 on June 13, 2008, from 12:00:00 to 12:01:42, Frequency Limits of .01-.02-10-20 Hz. Source: [28].

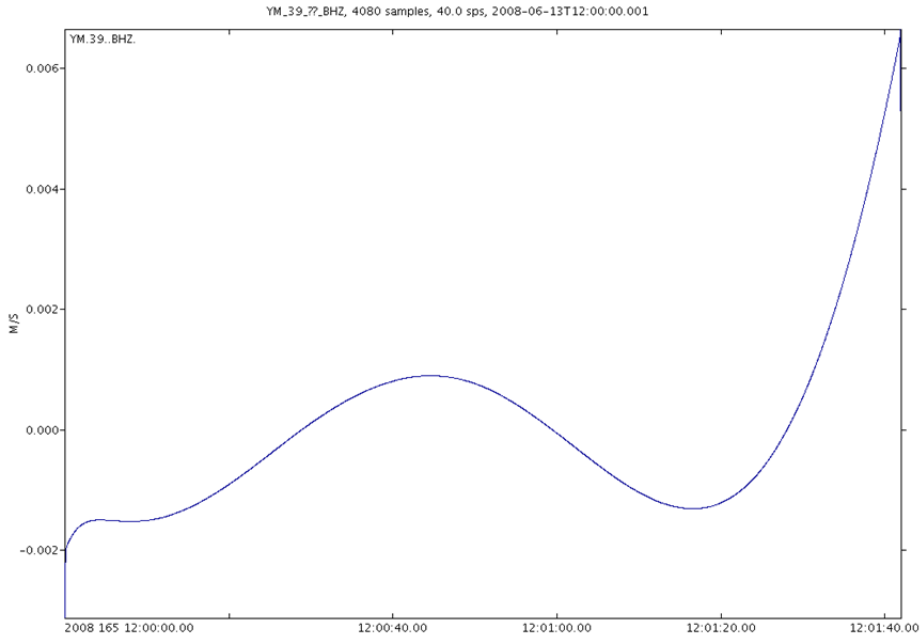

Figure 30. TSWS Plot of YM 39 on June 13, 2008, from 12:00:00 to 12:01:42, Frequency Limits of .01-.02-10-20 Hz, Remove Mean Deselected. Source: [28].

Figure 31 is a FAP calibrated plot of the same time period without “remove trend” applied. This behavior of the TSWS led to the conclusion that other calibration methods were needed besides using the user-friendly TSWS. If the frequency limits are applied correctly, the instrument correction is applied, and “remove mean” is selected, the amplitude of TSWS plots can still differ from the FAP, PZ, and RESP calibrated plots, but the shape of the signal is nearly identical to the other calibration methods.

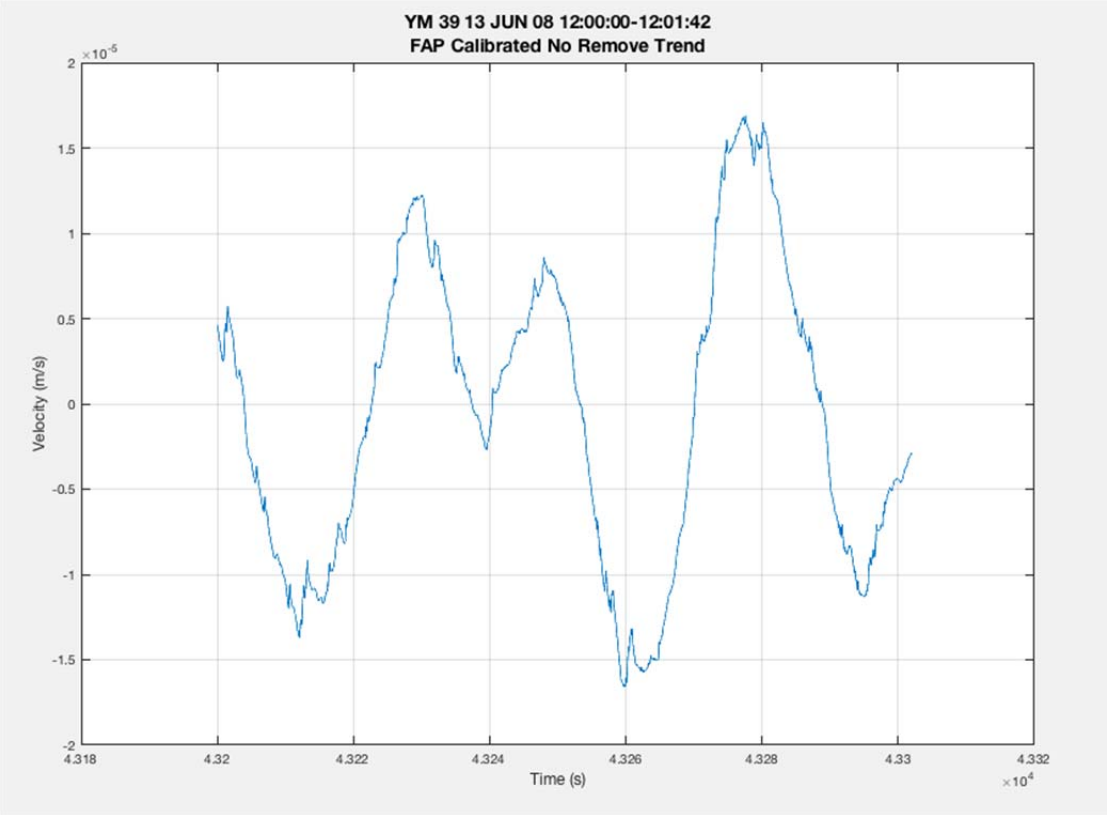

Figure 31. MATLAB Plot of YM 39 on June 13, 2008, 12:00:00 to 12:01:42, Frequency Limits of .01-.02-10-20 Hz, FAP Calibrated, Remove Trend Not Completed.

The remaining SAC calibration methods produced very similar results if the frequency limits were set the same. It was initially thought that FAP produced superior results to both a RESP and PZ calibrated file, but it was later discovered that FAP, RESP, and PZ calibrated files are nearly identical. Figures 32 and 33

show four different methods to gain calibrated data for both OBSs. Figure 32 is from YM 39 on June 13, 2008, and Figure 33 is from 7D J65A on November 15, 2011. Of note, all the plots are nearly identical, but the TSWS produces different amplitudes in Figure 32.

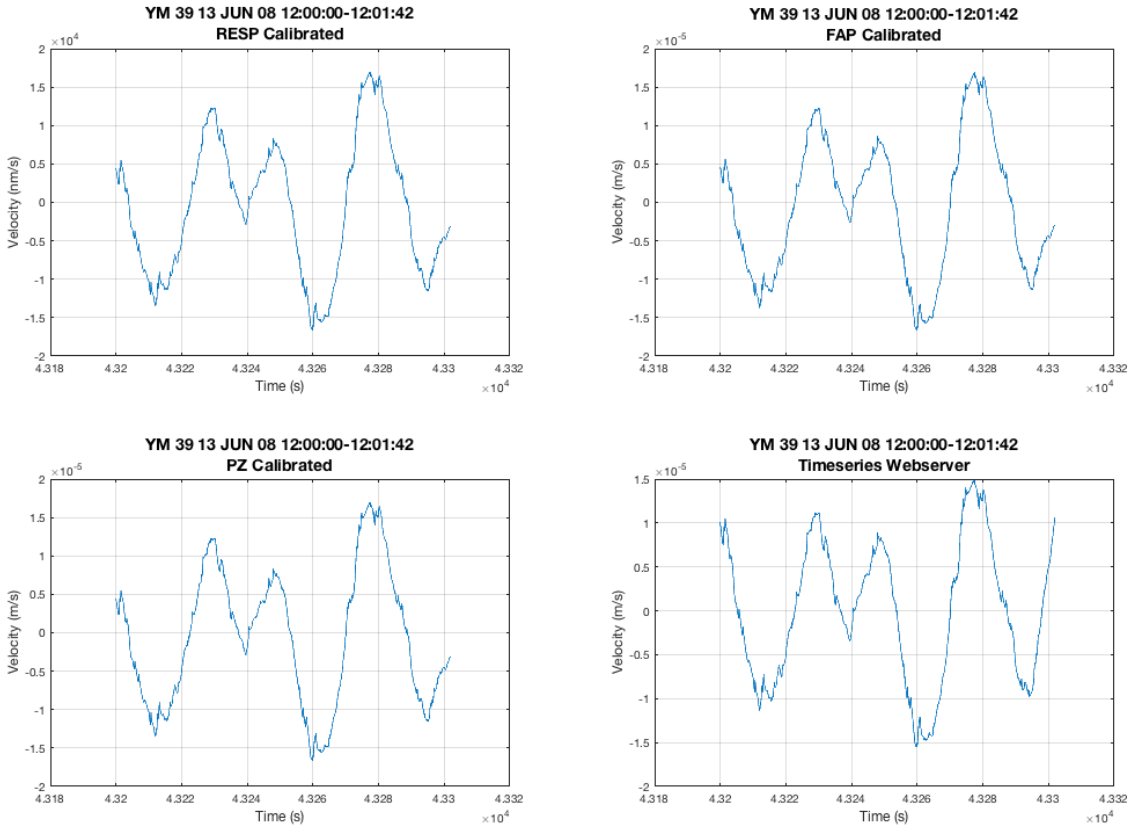

Figure 32. MATLAB Plot of Different Calibration Methods for YM 39 on June 13, 2008.

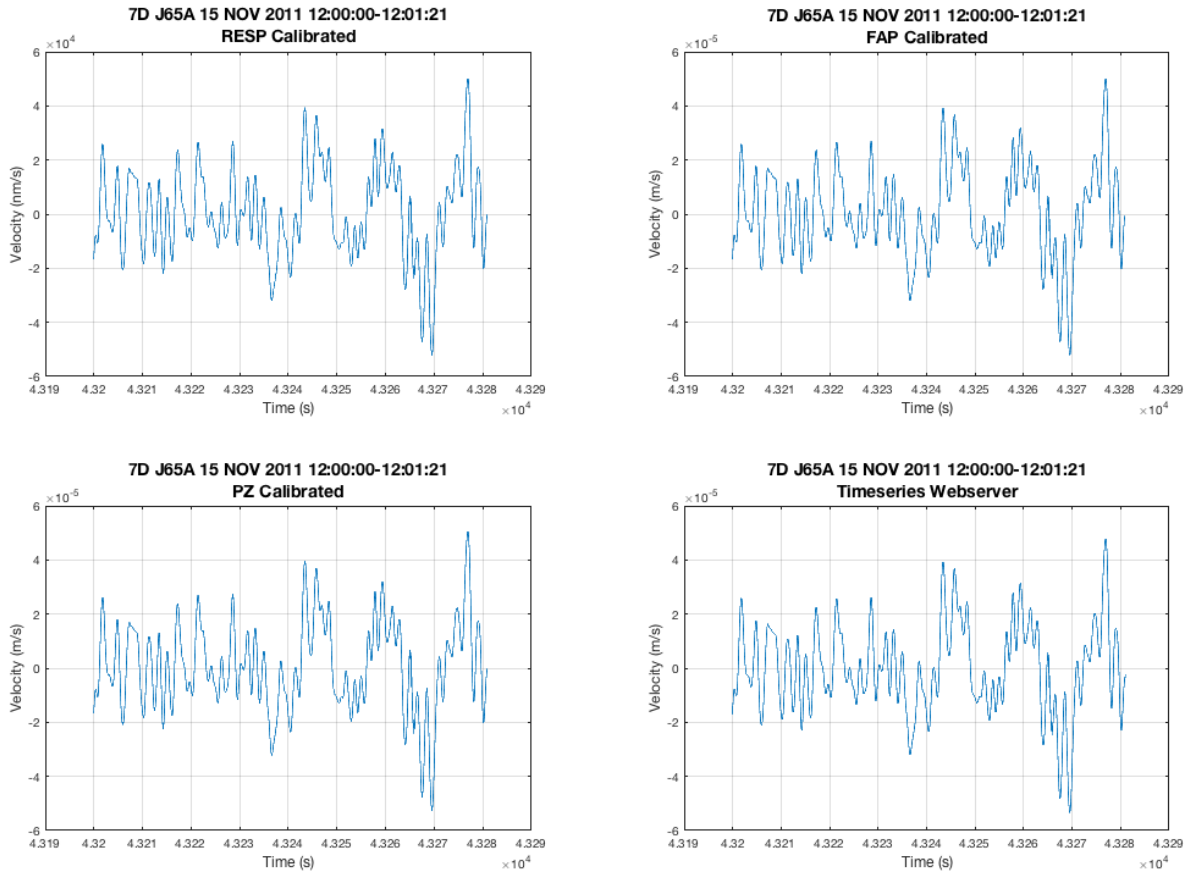

Figure 33. MATLAB Plot of Different Calibration Methods for 7D J65A on November 15, 2011.

Because of the similarity of the data from the three SAC calibration techniques and because of the work already completed with FAP files, the FAP calibration technique was used for the data in this thesis. Any of the methods available with the SAC transfer, either FAP, RESP, or PZ files, would have been sufficient for use.

Some idiosyncrasies with the software proved to hold additional challenges. Each time a transfer command in SAC was used, the command line involved a "from" *type of file* (i.e. RESP, PZ, FAP) and an optional "to" *desired units* (e.g., velocity and displacement). Figure 21 is an example of transfer with a "to vel" (to velocity) command. The default waveform is displacement, so if a "to none" line is entered, the SAC manual [24] states that the output will default to

displacement. If no “to” line is entered (left blank), SAC will assume it is “to none” [24]. A transfer with a FAP file, though, does not necessarily follow the SAC manual, which led to an assumption that calibrated files were in units of velocity when the files output were actually acceleration. Figure 34 summarizes the SAC peculiarities with the transfer command that led to some analysis challenges.

	to velocity	to none	No entry (blank)
EVALRESP	VEL	DISP	VEL
POLEZERO	VEL	DISP	DISP
FAP	ACC	VEL	VEL

Figure 34. Summary of SAC Transfer Output.

F. SUMMARIZED DATA ANALYSIS STEPS

The steps described in this chapter are summarized in Figure 35.

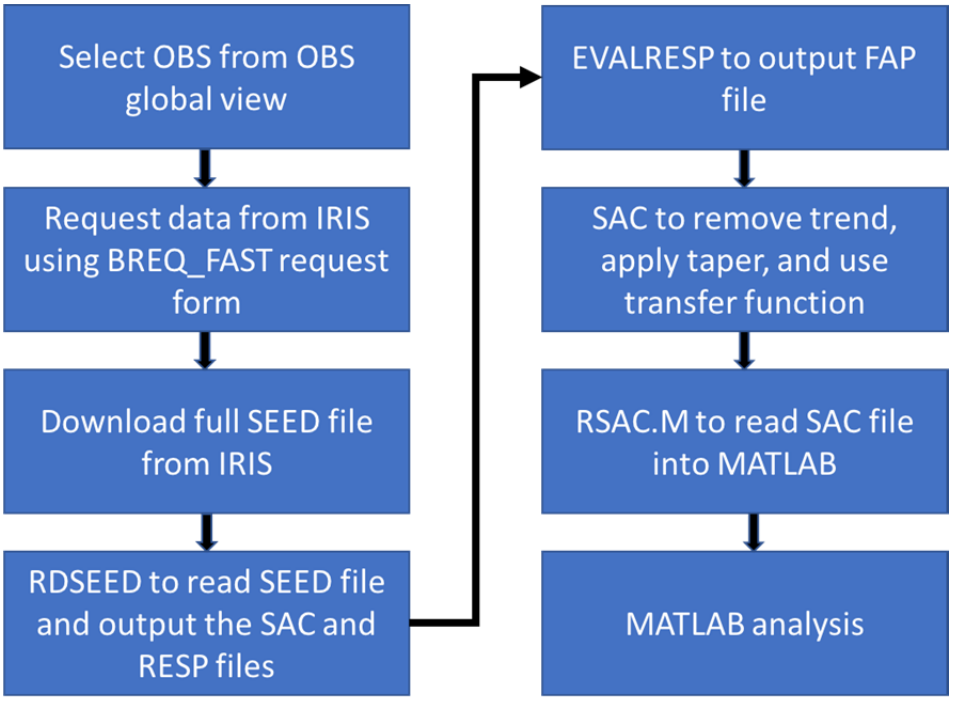

Figure 35. Methodology and Data Analysis Summary.

THIS PAGE INTENTIONALLY LEFT BLANK

V. RESULTS

A. POWER SPECTRAL DENSITY

1. YM 39 and YM 38

YM 39 was the most erratic of the OBSs sampled. It had the highest variation in standard deviation and the largest variation in percentage of time spent above max amplitude. Most samples did not have at least one hour of quiescent time and had to be analyzed with the high amplitude vibration analysis code. In most instances for YM 39, the PSDs taken from the quiescent periods displayed a decreasing amplitude with increasing frequency and no apparent narrowband frequencies as illustrated in Figure 36; however, the decibel levels differed from sample to sample. Discrete frequencies do show up in the PSDs of the entire 24-hour period, which is displayed in Figure 37.

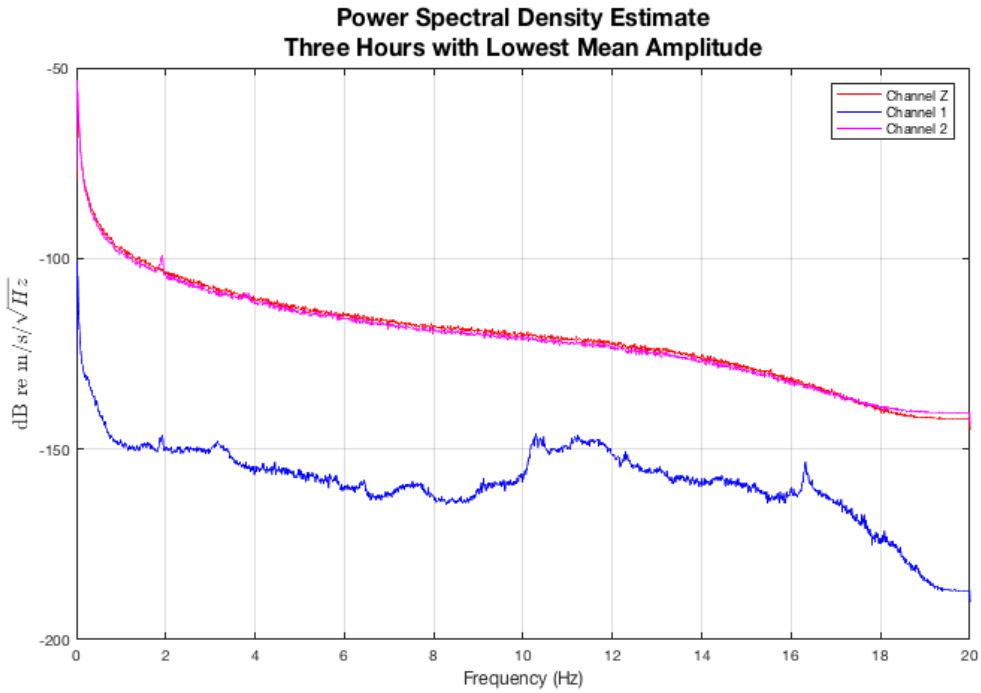

Figure 36. YM 39, PSD from August 1, 2008, Quiescent Period (Three Hours with Lowest Mean Amplitude).

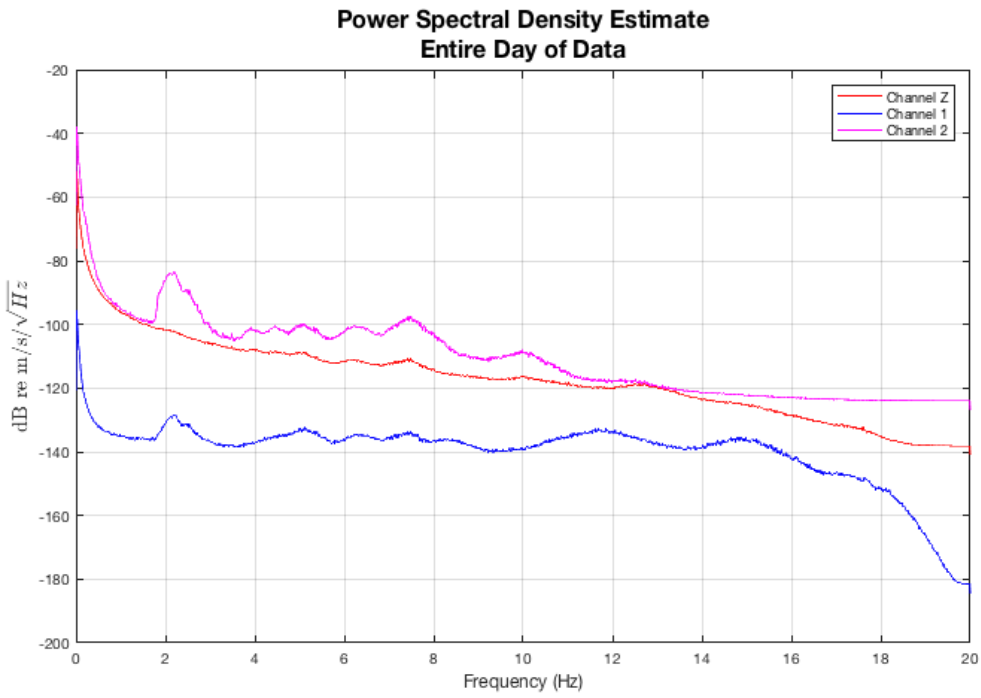

Figure 37. YM 39, August 1, 2008, PSD for Entire Day

If the PSD for channel Z is graphed on a logarithmic x and y axis, it appears almost as a straight line as in Figure 38. Most spectral densities for YM 39 channel Z follow this pattern with only slight variations from the overall slope. The velocity time series plot responsible for this PSD, Figure 39, represents a typical appearance of the majority of the days for YM 39.

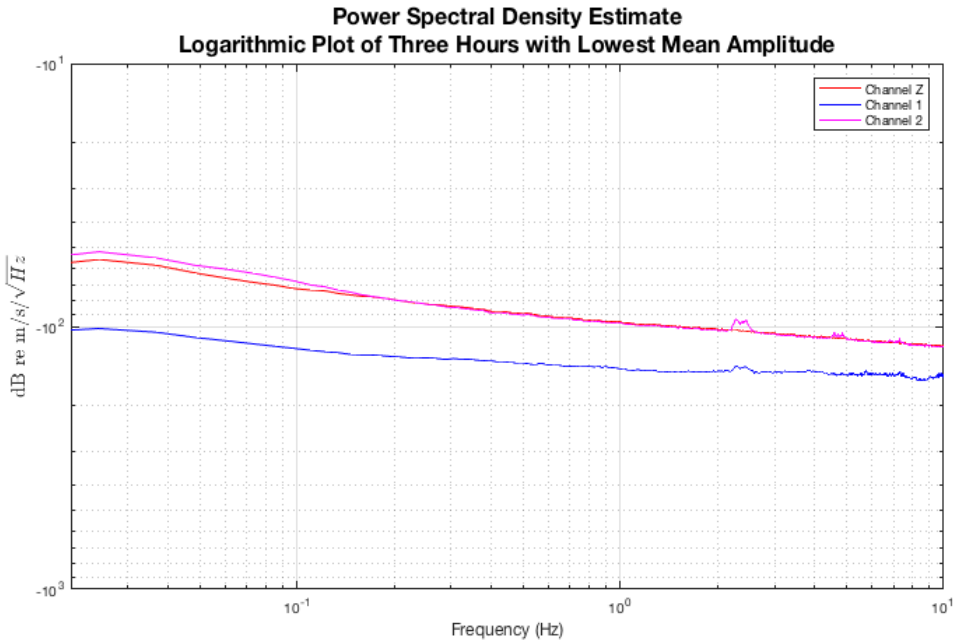

Figure 38. YM 39, August 1, 2008, PSD with Logarithmic Axes.

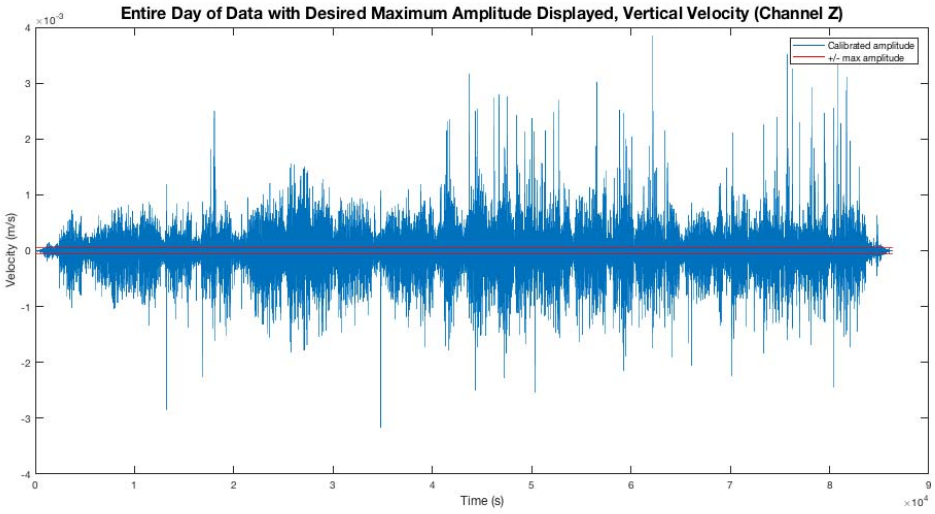

Figure 39. YM 39 Velocity Time Series, August 1, 2008.

For the low frequency range, shown in Figure 40, most of YM 39's PSDs exhibited a steady decline with the same overall pattern from month to month. However, even though the overall shape and slope remained consistent, the decibel level varied greatly from sample to sample and was far more inconsistent

than the other OBSs. The drop off in decibel levels close to 0 Hz is due to the bandpass filter, which starts with a taper at .01 Hz.

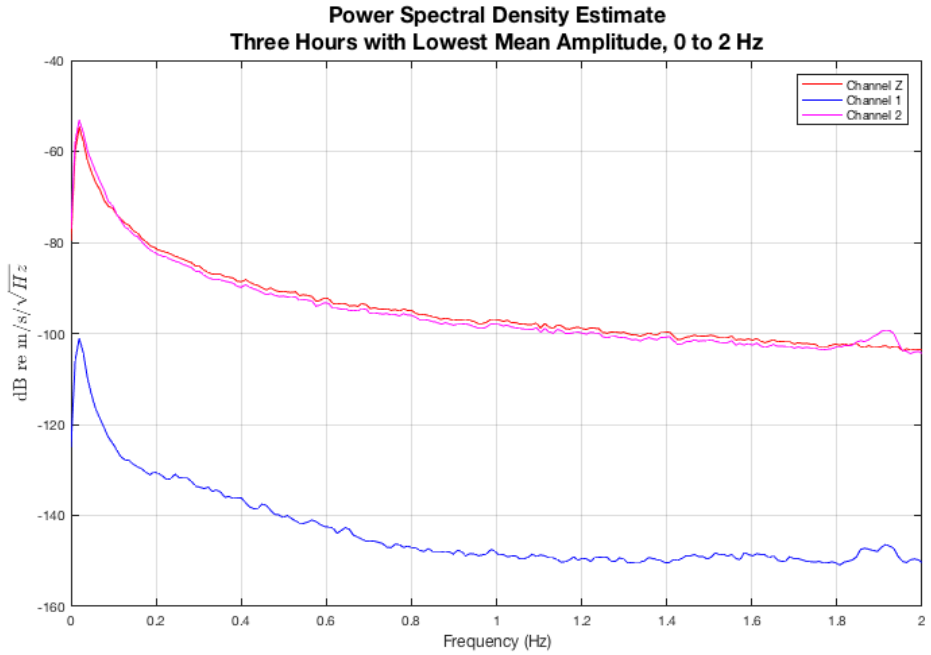

Figure 40. YM 39, PSD, August 1, 2008, 0 to 2 Hz.

YM 38, however, had the lowest amplitudes of all four OBSs, especially in the vertical channel. Channel 1 and channel 2 exhibited much higher amplitudes than channel Z for all days sampled. This is shown by the fact that the decibel level of the vertical channel hovered around 10 to 20 dB less than the horizontal channels. The channel Z plot showed hints of discrete frequencies, especially around 4 Hz, 6 Hz, and 8 Hz, but the appearance of the discrete frequencies differed slightly from month to month like in Figure 41 where the discrete frequencies are located at approximately 4 Hz and 7 Hz. A visual comparison of plots between YM 38 and YM 39 on the same dates revealed no common discrete frequencies and different appearances of the time series plots. In particular, YM 38 was quieter than YM 39 by around 2 orders of magnitude. Figure 41 displays a typical YM 38 PSD for a quiescent period. Figure 42 is from

the same sample between 0 to 2 Hz. Most 24-hour samples from YM 38 never had any amplitude spikes above the max amplitude threshold.

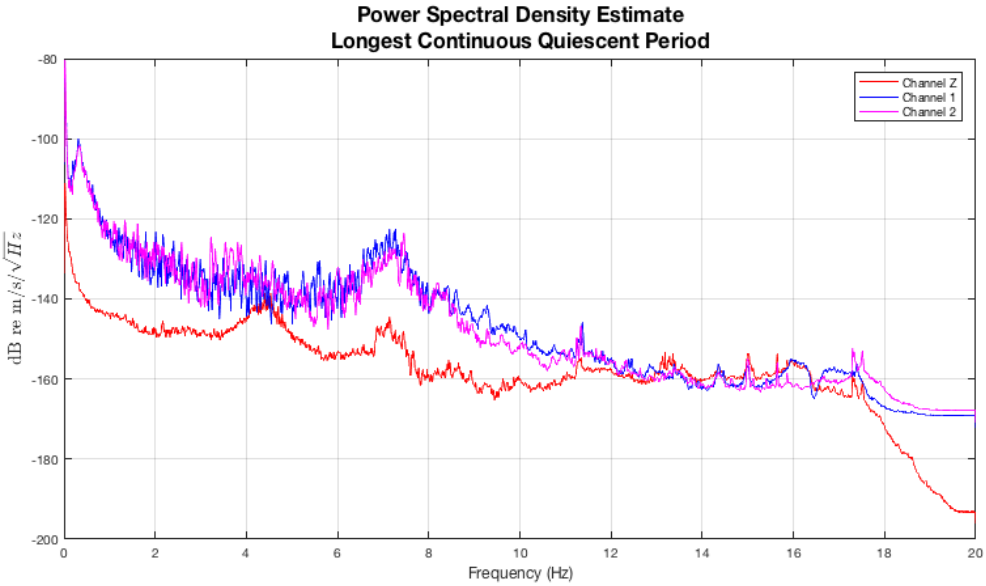

Figure 41. YM 38, PSD for Quiescent Period, August 1, 2008.

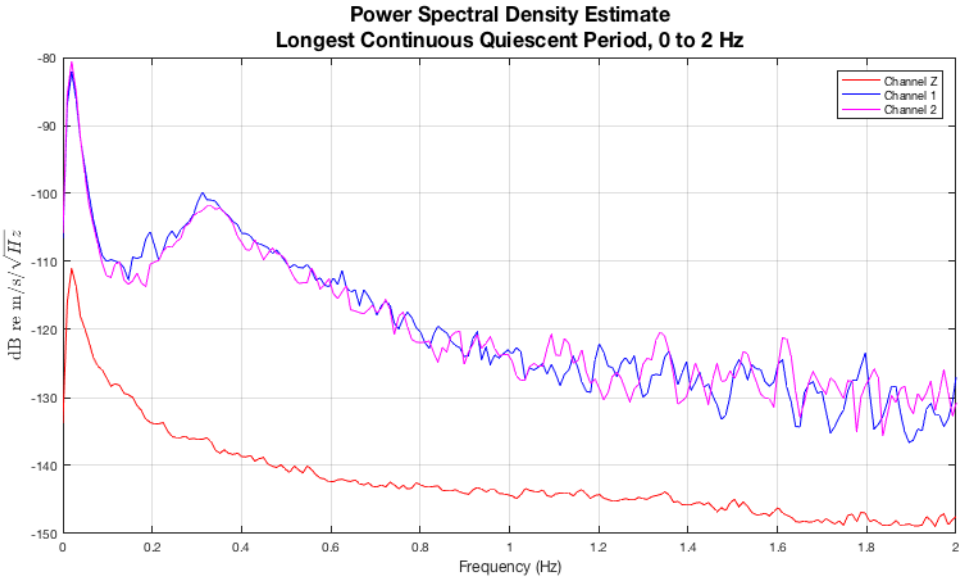

Figure 42. YM 38, PSD for Quiescent Period, August 1, 2008, 0 to 2 Hz.

The sample from August 1, 2008 is an example of one of the few days when the amplitude crossed the maximum amplitude threshold. As displayed in Figure 43, there are two large amplitude occurrences. Figure 44 is a close-up of the largest amplitude spike, and the amplitude increase does not appear to cause any ringing on the plot.

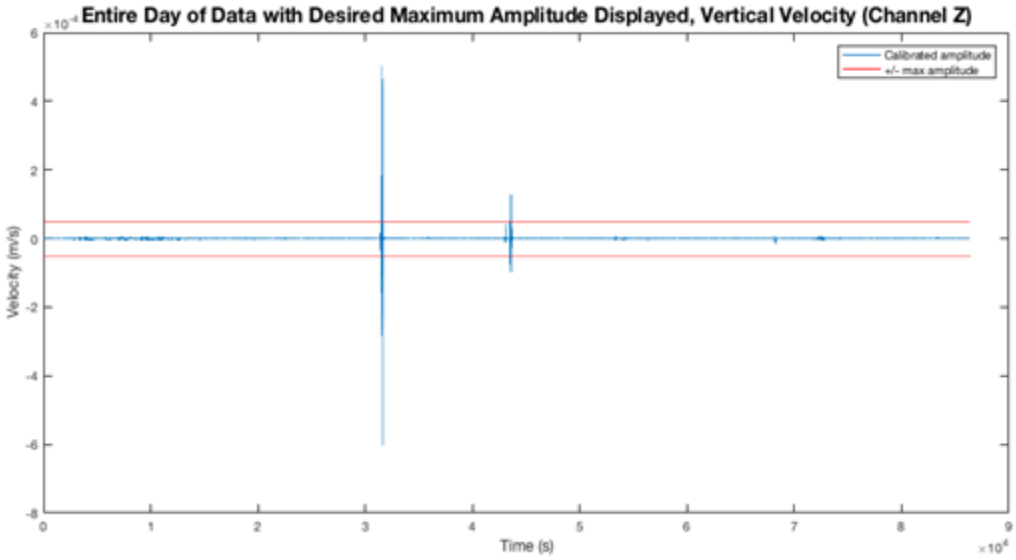

Figure 43. YM 38, Velocity Time Series, August 1, 2008.

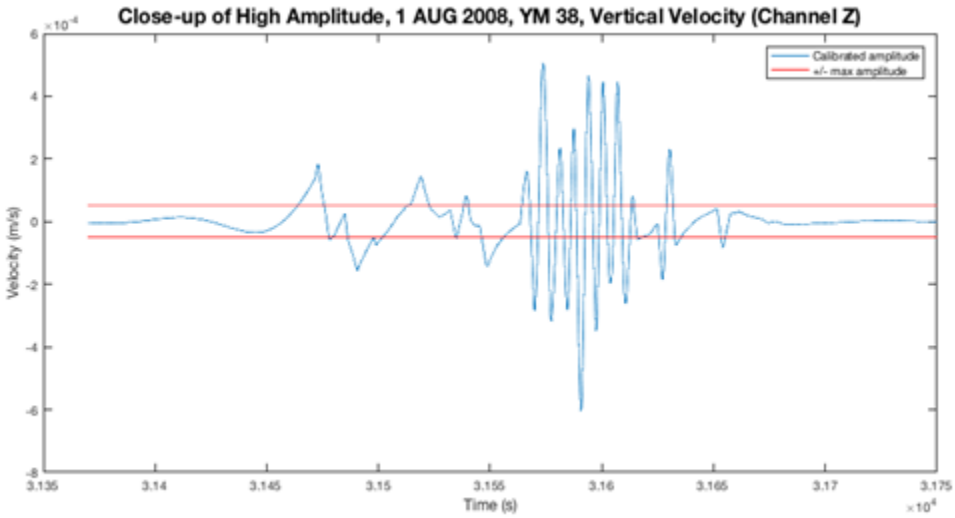

Figure 44. YM 38, August 1, 2008, Close-Up of Highest Amplitude Event in Velocity Time Series

Unlike in OBS YM 39, most of the high amplitudes in the horizontal channels do not show up in the vertical channel. Figure 45 is a depiction of channel 1 from YM 38 on August 1, 2008. The higher amplitudes in the beginning of the day do not translate into a high response in channel Z, but the two high-amplitude occurrences after the $3x10^4$ second mark and $4x10^4$ second mark do appear in the vertical channel.

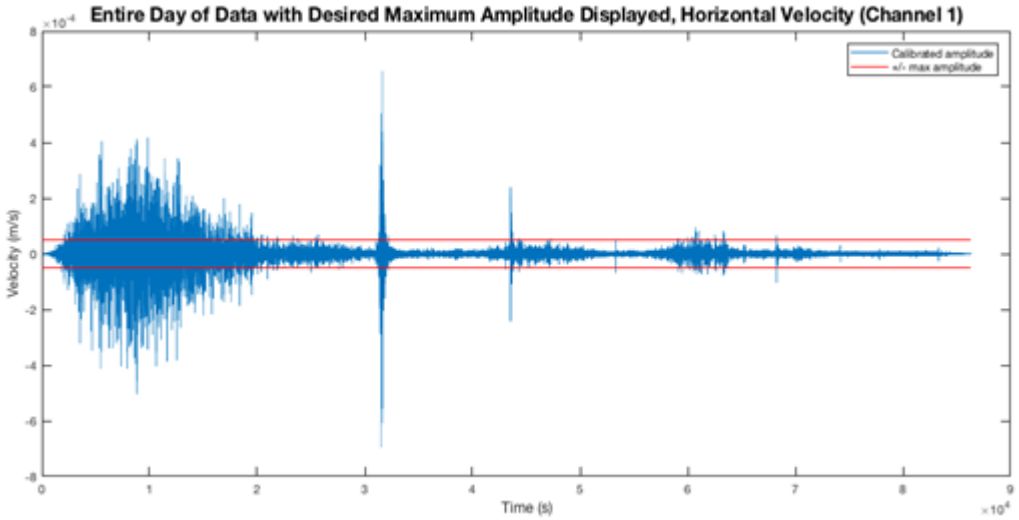

Figure 45. YM 38 Velocity Time Series, Channel 1, August 1, 2008.

Although YM 38 and YM 39 were located in the Luzon Strait in close proximity, the two OBSs displayed vastly different results. YM 39 was not consistent, and YM 38 displayed much lower vertical vibrational disturbances.

2. 7D J65A and 7D J73A

Both OBSs west of the Strait of Juan de Fuca, 7D J65A and 7D J73A display similar and consistent results. 7D J65A exhibits the same consistent pattern almost every day where channel Z peaked at 8 to 9 Hz with varying decibel levels. Figures 46 and 47 depict the two 7D J65A plots with maximum and minimum decibel levels at around 9 Hz. Channel Z in Figure 46 peaks at around -130 dB and in Figure 47 peaks at around -150 dB.

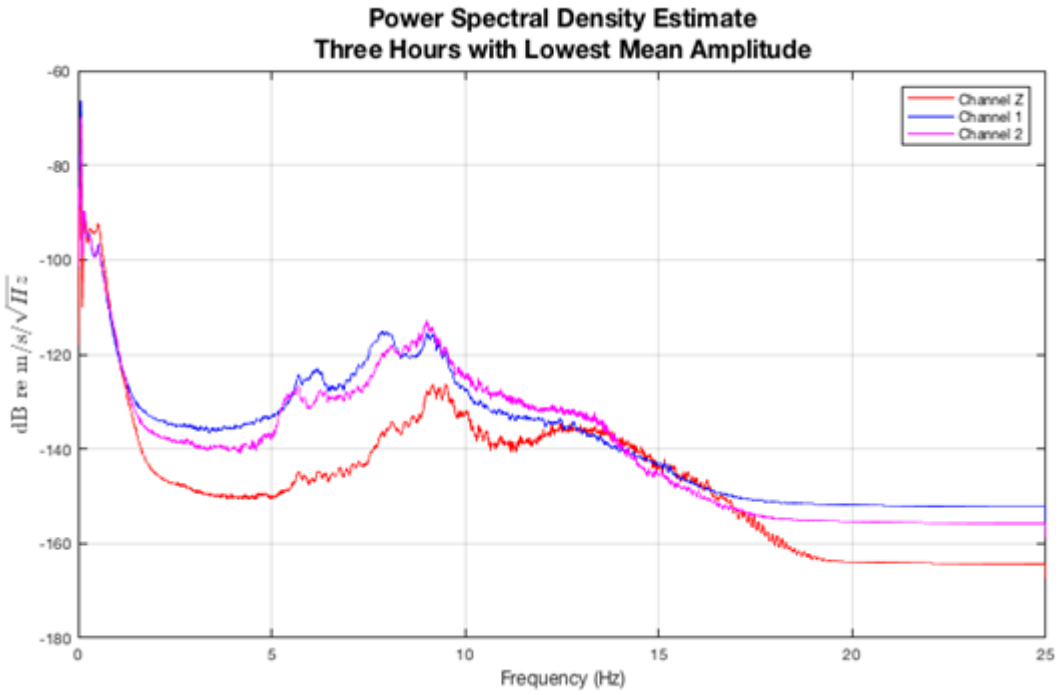

Figure 46. 7D J65A, PSD of Quiescent Period (Three Hours with Lowest Mean Amplitude), February 15, 2012.

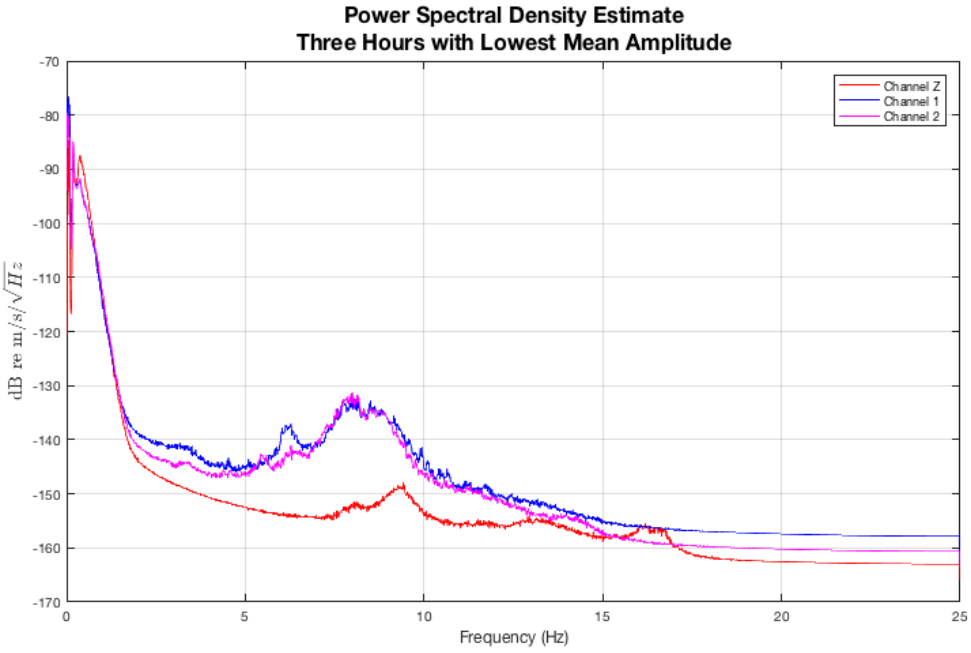

Figure 47. 7D J65A, PSD of Quiescent Period (Three Hours with Lowest Mean Amplitude), March 1, 2012.

Figure 48 is from 7D J73A, March 1, 2012, and shows an increase in decibels after 10 Hz. Even though a low-pass taper is applied at 10 Hz, 7D J73A's decibel levels continue to increase after this taper is applied. Decibel levels for channel Z peak after the taper from as low as -160 dB to as high as -130 dB. This pattern of decibel level increase after the taper is present in nearly every sample.

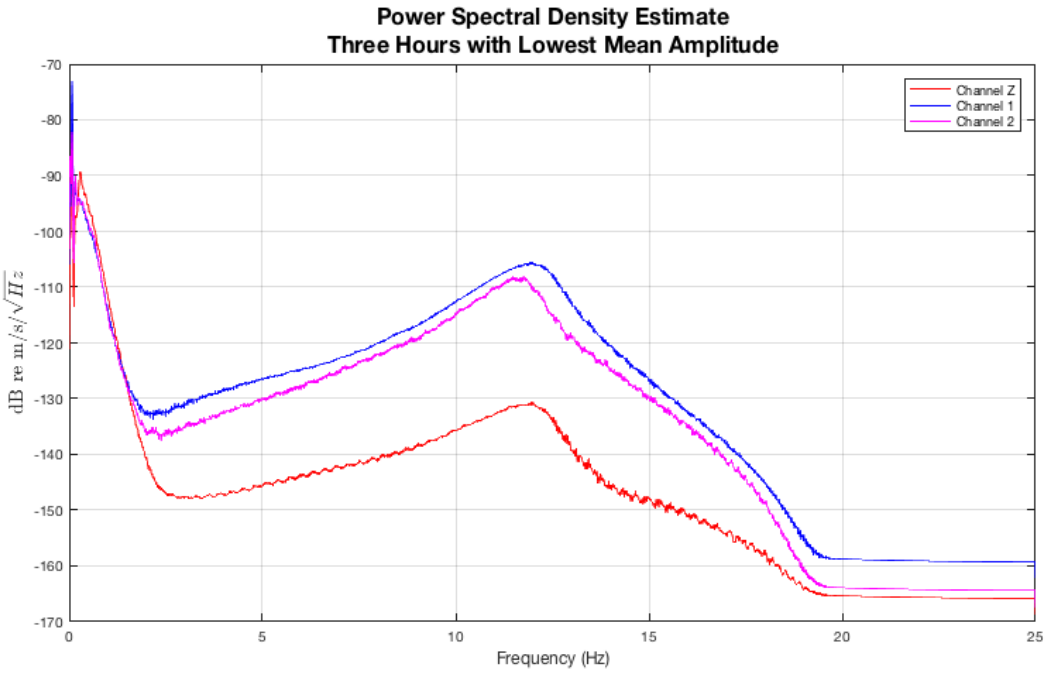

Figure 48. 7D J73A, PSD of Quiescent Period (Three Hours with Lowest Mean Amplitude), March 1, 2012.

From 0 to 2 Hz, 7D J65A and 7D J73A are similar, with both OBSs peaking at around 0.2 Hz and then displaying a steady, almost linear, decline after the peak. Figures 49 and 50 depict 0 to 2 Hz from both OBSs on the same day, March 1, 2012.

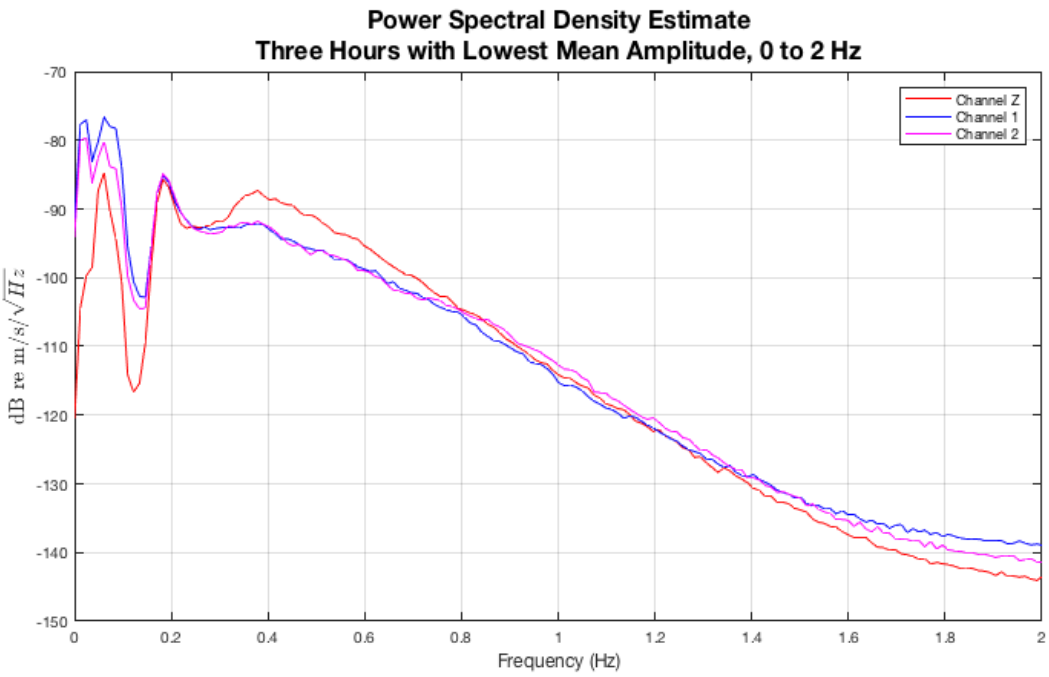

Figure 49. 7D J65A, PSD of Quiescent Period (Three Hours with Lowest Mean Amplitude), March 1, 2012, 0 to 2 Hz.

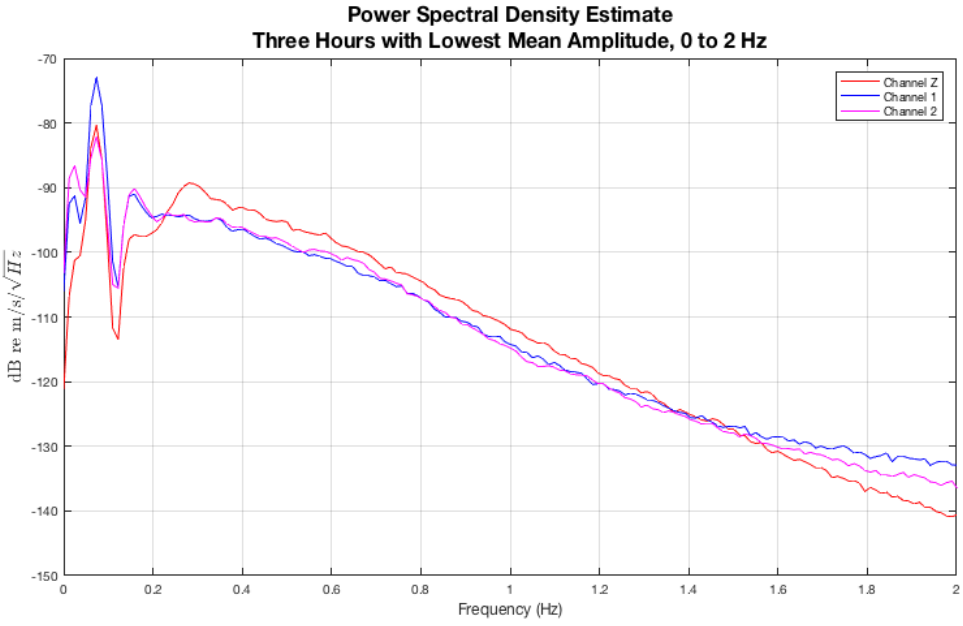

Figure 50. 7D J73A, PSD of Quiescent Period (Three Hours with Lowest Mean Amplitude), March 1, 2012, 0 to 2 Hz.

3. PSD Conclusion

Figures 51 and 52 summarize the OBS PSD variability, focusing in on 1 Hz and 5 Hz. The decibel levels for both 1 Hz and 5 Hz are graphed per sample for all samples taken. The results show fairly steady decibel levels for all OBSs at the frequencies except YM 39, which is the least consistent and noisiest of all the OBSs sampled. The decibel levels at 5 Hz are similar for YM 38 and the two OBSs located west of the Strait of Juan de Fuca. At 1 Hz, though, 7D J65A and 7D J73A are consistently stronger. Tables listing all the values in Figures 51 and 52 are located in Annex B.

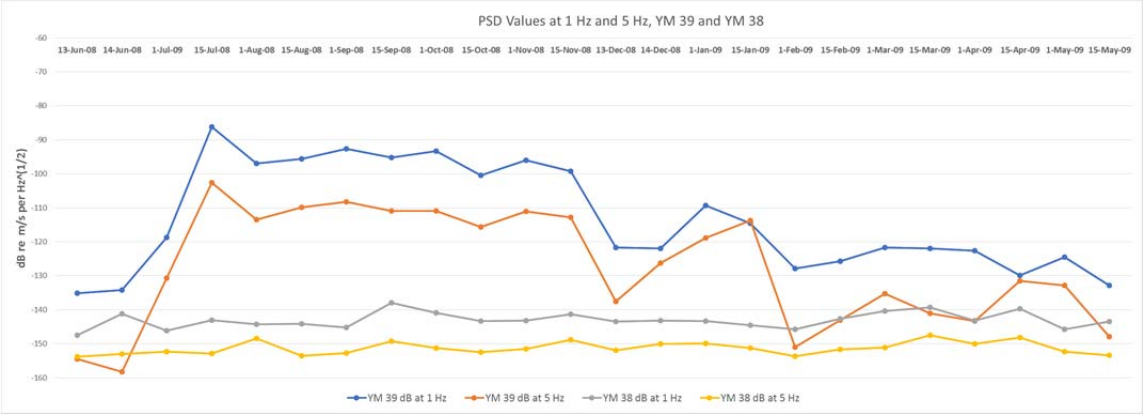

Figure 51. Quiescent PSD Values at 1 Hz and 5 Hz for YM 39 and YM 38.

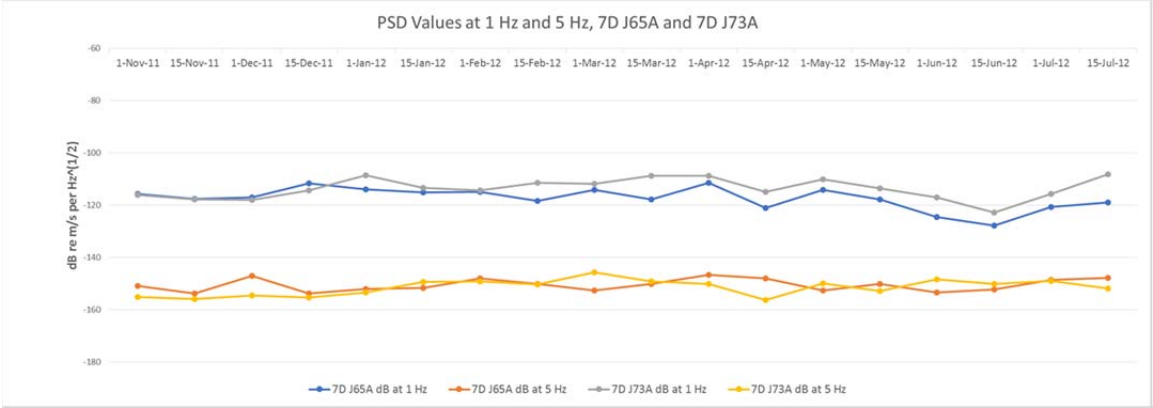

Figure 52. Quiescent PSD Values at 1 Hz and 5 Hz for 7D J65A and J73A.

Although acceleration is not discussed in Results, acceleration can be obtained from the velocity data used in all of the figures by using Equation 21, where a is acceleration, ω is angular frequency, and v is velocity. Appendix B contains rms acceleration for all vertical channels.

$$a = i\omega v \tag{21}$$

B. AMPLITUDE HISTOGRAMS

1. 7D J65A and 7D J73A

Amplitude histograms were generally viewed with a logarithmic y-axis so that more details were available. However, any velocity time series plot that was consistent and without multiple large amplitude spikes appeared Gaussian if viewed without a logarithmic axis. Most of the 7D J65A and 7D J73A amplitude histograms were Gaussian in appearance. Every amplitude histogram from these two OBSs viewed on a logarithmic scale looked similar to either Figure 53 or Figure 56. Figure 53 is from OBS 7D J73A, November 1, 2011. Figure 54 displays the same histogram, but with a non-logarithmic y-axis. The channel Z time series plot represented by these histograms is shown in Figure 55.

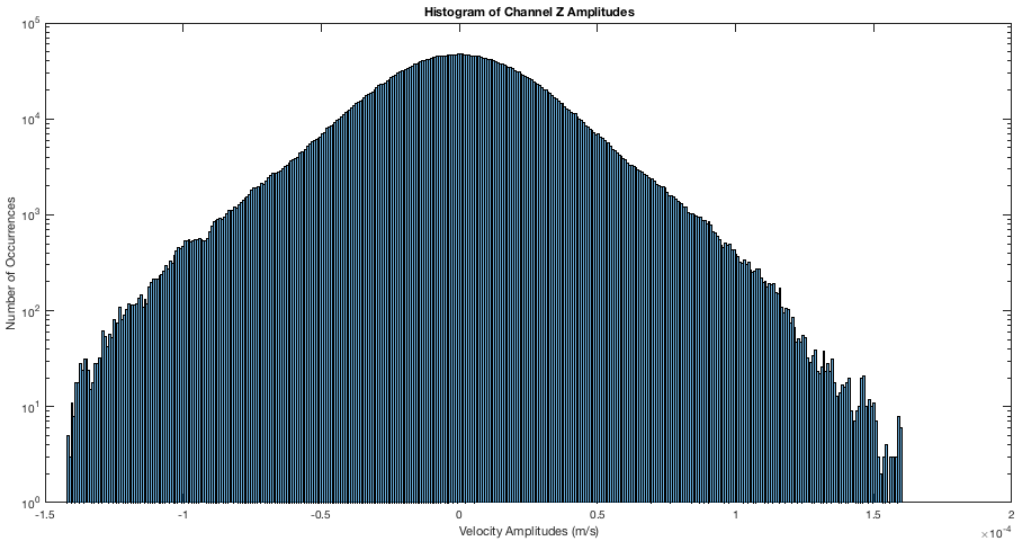

Figure 53. 7D J73A, Amplitude Histogram, November 1, 2011.

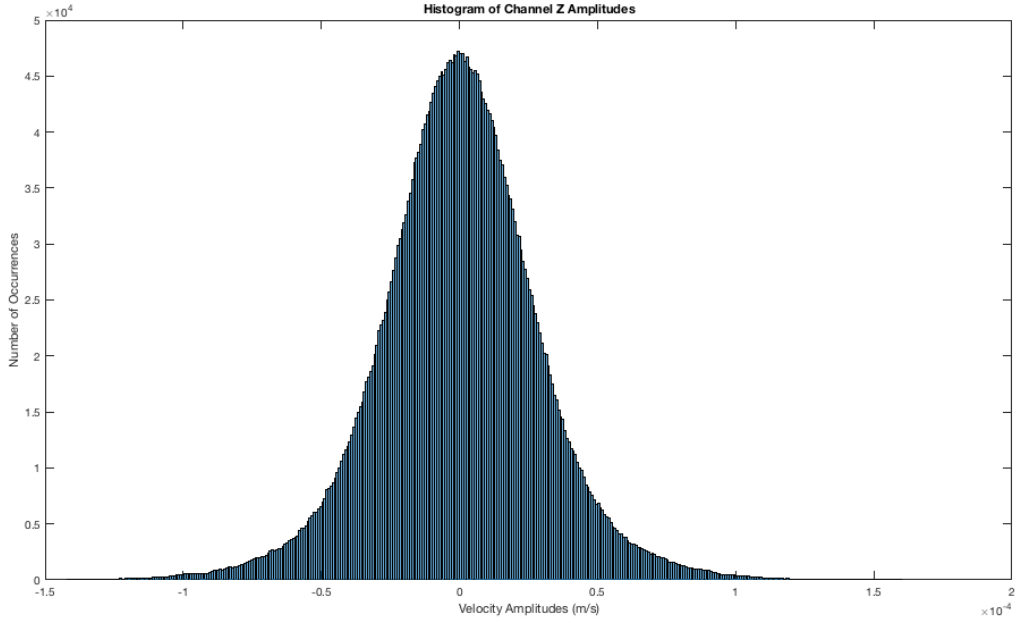

Figure 54. 7D J73A, Amplitude Histogram, November 1, 2011, Non-Logarithmic.

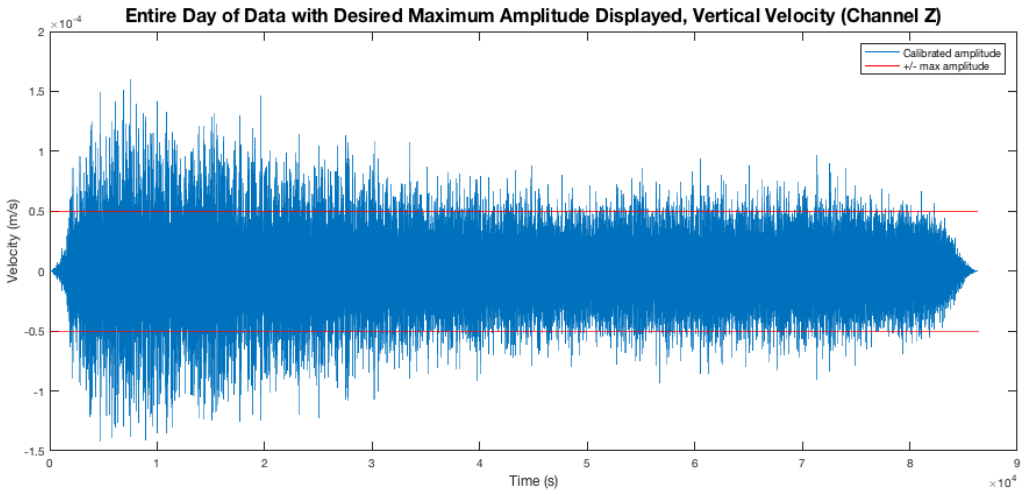

Figure 55. 7D J73A, Velocity Time Series, November 1, 2011.

Figure 56 displays a narrower histogram in a logarithmic plot. Such narrow histograms were also common in many of the days from 7D J65A and 7D J73A. The histogram in Figure 56 naturally has a smaller number of amplitude events that surpass the amplitude threshold. Figures 57 and 58 display the same information in non-logarithmic plots, but Figure 58 is a close-up displaying the single, larger amplitude events that occurred throughout this sample day. Figure 59 is the velocity time series plot of channel Z for July 1, 2012, represented by the histograms in Figures 56 through 58. Both OBSs are consistent enough that the wider and narrow histograms in Figure 53 and Figure 56 are representative of the range of standard deviation and shapes of all the data investigated.

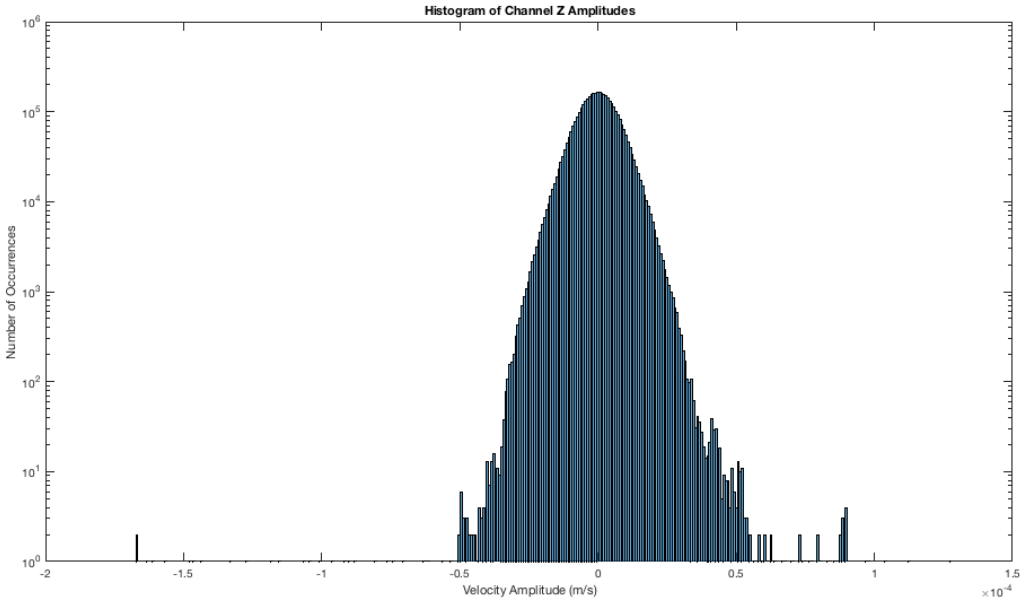

Figure 56. 7D J73A, Amplitude Histogram, July 1, 2012.

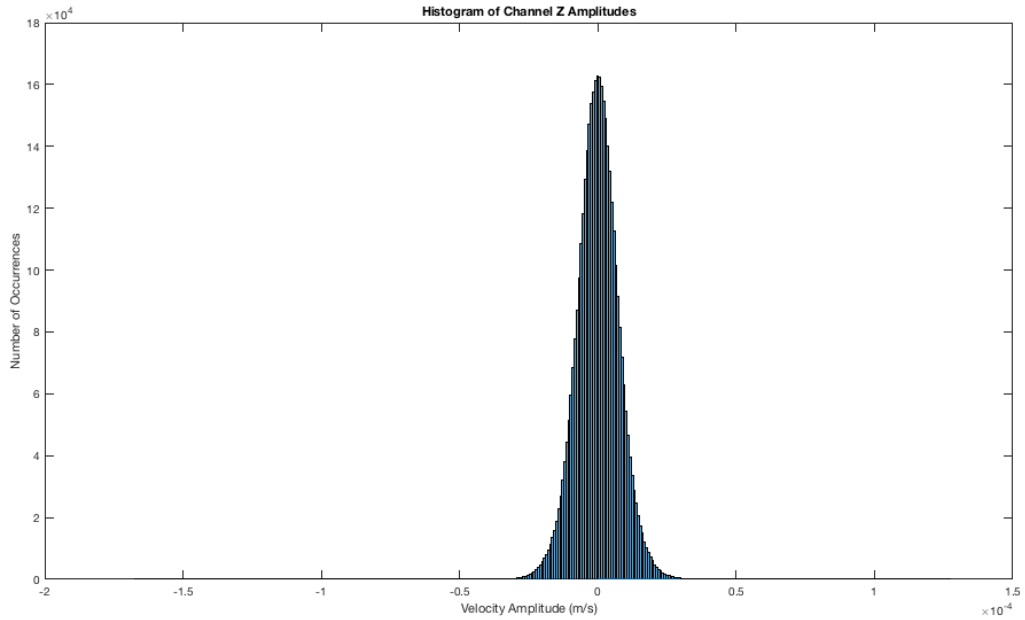

Figure 57. 7D J73A, Amplitude Histogram, July 1, 2012, Non-Logarithmic.

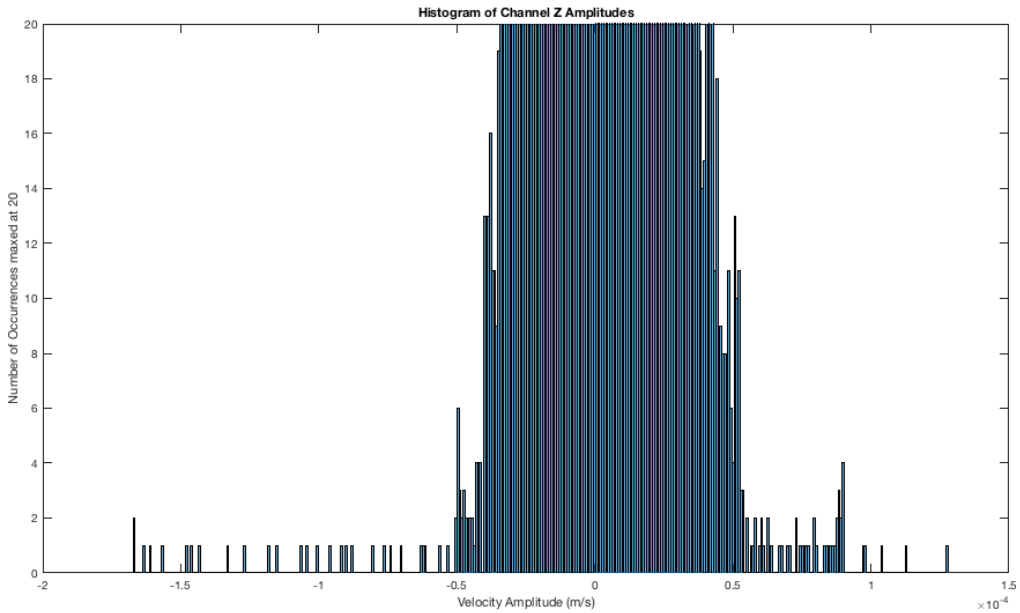

Figure 58. 7D J73A, Amplitude Histogram, July 1, 2012, Close-Up Non-Logarithmic.

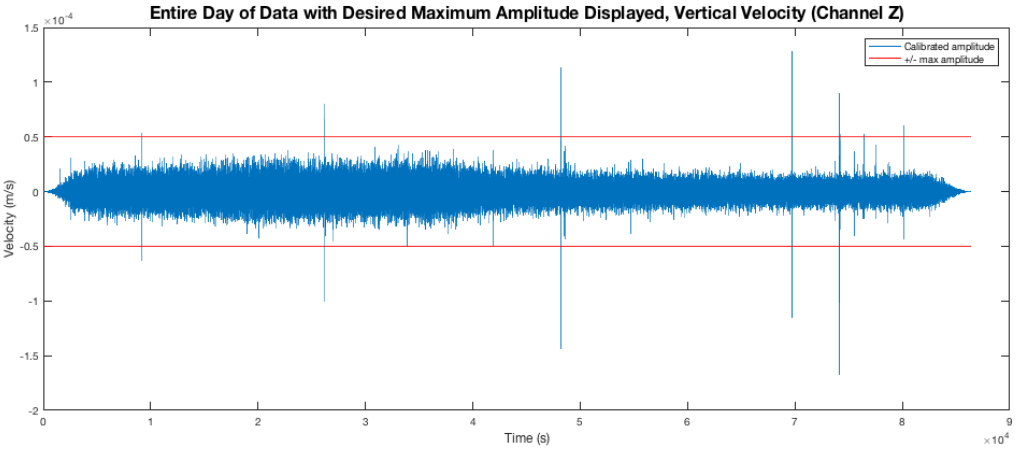

Figure 59. 7D J73A, Velocity Time Series, July 1, 2012, Channel Z.

2. YM 39 and YM 38

For the YM 39 and YM 38 OBSs, the non-logarithmic amplitude histograms miss many details otherwise available with a logarithmic plot. Many

time series plots for both YM 38 and YM 39 involve long, relatively quiet time periods followed by shorter periods of higher amplitude vibrations. Figure 60 from June 13, 2008, displays this type of time series plot. The amplitude histogram in Figure 61 is logarithmic, and the amplitude histogram in Figure 62 is not and misses useful specifics provided in Figure 61. Many of the histograms for YM 38 and YM 39 have similar appearances, although the samples from YM 38 were up to two orders of magnitude smaller in standard deviation.

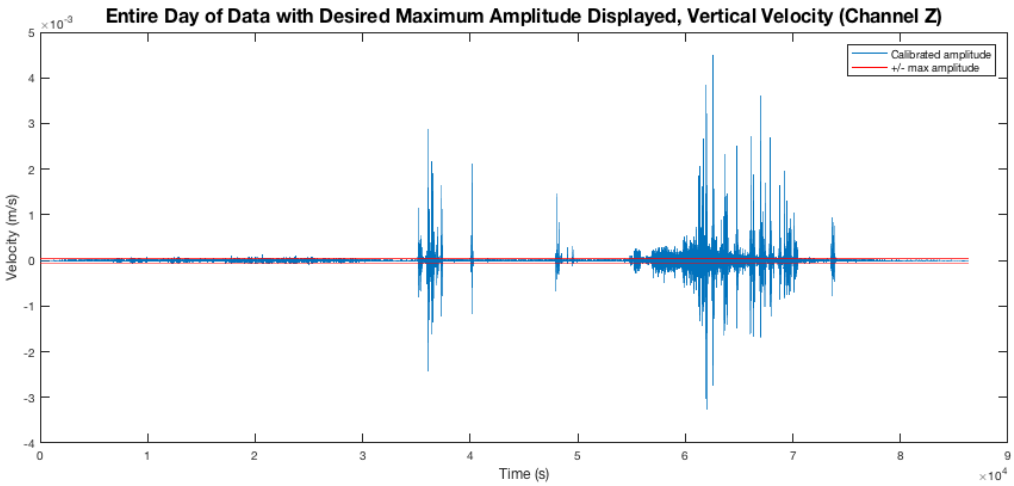

Figure 60. YM39, Velocity Time Series, June 13, 2008, Channel Z.

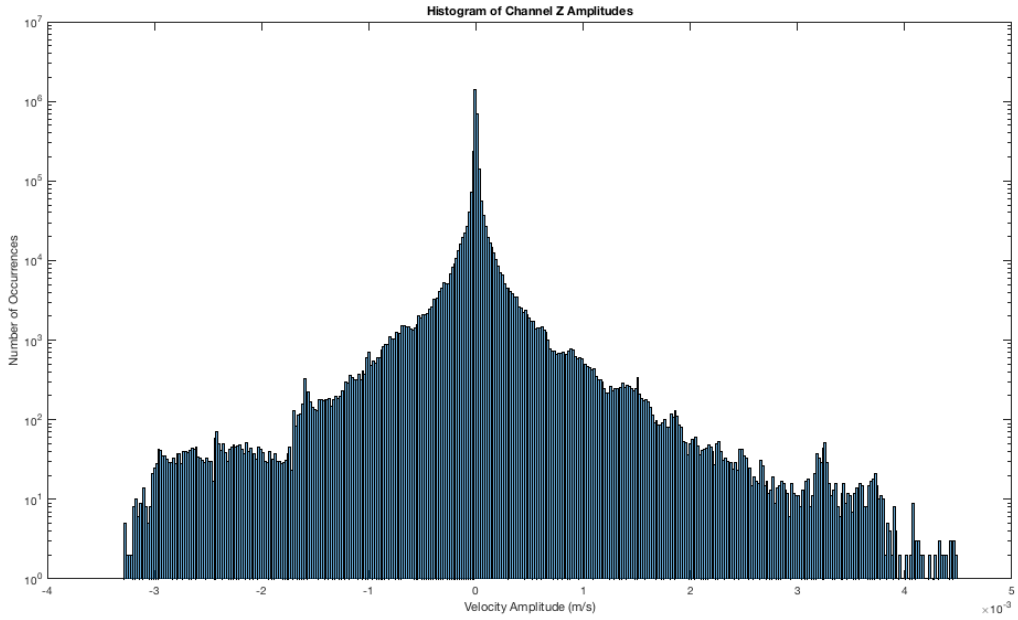

Figure 61. YM 39, Amplitude Histogram, June 13, 2008.

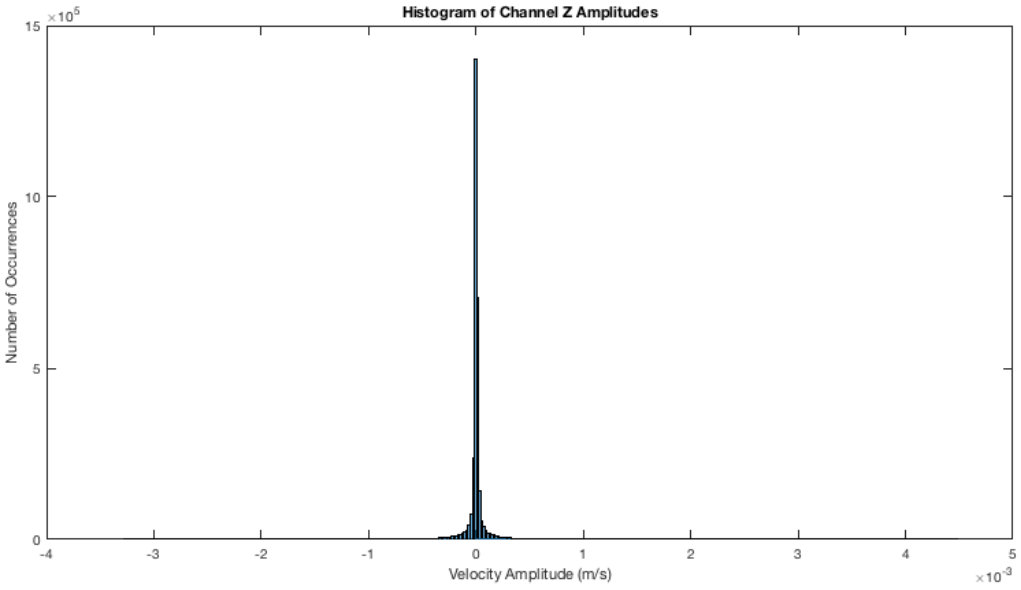

Figure 62. YM 39 Amplitude Histogram, Non-Logarithmic, June 13, 2008.

Multiple amplitude histograms from both YM 38 and YM 39 appear in a crown-type shape shown in Figure 63. Figure 64 is the time series plot for the same day, February 1, 2009. This histogram illustrates the common shape for the plots when there were calm periods interrupted by multiple, almost impulsive, amplitude spikes. Figures 65 and 66, from August 1, 2008, display the same behavior with YM 38 but at a much smaller amplitude. Initially this behavior was thought to be electronic clipping, but there are histogram examples with the same appearance but increased amplitude. The vibrations arrive and are symmetric with an equal positive and negative amplitude response.

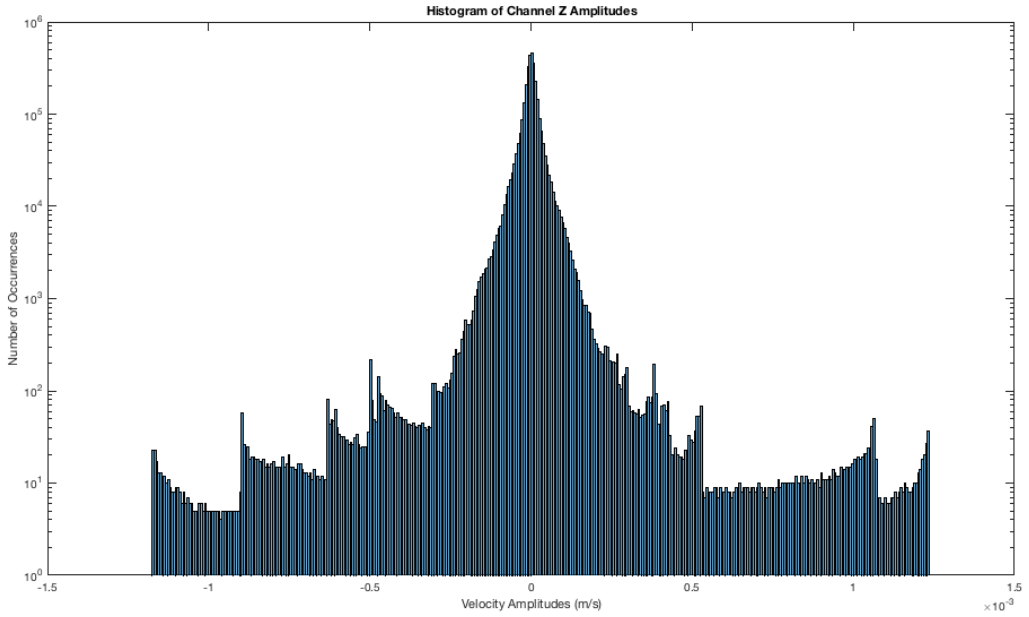

Figure 63. YM 39, Amplitude Histogram, February 1, 2009.

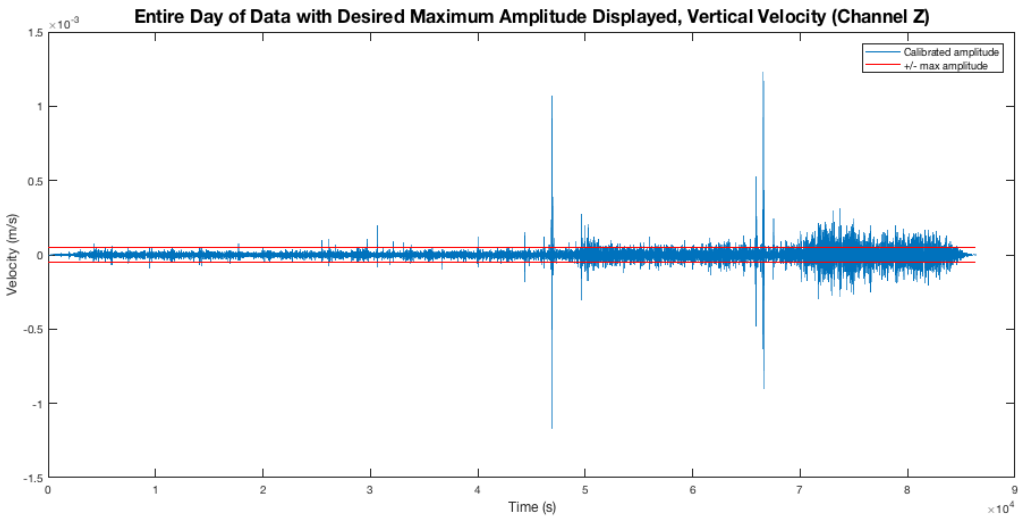

Figure 64. YM 39, Velocity Time Series, February 1, 2009.

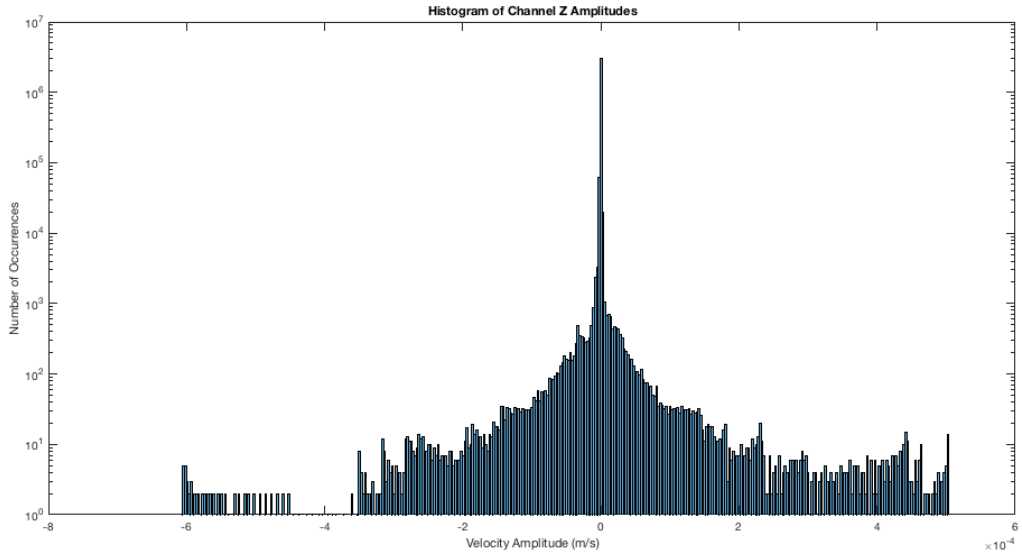

Figure 65. YM 38, Amplitude Histogram, August 1, 2008.

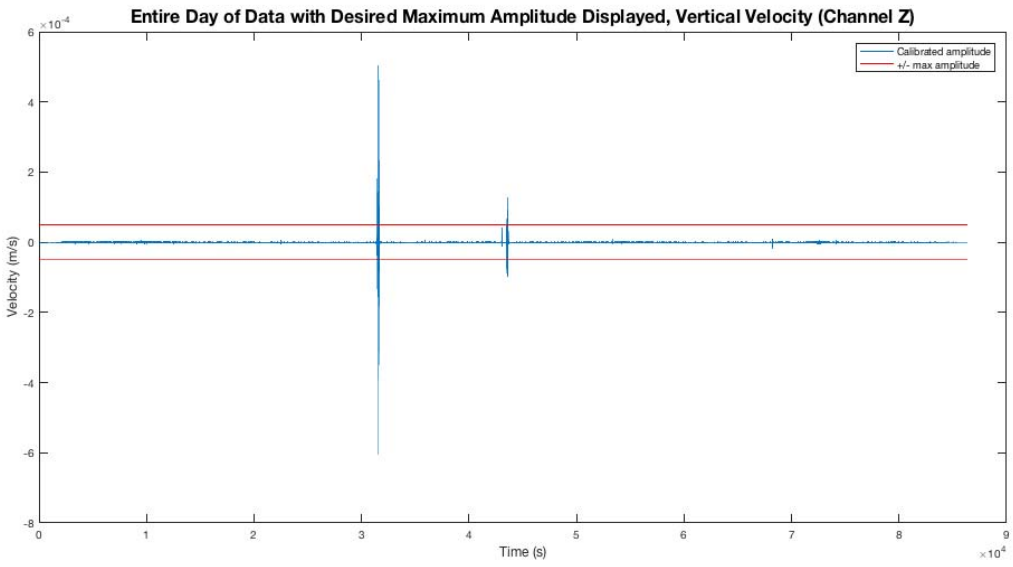

Figure 66. YM 38, Velocity Time Series, August 1, 2008, Channel Z.

3. Amplitude Histogram Conclusion

The histograms for both the OBSs located west of the Strait of Juan de Fuca proved that the data these two OBSs collected was consistent with few outliers. This led to amplitude histograms with the appearance of a normal distribution. Many samples taken from the OBSs in the Luzon Strait displayed long, relatively quiet periods, which were abruptly interrupted by higher amplitude seismic readings. These particular events were responsible for the crown-type shapes in Figures 63 and 65.

C. HISTOGRAMS OF HIGH AMPLITUDE PULSE WIDTHS AND HISTOGRAMS OF TIME BETWEEN HIGH AMPLITUDE PULSES

Two types of histograms were based on a maximum entered amplitude threshold: a histogram of the width of pulses that exceeded the maximum amplitude and a histogram of times between these pulses. As mentioned in Chapter IV, the maximum amplitude threshold chosen for this thesis was $5x10^{-5}$ m/s. Although this threshold was higher than the standard deviation of any OBS except for YM 39, all of the OBSs have occurrences where the amplitude

surpasses this line. This threshold proved to be a good indicator of high amplitude, non-quiescent activity.

1. 7D J65A and 7D J73A

Both OBSs west of the Strait of Juan de Fuca spent around 6% of the sampled time above the maximum amplitude threshold. For these OBSs, the maximum signal length above the maximum amplitude threshold was around 6 seconds, but the majority of these high amplitude signals were 1 second or less in length. Figure 67 is a representative histogram of signals that exceeded the maximum amplitude threshold for both 7D J65A and 7D J73A. Figure 68 is the time series associated with this histogram.

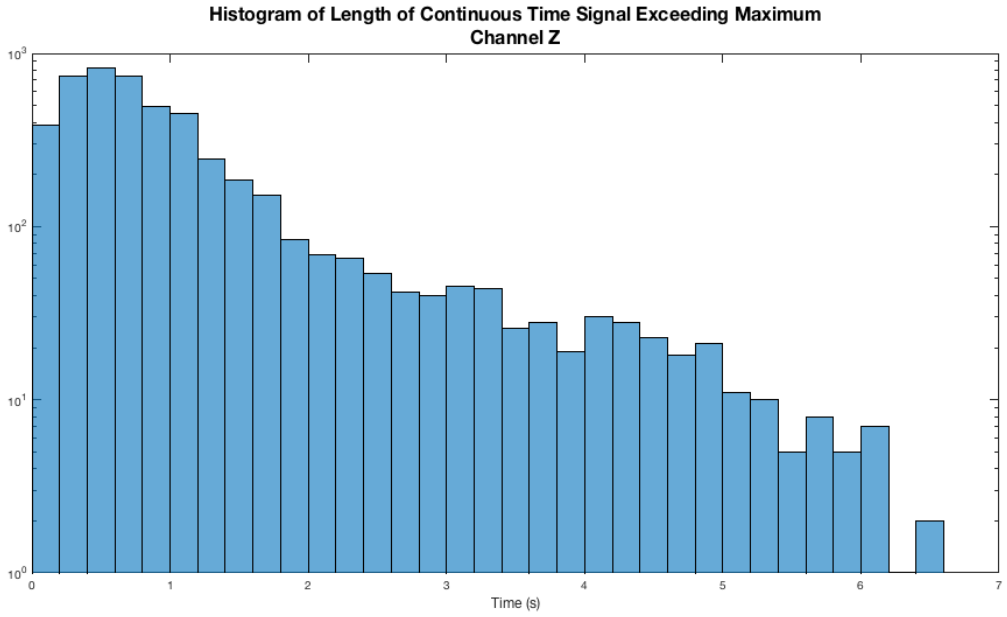

Figure 67. 7D J65A, November 15, 2011, Width of Signals Exceeding Maximum Amplitude Threshold

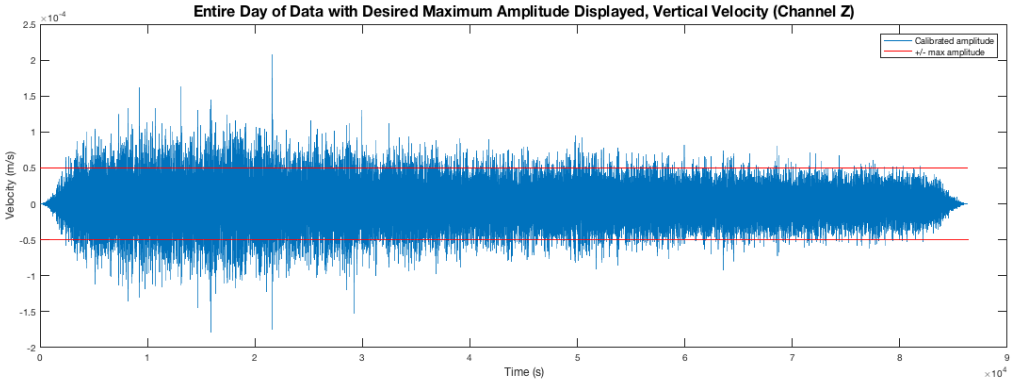

Figure 68. 7D J65A, November 15, 2011, Velocity Time Series

The vast majority of times between signals that exceeded the maximum amplitude was 1 second or less. Figures 69 and 70 display time between events, and Figure 71 is a close up with a bin width of 1 second. The higher amplitude signals occur in groups, which explains the large number of occurrences of the 1 second or less bin.

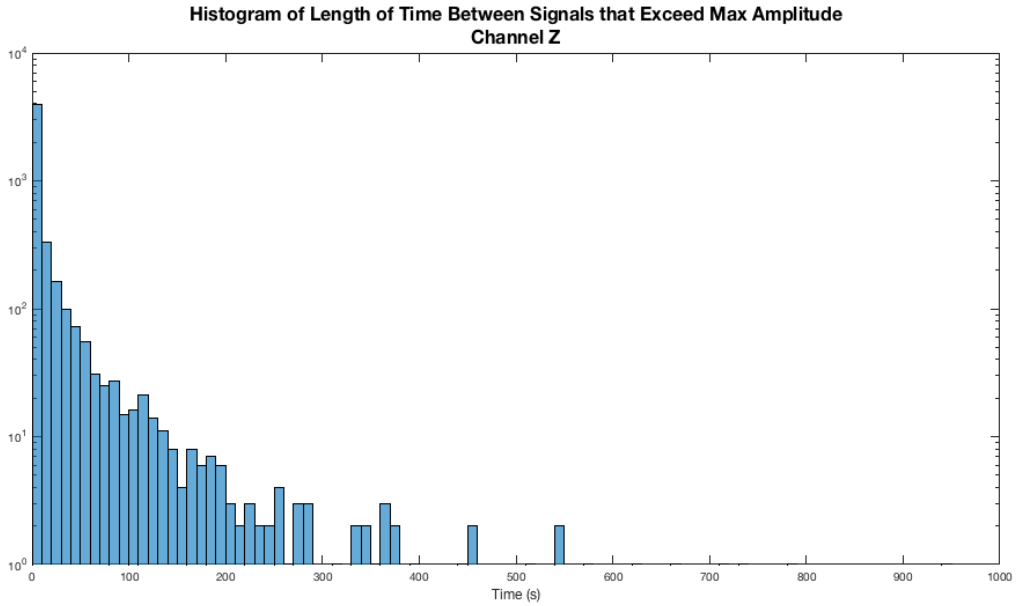

Figure 69. 7D J65A, November 15, 2011, Time Between Signals That Exceed Maximum Amplitude

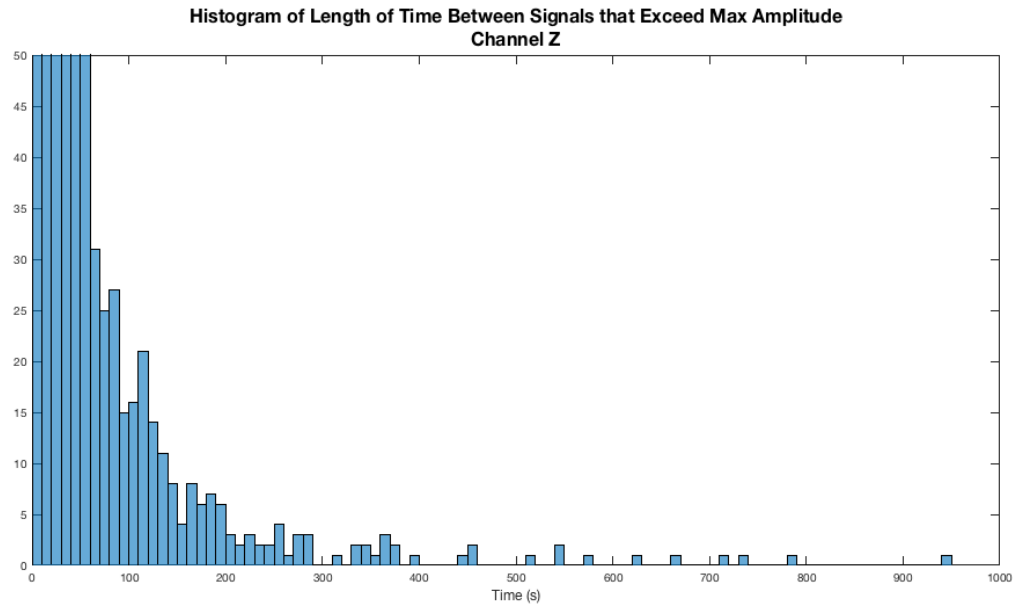

Figure 70. 7D J65A, November 15, 2011, Time Between Signals That Exceed Maximum Amplitude, Non-Logarithmic

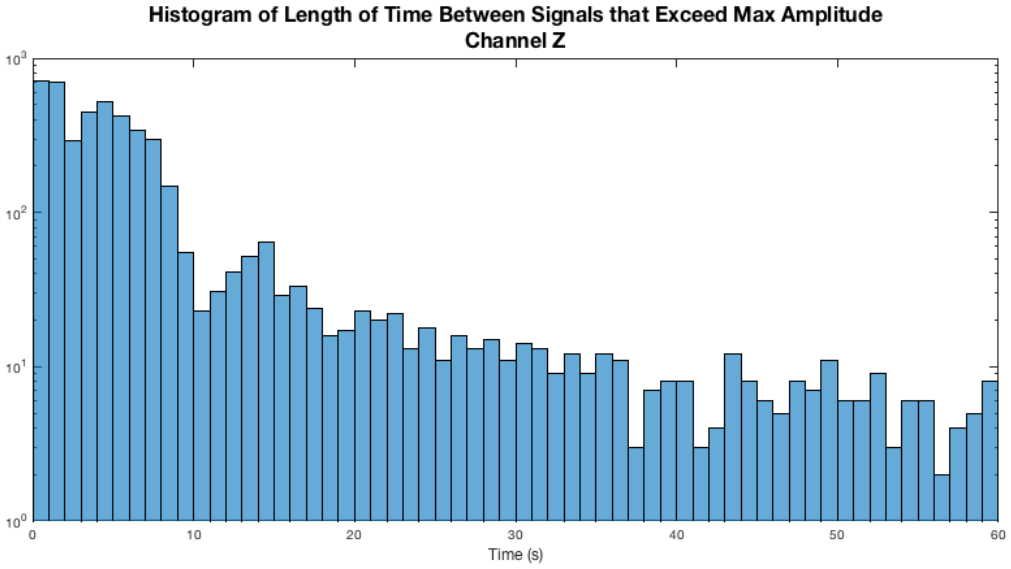

Figure 71. 7D J65A, November 15, 2011, Time Between Signals That Exceed Maximum Amplitude

2. YM 39 AND YM 38

OBS YM 39 spent an average of 52% of time above the maximum amplitude threshold over all the days sampled, although the percentage of time spent above the threshold varied significantly from 1% to 91% per day sampled. The sample from March 15, 2009, spent 54% of the time above the threshold, which is close to the overall YM 39 average of 52%. Figure 72 depicts the time series of channel Z from March 15, 2009. Figure 73 is the histogram of signal widths above the maximum amplitude threshold, and Figure 74 displays the times between these signals. Figure 75 is non-logarithmic, and displays the single occurrences where the largest time period between signals is almost five minutes.

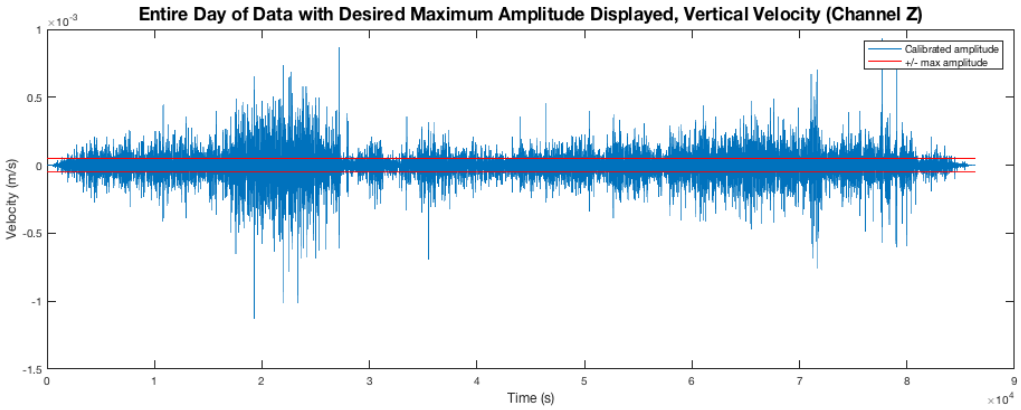

Figure 72. YM 39, March 15, 2009, Velocity Time Series

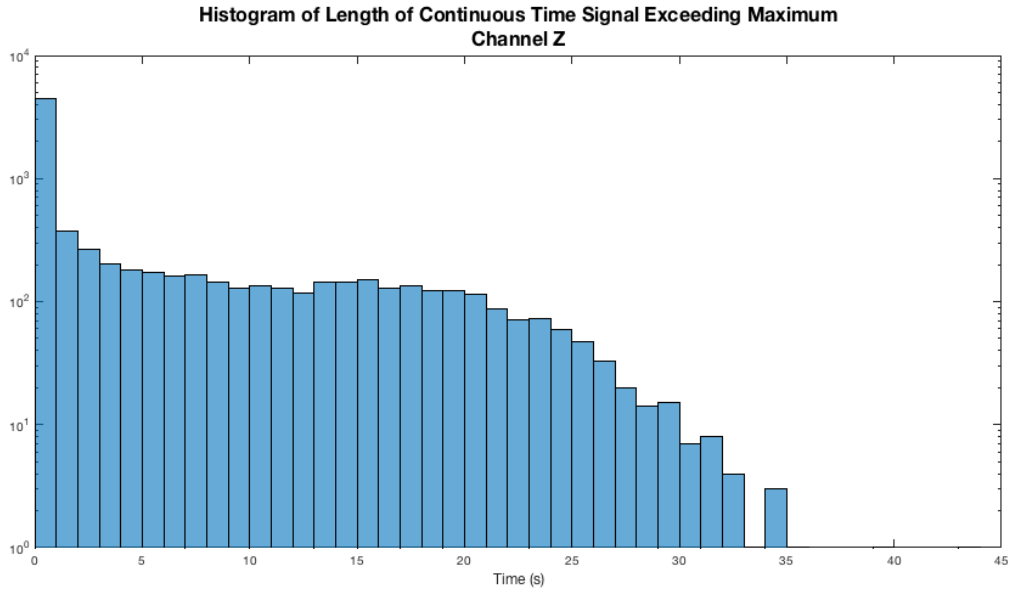

Figure 73. YM 39, March 15, 2009, Width of Signals Exceeding Maximum Amplitude Threshold

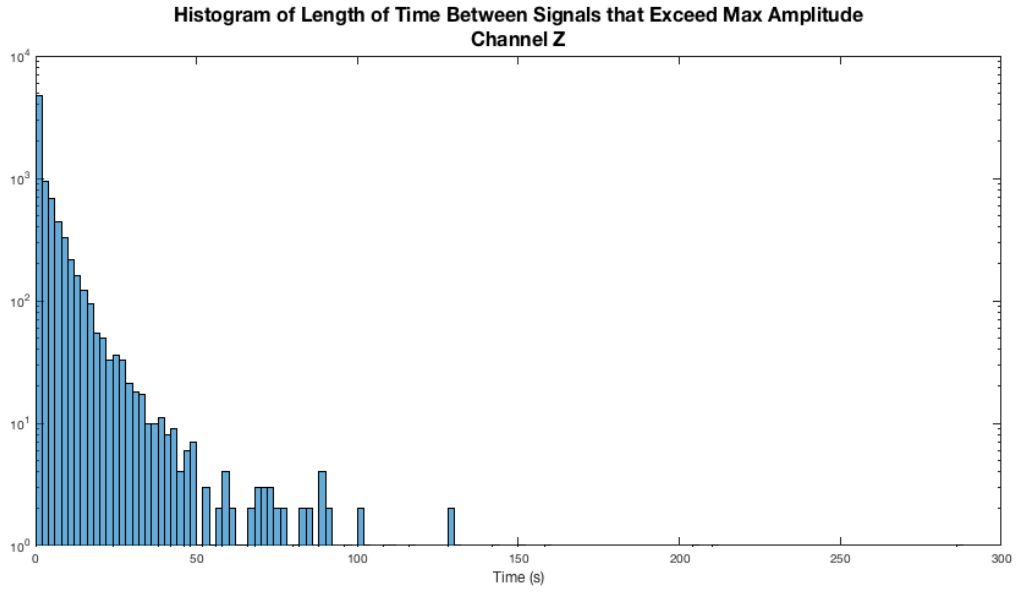

Figure 74. YM 39, March 15, 2009, Time Between Signals That Exceed Maximum Amplitude Threshold

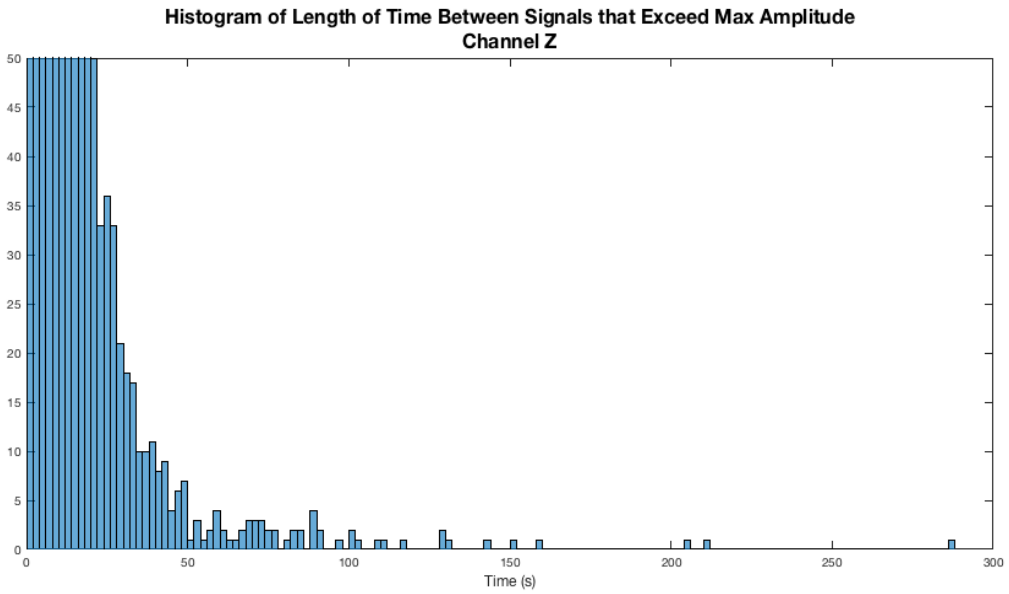

Figure 75. YM 39, March 15, 2009, Time Between Signals That Exceed Maximum Amplitude Threshold

3. Conclusion

It was anticipated that the length of time between high amplitude signals would be short for the days with a high percentage of time spent above the maximum amplitude threshold. What was unexpected, however, was the fact that the majority of times between high amplitude signals were 1 second or less for an OBS that spent only 7% of its time above the maximum amplitude (Figure 68). This confirms that the high amplitude signals tend to occur in groups. The maximum time spent between signals on this same day was 16 minutes, but this only occurred once in a 24 hour sample. Table 2 summarizes the extremes of the OBSs.

Table 2. Maximum and Minimum Standard Deviations and Times Spent Above the Maximum Amplitude for All OBSs

OBS	Max standard deviation observed (μm/s)	Min standard deviation observed (μm/s)	Max % of time spent above max amplitude	Min % of time spent above max amplitude
YM 39	662	16.1	91	1
YM 38	7.3	0.23	0.16	0
7D J65A	117	7.2	24	0
7D J73A	39.9	7.6	21	0

VI. CONCLUSIONS AND RECOMMENDATIONS

A. METHODOLOGY

The global view on the IRIS website proved useful in the selection of OBSs that were co-located in significant geographic chokepoints. IRIS also made it convenient to select the OBS directly, view the detailed information, and request the data directly from the OBS information webpage. The publicly available seismic processing software on the IRIS website was essential in obtaining calibrated data from the raw data. Manual calibration was attempted, but the IRIS software, which was designed by the seismology community, was quite capable once familiarity with the software was established. There were multiple paths to calibrated data, especially using the SAC transfer function, but the novice user will need to ensure that the SAC transfer output is in the units that he/she is expecting. A Mac computer, or a Unix-based operating system, is required to operate the IRIS software. The MATLAB rsac.m function was a convenient method to convert SAC data to a MATLAB format.

B. RESULTS

Out of the four OBSs, three proved consistent from month to month in their individual discrete frequencies and decibel levels, but there were no common discrete frequencies between OBSs that were located in the same geographic area. YM 39 in the Luzon Strait was erratic with large differences in decibel levels from sample to sample. The amplitude histograms for 7D J65A and 7D J73A displayed what appeared to be normal distributions, with the exception of a couple of outliers with some seismic activity noted. YM 39 and YM 38 displayed oddly shaped amplitude histograms that were the result of long quiescent periods interrupted by large, impulsive seismic activity. The histograms based on the maximum amplitude threshold showed that the higher amplitude vibrations occurred in groups, with the vast majority of counts occurring with a second or less between events. Even the histograms from samples where the

percentage of time spent above the maximum amplitude threshold was low showed results where the vast majority of time between signals was one second or less.

The extreme differences between YM 38 and YM 39 lead to questions about environmental effects on YM 39 that are not affecting YM 38. Even though YM 38 exhibited some high-amplitude activity on occasion, it was far more quiet and consistent than YM 39. There was not much in the way of commonality between these two OBSs despite their close proximity in the same geographic area.

7D J65A and 7D J73A had close values in decibel levels, standard deviation, and percentage of time spent above the maximum amplitude threshold in almost every sample taken on the same day, with the exception of a couple of outliers higher amplitude seismic events. It would appear that west of the Strait of Juan de Fuca is a fairly homogeneous location with regard to environmental factors on the ocean floor.

C. RECOMMENDATIONS FOR FUTURE RESEARCH

1. Transfer Functions to Reduce Long Period Noise

Pressure from infragravity waves on the surface of the ocean can penetrate to the ocean floor causing deformation of the ocean floor [5]. According to [5], these pressure variations are the source of long period seismic noise, from around 30 seconds to 100 or more seconds (1 to 3.3 mHz). These pressure variations are also picked up by the DPG. Therefore, a transfer function can be developed that can get rid of the seismic noise caused by the surface waves. This could also possibly be used to take noise out of any future bottom mounted sensor.

2. Environmental Effects in the Luzon Strait

The extreme differences between the two OBSs in the Luzon Strait present questions about environmental effects on YM 39 that are not affecting

YM 38. The Luzon Strait is known for its large internal wave activity, and investigating a correlation between this activity with OBS results would be an interesting study. A detailed study of currents and tides in the local region combined with OBS results could also prove useful.

3. Correlation of Data with Other OBS in Luzon Strait, Possible Mechanical Failure of YM 39

Other OBSs in the neighborhood of YM 38 and YM 39 could be inspected to correlate the results obtained in this thesis. IRIS data problem reports were searched, but no OBSs in the YM network were listed. Currently, then, there are no indications of a mechanical failure of YM 39, but additional data could be explored to both confirm the results and rule out any mechanical failure of YM 39.

4. Electronic Noise Floor of OBSs

The electronic noise floors of the OBSs were not found during the research for this thesis, and it is possible that the amplitude histograms with a Gaussian appearance were the result of OBS electronic noise. Thus, the OBSs could be limited by the electronic noise floor during quiescent periods. No instrument noise models were found that provide the rough order of magnitude of the electronic noise floor, and any future study should explore these questions further. In particular, it would be valuable to have confidence in the ability of OBS sensors to accurately measure ocean accelerations down to 10^{-6} m/s^2 without running into the electronic noise floor.

5. OBS Requests

The OBSIP website [4] contains information for researchers to request OBSIP instrument usage, and the OBSIP allows their OBS equipment to be available to other government research or educational institutions [4]. Therefore, LLNL or NPS could request usage of OBSs in other areas of interest.

THIS PAGE INTENTIONALLY LEFT BLANK

APPENDIX A. MATLAB CODE

A. VIBRATION ANALYSIS CODE

```
function vibration_analysis(rsac_channel_Z,max_amp,Fs,rsac_channel_1,rsac_channel_2)
%  OBS, ocean bottom seismometer, maximum amplitude, BHZ, sampling frequency
%
%  Purpose:  Takes three calibrated channels of OBS data, OBS sampling
%  frequency, and maximum desired amplitude, and finds the maximum
%  quiescent period (at least 1 hour in length where the amplitude
%  does not exceed maximum amplitude).  Function outputs an amplitude (m/s)
%  vs time plot (for all three channels), the mean and standard deviation
%  of entire sample amplitude, power spectral densities of longest
%  quiescent period, a percentage of time spent above maximum desired
%  amplitude, a histogram of amplitudes, a histogram of lengths of signals
%  greater than max desired amplitude, and a histogram of time periods
%  between signals that exceed maximum amplitude.
%
%  Output Variables:
%     std_z = standard deviation of channel z amplitude
%     percentage_time_above_max_amp = percentage of time where amplitude
%     is greater than max amplitude
%
%  Input Variables:
%     rsac_channel_Z = vertical .sac file after it has been read through
%     rsac.m
%     max_amp = desired maximum amplitude (m/s)
%     Fs = sampling frequency of OBS (Hz)
%     rsac_channel_1 = channel 1 .sac file after it has been read through
%     rsac.m
%     rsac_channel_2 = channel 2 .sac file after it has been read through
%     rsac.m
%
%  Local Variables:
%     cal_data = calibrated vertical channel amplitude (m/s)
%     time = time (seconds)
%     PKS = value of peaks greater than max amplitudel (m/s)
%     LOCS = vector of location of PKS (integer location)
%     loop_index = binary file (index) for location of PKS
%     loop_index_logical = logical version of loop_index
%     cal_data1 = same as cal_data, but modified to zero-out peak
%           locations (m/s)
%     PKS2 = value of peaks in second peaks-finding function (m/s)
%     LOCS2 = vector of location of PKS2
%     loop_index_logical2=logical version of modified loop_index
%     cal_data2 = same as cal_data1, but modified to zero-out additional
%           peaks (m/s)
%     cal_data3 = same as cal_data2, but modified to contain longest
%           quiescent occurrence only (m/s)
%     largest_quiescent_index = index locating the largest quiescent
%           period
%     channel1_cal_data = calibrated amplitude of channel 1 (m/s)
```

```
%       channel2_cal_data = calibrated amplitude of channel 2 (m/s)
%       time_quiescent = time location of longest quiescent period (s)
%       N = FFT length
%       overlap = pwelch overlap value
%       Pxx = channel Z distribution of power per unit of freq, but in this
%             application units of [m/s/sqrt(Hz)]
%       F, F1, F2 = Frequency (Hz)
%       Pxx1 = channel 1 distribution of power per unit of freq, but in this
%             application units of [m/s/sqrt(Hz)]
%       Pxx2 = channel 2 distribution of power per unit of freq, but in this
%             application units of [m/s/sqrt(Hz)]
%       index = index locating where cal_data is greater than the maximum
%             amplitude
%       above_max_amp_time = time where cal_data is greater than maximum
%             amplitude (s)
%       outlier = logical index location where Z-amplitude is greater than
%             maximum amplitude
%       cal_data_update = same as cal_data, but only contains amplitudes
%             greater than maximum amplitude.  (m/s)
%       W = vector with lengths of signals that exceed max amplitude
%       S = vector that contains different lengths of time between signals
%             that exceed max amplitude
%
%       Functions Called:  None.
%
%       Filename: vibration_analysis.m
%       Written by: Jeremy R. Hankins

cal_data=rsac_channel_Z(:,2);
time=rsac_channel_Z(:,1);
cal_data_qplot=cal_data;
rsac1_qplot=rsac_channel_1(:,2);
rsac2_qplot=rsac_channel_2(:,2);
% plot amplitude (m/s) vs. time (s) for all channels

figure
plot(time,cal_data)
hold on
plot([time(1) time(length(time))],[max_amp max_amp],'r-')
hold on
plot([time(1) time(length(time))],[-max_amp -max_amp],'r-')
ylabel('Velocity (m/s)','Fontsize',12)
xlabel('Time (s)','Fontsize',12)
title('Entire Day of Data with Desired Maximum Amplitude Displayed, Vertical Velocity (Channel
Z)','Fontsize',16)
legend('Calibrated amplitude','+/- max amplitude')

figure
plot(time,rsac_channel_1(:,2))
hold on
plot([time(1) time(length(time))],[max_amp max_amp],'r-')
hold on
plot([time(1) time(length(time))],[-max_amp -max_amp],'r-')
ylabel('Velocity (m/s)','Fontsize',12)
xlabel('Time (s)','Fontsize',12)
```

```
title('Entire Day of Data with Desired Maximum Amplitude Displayed, Horizontal Velocity
(Channel 1)','Fontsize',16)
legend('Calibrated amplitude','+/- max amplitude')

figure
plot(time,rsac_channel_2(:,2))
hold on
plot([time(1) time(length(time))],[max_amp max_amp],'r-')
hold on
plot([time(1) time(length(time))],[-max_amp -max_amp],'r-')
ylabel('Velocity (m/s)','Fontsize',12)
xlabel('Time (s)','Fontsize',12)
title('Entire Day of Data with Desired Maximum Amplitude Displayed, Horizontal Velocity
(Channel 2)','Fontsize',16)
legend('Calibrated amplitude','+/- max amplitude')

rsac_channel_1=rsac_channel_1(:,2);
rsac_channel_2=rsac_channel_2(:,2);

% find the peaks above the maximum amplitude

[PKS,LOCS]=findpeaks(abs(cal_data),'MinPeakHeight',max_amp);

% for-loop to create index locating where time between peaks is at least an
% hour
for i=1:length(LOCS);
   if i==1
      if time(LOCS(i))-time(1)>=(60*60);
         loop_index(1:LOCS(i))=0;
      else loop_index(1:LOCS(i))=1;
      end

   elseif i>1 && i<length(LOCS);
      if time(LOCS(i))-time(LOCS(i-1))>=(60*60)
         loop_index(LOCS(i-1):LOCS(i))=0;
      else loop_index(LOCS(i-1):LOCS(i))=1;
      end

   elseif i==length(LOCS);
      if length(time)-time(LOCS(i))>=(60*60)
         loop_index(LOCS(i):length(time))=0;
      else loop_index(LOCS(i):length(time))=1;
      end
   end
end

loop_index_logical=logical(loop_index);

cal_data1=cal_data;

cal_data1(loop_index_logical)=0;

% get rid of remaining peaks (which are located directly next to previous
% peak locations)
```

```
[PKS2,LOCS2]=findpeaks(abs(cal_data1),'MinPeakHeight',max_amp);

for i=1:length(LOCS2)
   loop_index(LOCS2(i)-60*Fs:LOCS2(i)+60*Fs)=1; %taking away 1 minute on either side of
remaining peaks
end

loop_index_logical2=logical(loop_index);

cal_data2=cal_data1;

cal_data2(loop_index_logical2)=0;

% find largest quiescent period

cal_data3=cal_data2;
largest_quiescent_index=ones(length(cal_data2),1);
X=diff(LOCS);
X=[LOCS(1)-1; X; length(cal_data2)-LOCS(length(LOCS))];  % need to add beginning length
I=find(X==max(X));

if I==1 && length(time(round(length(time)*.05):LOCS(I)))>=60*60*Fs
   largest_quiescent_index(round(length(time)*.05):LOCS(I))=0;
elseif I==1 && length(time(round(length(time)*.05):LOCS(I)))<60*60*Fs
   I=find(X==max(X(2:length(X))));
end

if I==length(X) && length(time(LOCS(I-1):length(cal_data2)-round(.05*length(time))))>=60*60*Fs
   largest_quiescent_index(LOCS(I-1):length(cal_data2)-round(.05*length(time)))=0;
elseif I==length(X) && length(time(LOCS(I-1):length(cal_data2)-
round(.05*length(time))))<60*60*Fs
   I=find(X==max(X(2:length(X)-1)));
end

if I>1 && I<length(X);
    largest_quiescent_index(LOCS(I-1):LOCS(I))=0;
end

% Ensure X is at least an hour
Y = X(I);
if Y<=60*60*Fs
   error='quiscent period not an hour use high amp vibration analysis'
elseif Y>60*60*Fs
   display('hour of quiescent found')
end

largest_quiescent_index=logical(largest_quiescent_index);
cal_data3(largest_quiescent_index)=0;

channel1_cal_data=rsac_channel_1;   %channel 1
channel1_cal_data(largest_quiescent_index)=0;

channel2_cal_data=rsac_channel_2;   %channel2
channel2_cal_data(largest_quiescent_index)=0;
```

```
time_quiescent=time(~largest_quiescent_index);

% plot longest quiescent period

figure
plot(time_quiescent,cal_data_qplot(~largest_quiescent_index))
hold on
plot([time_quiescent(1) time_quiescent(length(time_quiescent))],[max_amp max_amp],'r-')
hold on
plot([time_quiescent(1) time_quiescent(length(time_quiescent))],[-max_amp -max_amp],'r-')
hold on
plot(time_quiescent,rsac1_qplot(~largest_quiescent_index),'g')
hold on
plot(time_quiescent,rsac2_qplot(~largest_quiescent_index),'m')
ylabel('Velocity (m/s)','Fontsize',12)
xlabel('Time (s)','Fontsize',12)
title('Longest Continuous Quiescent Period (Based on Channel Z)','Fontsize',16)
legend('Calibrated amplitude, channel Z','+/- max amplitude','+/- max amplitude','Calibrated
amplitude, channel 1','Calibrated amplitude, channel 2')

% Power Spectral Density of quiescent period

N=2^12;
overlap=N/2;

figure
[Pxx,F]=pwelch(cal_data3(~largest_quiescent_index),hamming(N),overlap,N,Fs);
[Pxx1,F1]=pwelch(channel1_cal_data(~largest_quiescent_index),hamming(N),overlap,N,Fs);
[Pxx2,F2]=pwelch(channel2_cal_data(~largest_quiescent_index),hamming(N),overlap,N,Fs);
plot(F,10*log10(Pxx),'r')
hold on
plot(F1,10*log10(Pxx1),'b')
hold on
plot(F2,10*log10(Pxx2),'m')
ylabel('dB re m/s/$$\sqrt{Hz}$$','Interpreter','Latex','Fontsize',14)
xlabel('Frequency (Hz)','Fontsize',12)
title({'Power Spectral Density Estimate','Longest Continuous Quiescent Period'},'Fontsize',16)
grid on
legend('Channel Z','Channel 1','Channel 2')

figure
plot(F,10*log10(Pxx),'r')
hold on
plot(F1,10*log10(Pxx1),'b')
hold on
plot(F2,10*log10(Pxx2),'m')
ylabel('dB re m/s/$$\sqrt{Hz}$$','Interpreter','Latex','Fontsize',14)
xlabel('Frequency (Hz)','Fontsize',12)
xlim([0 2])
title({'Power Spectral Density Estimate','Longest Continuous Quiescent Period, 0 to 2
Hz'},'Fontsize',16)
grid on
legend('Channel Z','Channel 1','Channel 2')

length_z=length(cal_data);
```

```
taperz=floor(.05*length_z);

length_1=length(rsac_channel_1);
taper1=floor(.05*length_1);

length_2=length(rsac_channel_2);
taper2=floor(.05*length_2);

cal_data=cal_data(taperz:length_z-taperz);
rsac_channel_1=rsac_channel_1(taper1:length_1-taper1);
rsac_channel_2=rsac_channel_2(taper2:length_2-taper2);

time=time(taperz:length_z-taperz);

% Find percentage of time above maximum amplitude

index=abs(cal_data)>=max_amp;
above_max_amp_time=time(index);
percentage_time_above_max_amp=(length(above_max_amp_time)/length(time))*100

% Create square wave where amplitude surpasses maximum amplitude for use in
% histogram.

cal_data_update=cal_data;
outlier=abs(cal_data_update) > max_amp;
cal_data_update(~outlier)=0;      % Sets entire signal below max amp to zero
cal_data_update(outlier)=sign(cal_data_update(outlier)); % This sets all
                % magnitudes above max amp to 1 (builds a square wave)

W=pulsewidth(abs(cal_data_update),Fs); % stores times of pulses above max amp

% W = pulsewidth(X) returns a vector, W, containing the time differences
% between the mid-reference level instants of the initial and final transitions
% of each positive-polarity pulse in the bilevel waveform, X.

[S,INITCROSS]=pulsesep(abs(cal_data_update),Fs);
S=[INITCROSS(1); S];

% S = pulsesep(X) returns the differences, S, between the mid-reference level
%instants of the final negative-going transitions of every positive-polarity
%pulse and the next positive-going transition. X is a bilevel waveform.

% [S,INITCROSS] = pulsesep(...) returns the mid-reference level instants,
% INITCROSS, of the first positive-polarity transitions.

figure
histogram(W)
set(gca,'Yscale','log')  % this gives you average time of pulses above max amp
title({'Histogram of Length of Continuous Time Signal Exceeding Maximum','Channel
Z'},'Fontsize',16)
xlabel('Time (s)','Fontsize',12)

figure
histogram(W)
ylim([0 50])
```

```
xlabel('Time (s)','Fontsize',12)
title({'Histogram of Length of Continuous Time Signal Exceeding Maximum','Channel
Z'},'Fontsize',16)

figure
histogram(S)
set(gca,'Yscale','log')
xlabel('Time (s)','Fontsize',12)
title({'Histogram of Length of Time Between Signals that Exceed Max Amplitude','Channel
Z'},'Fontsize',16)

figure
histogram(S)
ylim([0 50])
xlabel('Time (s)','Fontsize',12)
title({'Histogram of Length of Time Between Signals that Exceed Max Amplitude','Channel
Z'},'Fontsize',16)

figure
histogram(cal_data,400)
set(gca,'Yscale','log')
xlabel('Velocity Amplitude (m/s)')
ylabel('Number of Occurrences')
title('Histogram of Channel Z Amplitudes')

figure
histogram(cal_data,400)
xlabel('Velocity Amplitude (m/s)')
ylabel('Number of Occurrences maxed at 20')
ylim([0 20])
title('Histogram of Channel Z Amplitudes')

std_z=std(cal_data)
```

B. HIGH AMPLITUDE VIBRATION ANALYSIS CODE

```
function
high_amp_vibration_analysis(rsac_channel_Z,max_amp,Fs,rsac_channel_1,rsac_channel_2)
%   OBS, ocean bottom seismometer, maximum amplitude, BHZ, sampling frequency
%
%   Purpose:  Run this function if the sample day too noisy for
%   vibration_analysis.m (not at least 1 hour in length where the amplitude
%   does not exceed maximum amplitude).  Takes three calibrated channels of
%   OBS data, OBS sampling frequency, and maximum desired amplitude, and
%   finds the three hours with lowest mean amplitude. Function outputs an
%   amplitude (m/s) vs time plot (for all three channels), the mean and
%   standard deviation of entire sample amplitude, power spectral densities
%   of three-hour with lowest mean, a percentage of time spent above maximum
%   desired amplitude, a histogram of amplitudes, a histogram of lengths of
%   signals greater than max desired amplitude, and a histogram of time
%   periods between signals that exceed maximum amplitude.
%
%   Sample needs to be at least 15 hours long for this function to work
%   properly.
```

```
%
%  Output Variables:
%     std_z = standard deviation of channel z amplitude
%     percentage_time_above_max_amp = percentage of time where amplitude
%     is greater than max amplitude
%
%  Input Variables:
%     rsac_channel_Z = vertical .sac file after it has been read through
%     rsac.m
%     max_amp = desired maximum amplitude (m/s)
%     Fs = sampling frequency of OBS (Hz)
%     rsac_channel_1 = channel 1 .sac file after it has been read through
%     rsac.m
%     rsac_channel_2 = channel 2 .sac file after it has been read through
%     rsac.m
%
%  Local Variables:
%     cal_data = calibrated vertical channel amplitude (m/s)
%     time = time (seconds)
%     length_z = length of cal_data (vector length), channel Z
%     taperz = amount to subtract from beginning/end of sample to get rid
%     of taper, channel Z
%     length_1 = vector length of channel 1 amplitude vector
%     taper1 = amount to subtract from beginning/end of sample to get rid
%     of taper, channel 1
%     length_2 = vector length of channel 2 amplitude vector
%     taper2 = amount to subtract from beginning/end of sample to get rid
%     of taper, channel 2
%     rsac_channel_1 = amplitude vector channel 1
%     rsac_channel_2 = amplitdue vector channel 2
%     second_3_hours_cal_data to twentyone_3_hours_cal_data = three-hour
%        blocks of time used to find three-hour time period with lowest mean
%        ampltidue
%     MEAN = vector containing mean values of three-hour blocks of time
%     Y = used in first if/elseif statement.  If size of sample much less
%     than 24 hours, Y variable helps assign correct area to apply taper
%     X = used in if/elseif statement to choose correct three-hour block
%     and assign variables to PSD
%     N = FFT length
%     overlap = pwelch overlap value
%     Pxx = channel Z distribution of power per unit of freq, but in this
%           application units of [m/s/sqrt(Hz)]
%     F, F1, F2 = Frequency (Hz)
%     Pxx1 = channel 1 distribution of power per unit of freq, but in this
%           application units of [m/s/sqrt(Hz)]
%     Pxx2 = channel 2 distribution of power per unit of freq, but in this
%           application units of [m/s/sqrt(Hz)]
%     index = index locating where cal_data is greater than the maximum
%           amplitude
%     above_max_amp_time = time where cal_data is greater than maximum
%           amplitude (s)
%     outlier = logical index location where Z-amplitude is greater than
%           maximum amplitude
%     cal_data_update = same as cal_data, but only contains amplitudes
%           greater than maximum amplitude.  (m/s)
```

```
%       W = vector with lengths of signals that exceed max amplitude
%       S = vector that contains different lengths of time between signals
%             that exceed max amplitude
%
%       Functions Called:  None.
%
%       Filename: high_amp_vibration_analysis.m
%       Written by: Jeremy R. Hankins

cal_data=rsac_channel_Z(:,2);
time=rsac_channel_Z(:,1);

length_z=length(cal_data);
taperz=floor(.05*length_z);

length_1=length(rsac_channel_1(:,2));
taper1=floor(.05*length_1);

length_2=length(rsac_channel_2(:,2));
taper2=floor(.05*length_2);

rsac_channel_1=rsac_channel_1(:,2);
rsac_channel_2=rsac_channel_2(:,2);

figure
plot(time,cal_data)
hold on
plot([time(1) time(length(time))],[max_amp max_amp],'r-')
hold on
plot([time(1) time(length(time))],[-max_amp -max_amp],'r-')
ylabel('Velocity (m/s)','Fontsize',12)
xlabel('Time (s)','Fontsize',12)
title('Entire Day of Data with Desired Maximum Amplitude Displayed, Vertical Velocity (Channel
Z)','Fontsize',16)
legend('Calibrated amplitude','+/- max amplitude')

figure
plot(time,rsac_channel_1)
hold on
plot([time(1) time(length(time))],[max_amp max_amp],'r-')
hold on
plot([time(1) time(length(time))],[-max_amp -max_amp],'r-')
ylabel('Velocity (m/s)','Fontsize',12)
xlabel('Time (s)','Fontsize',12)
title('Entire Day of Data with Desired Maximum Amplitude Displayed, Horizontal Velocity
(Channel 1)','Fontsize',16)
legend('Calibrated amplitude','+/- max amplitude')

figure
plot(time,rsac_channel_2)
hold on
plot([time(1) time(length(time))],[max_amp max_amp],'r-')
hold on
plot([time(1) time(length(time))],[-max_amp -max_amp],'r-')
ylabel('Velocity (m/s)','Fontsize',12)
```

```
xlabel('Time (s)','Fontsize',12)
title('Entire Day of Data with Desired Maximum Amplitude Displayed, Horizontal Velocity
(Channel 2)','Fontsize',16)
legend('Calibrated amplitude','+/- max amplitude')

% Divide sample into 3 hour time blocks, exluding taper at beginning and
% end of sample.  3 hour block that includes taper could be less/more
% than three hours.  Amount less/more depends on length of sample.

% if/elseif statement covers files as short as 15 hours

second_3_hours_cal_data=cal_data(taperz:4*60*60*Fs);
third_3_hours_cal_data=cal_data(2*60*60*Fs:5*60*60*Fs);
fourth_3_hours_cal_data=cal_data(3*60*60*Fs:6*60*60*Fs);
fifth_3_hours_cal_data=cal_data(4*60*60*Fs:7*60*60*Fs);
sixth_3_hours_cal_data=cal_data(5*60*60*Fs:8*60*60*Fs);
seventh_3_hours_cal_data=cal_data(6*60*60*Fs:9*60*60*Fs);
eighth_3_hours_cal_data=cal_data(7*60*60*Fs:10*60*60*Fs);
nine_3_hours_cal_data=cal_data(8*60*60*Fs:11*60*60*Fs);
ten_3_hours_cal_data=cal_data(9*60*60*Fs:12*60*60*Fs);
eleven_3_hours_cal_data=cal_data(10*60*60*Fs:13*60*60*Fs);
twelve_3_hours_cal_data=cal_data(11*60*60*Fs:14*60*60*Fs);
if length(cal_data)/(Fs*60*60)>=23;
   Y=20;
   thirteen_3_hours_cal_data=cal_data(12*60*60*Fs:15*60*60*Fs);
   fourteen_3_hours_cal_data=cal_data(13*60*60*Fs:16*60*60*Fs);
   fifteen_3_hours_cal_data=cal_data(14*60*60*Fs:17*60*60*Fs);
   sixteen_3_hours_cal_data=cal_data(15*60*60*Fs:18*60*60*Fs);
   seventeen_3_hours_cal_data=cal_data(16*60*60*Fs:19*60*60*Fs);
   eighteen_3_hours_cal_data=cal_data(17*60*60*Fs:20*60*60*Fs);
   nineteen_3_hours_cal_data=cal_data(18*60*60*Fs:21*60*60*Fs);
   twenty_3_hours_cal_data=cal_data(19*60*60*Fs:22*60*60*Fs);
   twentyone_3_hours_cal_data=cal_data(20*60*60*Fs:length_z-taperz);
elseif length(cal_data)/(Fs*60*60)>=22 && length(cal_data)/(Fs*60*60) < 23;
   Y=19;
   thirteen_3_hours_cal_data=cal_data(12*60*60*Fs:15*60*60*Fs);
   fourteen_3_hours_cal_data=cal_data(13*60*60*Fs:16*60*60*Fs);
   fifteen_3_hours_cal_data=cal_data(14*60*60*Fs:17*60*60*Fs);
   sixteen_3_hours_cal_data=cal_data(15*60*60*Fs:18*60*60*Fs);
   seventeen_3_hours_cal_data=cal_data(16*60*60*Fs:19*60*60*Fs);
   eighteen_3_hours_cal_data=cal_data(17*60*60*Fs:20*60*60*Fs);
   nineteen_3_hours_cal_data=cal_data(18*60*60*Fs:21*60*60*Fs);
   twenty_3_hours_cal_data=cal_data(19*60*60*Fs:length_z-taperz);
   twentyone_3_hours_cal_data=1E10;
elseif length(cal_data)/(Fs*60*60)>=21 && length(cal_data)/(Fs*60*60) < 22;
   Y=18;
   thirteen_3_hours_cal_data=cal_data(12*60*60*Fs:15*60*60*Fs);
   fourteen_3_hours_cal_data=cal_data(13*60*60*Fs:16*60*60*Fs);
   fifteen_3_hours_cal_data=cal_data(14*60*60*Fs:17*60*60*Fs);
   sixteen_3_hours_cal_data=cal_data(15*60*60*Fs:18*60*60*Fs);
   seventeen_3_hours_cal_data=cal_data(16*60*60*Fs:19*60*60*Fs);
   eighteen_3_hours_cal_data=cal_data(17*60*60*Fs:20*60*60*Fs);
   nineteen_3_hours_cal_data=cal_data(18*60*60*Fs:length_z-taperz);
   twenty_3_hours_cal_data=1E10;
   twentyone_3_hours_cal_data=1E10;
```

```
elseif length(cal_data)/(Fs*60*60)>=20 && length(cal_data)/(Fs*60*60) < 21;
    Y=17;
    thirteen_3_hours_cal_data=cal_data(12*60*60*Fs:15*60*60*Fs);
    fourteen_3_hours_cal_data=cal_data(13*60*60*Fs:16*60*60*Fs);
    fifteen_3_hours_cal_data=cal_data(14*60*60*Fs:17*60*60*Fs);
    sixteen_3_hours_cal_data=cal_data(15*60*60*Fs:18*60*60*Fs);
    seventeen_3_hours_cal_data=cal_data(16*60*60*Fs:19*60*60*Fs);
    eighteen_3_hours_cal_data=cal_data(17*60*60*Fs:length_z-taperz);
    nineteen_3_hours_cal_data=1E10;
    twenty_3_hours_cal_data=1E10;
    twentyone_3_hours_cal_data=1E10;
elseif length(cal_data)/(Fs*60*60)>=19 && length(cal_data)/(Fs*60*60) < 20;
    Y=16;
    thirteen_3_hours_cal_data=cal_data(12*60*60*Fs:15*60*60*Fs);
    fourteen_3_hours_cal_data=cal_data(13*60*60*Fs:16*60*60*Fs);
    fifteen_3_hours_cal_data=cal_data(14*60*60*Fs:17*60*60*Fs);
    sixteen_3_hours_cal_data=cal_data(15*60*60*Fs:18*60*60*Fs);
    seventeen_3_hours_cal_data=cal_data(16*60*60*Fs:length_z-taperz);
    eighteen_3_hours_cal_data=1E10;
    nineteen_3_hours_cal_data=1E10;
    twenty_3_hours_cal_data=1E10;
    twentyone_3_hours_cal_data=1E10;
elseif length(cal_data)/(Fs*60*60)>=18 && length(cal_data)/(Fs*60*60) < 19;
    Y=15;
    thirteen_3_hours_cal_data=cal_data(12*60*60*Fs:15*60*60*Fs);
    fourteen_3_hours_cal_data=cal_data(13*60*60*Fs:16*60*60*Fs);
    fifteen_3_hours_cal_data=cal_data(14*60*60*Fs:17*60*60*Fs);
    sixteen_3_hours_cal_data=cal_data(15*60*60*Fs:length_z-taperz);
    seventeen_3_hours_cal_data=1E10;
    eighteen_3_hours_cal_data=1E10;
    nineteen_3_hours_cal_data=1E10;
    twenty_3_hours_cal_data=1E10;
    twentyone_3_hours_cal_data=1E10;
elseif length(cal_data)/(Fs*60*60)>=17 && length(cal_data)/(Fs*60*60) < 18;
    Y=14;
    thirteen_3_hours_cal_data=cal_data(12*60*60*Fs:15*60*60*Fs);
    fourteen_3_hours_cal_data=cal_data(13*60*60*Fs:16*60*60*Fs);
    fifteen_3_hours_cal_data=cal_data(14*60*60*Fs:length_z-taperz);
    sixteen_3_hours_cal_data=1E10;
    seventeen_3_hours_cal_data=1E10;
    eighteen_3_hours_cal_data=1E10;
    nineteen_3_hours_cal_data=1E10;
    twenty_3_hours_cal_data=1E10;
    twentyone_3_hours_cal_data=1E10;
elseif length(cal_data)/(Fs*60*60)>=16 && length(cal_data)/(Fs*60*60) < 17;
    Y=13;
    thirteen_3_hours_cal_data=cal_data(12*60*60*Fs:15*60*60*Fs);
    fourteen_3_hours_cal_data=cal_data(13*60*60*Fs:length_z-taperz);
    fifteen_3_hours_cal_data=1E10;
    sixteen_3_hours_cal_data=1E10;
    seventeen_3_hours_cal_data=1E10;
    eighteen_3_hours_cal_data=1E10;
    nineteen_3_hours_cal_data=1E10;
    twenty_3_hours_cal_data=1E10;
    twentyone_3_hours_cal_data=1E10;
```

```
elseif length(cal_data)/(Fs*60*60)>=15 && length(cal_data)/(Fs*60*60) < 16;
    Y=12;
    thirteen_3_hours_cal_data=cal_data(12*60*60*Fs:length_z-taperz);
    fourteen_3_hours_cal_data=1E10;
    fifteen_3_hours_cal_data=1E10;
    sixteen_3_hours_cal_data=1E10;
    seventeen_3_hours_cal_data=1E10;
    eighteen_3_hours_cal_data=1E10;
    nineteen_3_hours_cal_data=1E10;
    twenty_3_hours_cal_data=1E10;
    twentyone_3_hours_cal_data=1E10;
end

MEAN=[mean(abs(second_3_hours_cal_data)),...
    mean(abs(third_3_hours_cal_data)),mean(abs(fourth_3_hours_cal_data)),...
    mean(abs(fifth_3_hours_cal_data)),mean(abs(sixth_3_hours_cal_data)),...
    mean(abs(seventh_3_hours_cal_data)),mean(abs(eighth_3_hours_cal_data)),...
    mean(abs(nine_3_hours_cal_data)),mean(abs(ten_3_hours_cal_data)),...
    mean(abs(eleven_3_hours_cal_data)),mean(abs(twelve_3_hours_cal_data)),...
    mean(abs(thirteen_3_hours_cal_data)),mean(abs(fourteen_3_hours_cal_data)),...
    mean(abs(fifteen_3_hours_cal_data)),mean(abs(sixteen_3_hours_cal_data)),...
    mean(abs(seventeen_3_hours_cal_data)),mean(abs(eighteen_3_hours_cal_data)),...
    mean(abs(nineteen_3_hours_cal_data)),mean(abs(twenty_3_hours_cal_data)),...
    mean(abs(twentyone_3_hours_cal_data))];

X=find(MEAN==min(MEAN))

% if/elseif statments to plot correct psd

if X==1
    psd_z=second_3_hours_cal_data;
    psd_1=rsac_channel_1(taper1:4*60*60*Fs);
    psd_2=rsac_channel_2(taper2:4*60*60*Fs);
elseif X==2
    psd_z=third_3_hours_cal_data;
    psd_1=rsac_channel_1(2*60*60*Fs:5*60*60*Fs);
    psd_2=rsac_channel_2(2*60*60*Fs:5*60*60*Fs);
elseif X==3
    psd_z=fourth_3_hours_cal_data;
    psd_1=rsac_channel_1(3*60*60*Fs:6*60*60*Fs);
    psd_2=rsac_channel_2(3*60*60*Fs:6*60*60*Fs);
elseif X==4
    psd_z=fifth_3_hours_cal_data;
    psd_1=rsac_channel_1(4*60*60*Fs:7*60*60*Fs);
    psd_2=rsac_channel_2(4*60*60*Fs:7*60*60*Fs);
elseif X==5
    psd_z=sixth_3_hours_cal_data;
    psd_1=rsac_channel_1(5*60*60*Fs:8*60*60*Fs);
    psd_2=rsac_channel_2(5*60*60*Fs:8*60*60*Fs);
elseif X==6
    psd_z=seventh_3_hours_cal_data;
    psd_1=rsac_channel_1(6*60*60*Fs:9*60*60*Fs);
    psd_2=rsac_channel_2(6*60*60*Fs:9*60*60*Fs);
elseif X==7
    psd_z=eighth_3_hours_cal_data;
```

```
    psd_1=rsac_channel_1(7*60*60*Fs:10*60*60*Fs);
    psd_2=rsac_channel_2(7*60*60*Fs:10*60*60*Fs);
elseif X==8
    psd_z=nine_3_hours_cal_data;
    psd_1=rsac_channel_1(8*60*60*Fs:11*60*60*Fs);
    psd_2=rsac_channel_2(8*60*60*Fs:11*60*60*Fs);
elseif X==9
    psd_z=ten_3_hours_cal_data;
    psd_1=rsac_channel_1(9*60*60*Fs:12*60*60*Fs);
    psd_2=rsac_channel_2(9*60*60*Fs:12*60*60*Fs);
elseif X==10
    psd_z=eleven_3_hours_cal_data;
    psd_1=rsac_channel_1(10*60*60*Fs:13*60*60*Fs);
    psd_2=rsac_channel_2(10*60*60*Fs:13*60*60*Fs);
elseif X==11
    psd_z=twelve_3_hours_cal_data;
    psd_1=rsac_channel_1(11*60*60*Fs:14*60*60*Fs);
    psd_2=rsac_channel_2(11*60*60*Fs:14*60*60*Fs);
elseif X==12
    psd_z=thirteen_3_hours_cal_data;
    if Y==12
        psd_1=rsac_channel_1(12*60*60*Fs:length_1-taper1);
        psd_2=rsac_channel_2(12*60*60*Fs:length_2-taper2);
    else
        psd_1=rsac_channel_1(12*60*60*Fs:15*60*60*Fs);
        psd_2=rsac_channel_2(12*60*60*Fs:15*60*60*Fs);
    end
elseif X==13
    psd_z=fourteen_3_hours_cal_data;
    if Y==13
        psd_1=rsac_channel_1(13*60*60*Fs:length_1-taper1);
        psd_2=rsac_channel_2(13*60*60*Fs:length_2-taper2);
    else
        psd_1=rsac_channel_1(13*60*60*Fs:16*60*60*Fs);
        psd_2=rsac_channel_2(13*60*60*Fs:16*60*60*Fs);
    end
elseif X==14
    psd_z=fifteen_3_hours_cal_data;
    if Y==14
        psd_1=rsac_channel_1(14*60*60*Fs:length_1-taper1);
        psd_2=rsac_channel_2(14*60*60*Fs:length_2-taper2);
    else
        psd_1=rsac_channel_1(14*60*60*Fs:17*60*60*Fs);
        psd_2=rsac_channel_2(14*60*60*Fs:17*60*60*Fs);
    end
elseif X==15
    psd_z=sixteen_3_hours_cal_data;
    if Y==15
        psd_1=rsac_channel_1(15*60*60*Fs:length_1-taper1);
        psd_2=rsac_channel_2(15*60*60*Fs:length_2-taper2);
    else
        psd_1=rsac_channel_1(15*60*60*Fs:18*60*60*Fs);
        psd_2=rsac_channel_2(15*60*60*Fs:18*60*60*Fs);
    end
elseif X==16
```

```
    psd_z=seventeen_3_hours_cal_data;
    if Y==16
        psd_1=rsac_channel_1(16*60*60*Fs:length_1-taper1);
        psd_2=rsac_channel_2(16*60*60*Fs:length_2-taper2);
    else
        psd_1=rsac_channel_1(16*60*60*Fs:19*60*60*Fs);
        psd_2=rsac_channel_2(16*60*60*Fs:19*60*60*Fs);
    end
elseif X==17
    psd_z=eighteen_3_hours_cal_data;
    if Y==17
        psd_1=rsac_channel_1(17*60*60*Fs:length_1-taper1);
        psd_2=rsac_channel_2(17*60*60*Fs:length_2-taper2);
    else
        psd_1=rsac_channel_1(17*60*60*Fs:20*60*60*Fs);
        psd_2=rsac_channel_2(17*60*60*Fs:20*60*60*Fs);
    end
elseif X==18
    psd_z=nineteen_3_hours_cal_data;
    if Y==18
        psd_1=rsac_channel_1(18*60*60*Fs:length_1-taper1);
        psd_2=rsac_channel_2(18*60*60*Fs:length_2-taper2);
    else
        psd_1=rsac_channel_1(18*60*60*Fs:21*60*60*Fs);
        psd_2=rsac_channel_2(18*60*60*Fs:21*60*60*Fs);
    end
elseif X==19
    psd_z=twenty_3_hours_cal_data;
    if Y==19;
        psd_1=rsac_channel_1(19*60*60*Fs:length_1-taper1);
        psd_2=rsac_channel_2(19*60*60*Fs:length_2-taper2);
    else
        psd_1=rsac_channel_1(19*60*60*Fs:22*60*60*Fs);
        psd_2=rsac_channel_2(19*60*60*Fs:22*60*60*Fs);
    end
elseif X==20
    psd_z=twentyone_3_hours_cal_data;
    psd_1=rsac_channel_1(20*60*60*Fs:length_1-taper1);
    psd_2=rsac_channel_2(20*60*60*Fs:length_2-taper2);

end

N=2^12;
overlap=N/2;

figure
[Pxx,F]=pwelch(psd_z,hamming(N),overlap,N,Fs);
[Pxx1,F1]=pwelch(psd_1,hamming(N),overlap,N,Fs);
[Pxx2,F2]=pwelch(psd_2,hamming(N),overlap,N,Fs);
plot(F,10*log10(Pxx),'r')
hold on
plot(F1,10*log10(Pxx1),'b')
hold on
plot(F2,10*log10(Pxx2),'m')
ylabel('dB re m/s/$$\sqrt{Hz}$$','Interpreter','Latex','Fontsize',14)
```

```
xlabel('Frequency (Hz)','Fontsize',12)
xlim([0 2])
title({'Power Spectral Density Estimate','Three Hours with Lowest Mean Amplitude, 0 to 2
Hz'},'Fontsize',16)
grid on
legend('Channel Z','Channel 1','Channel 2')

figure
plot(F,10*log10(Pxx),'r')
hold on
plot(F1,10*log10(Pxx1),'b')
hold on
plot(F2,10*log10(Pxx2),'m')
ylabel('dB re m/s/$$\sqrt{Hz}$$','Interpreter','Latex','Fontsize',14)
xlabel('Frequency (Hz)','Fontsize',12)
title({'Power Spectral Density Estimate','Three Hours with Lowest Mean Amplitude'},'Fontsize',16)
grid on
legend('Channel Z','Channel 1','Channel 2')

% get rid of taper for plot and histograms
cal_data=cal_data(taperz:length_z-taperz);
rsac_channel_1=rsac_channel_1(taper1:length_1-taper1);
rsac_channel_2=rsac_channel_2(taper2:length_2-taper2);
time=time(taperz:length_z-taperz);

% psd for entire day of data
figure
[Pxx,F]=pwelch(cal_data,hamming(N),overlap,N,Fs);
[Pxx1,F1]=pwelch(rsac_channel_1,hamming(N),overlap,N,Fs);
[Pxx2,F2]=pwelch(rsac_channel_2,hamming(N),overlap,N,Fs);
plot(F,10*log10(Pxx),'r')
hold on
plot(F1,10*log10(Pxx1),'b')
hold on
plot(F2,10*log10(Pxx2),'m')
ylabel('dB re m/s/$$\sqrt{Hz}$$','Interpreter','Latex','Fontsize',14)
xlabel('Frequency (Hz)','Fontsize',12)
title({'Power Spectral Density Estimate','Entire Day of Data'},'Fontsize',16)
grid on
legend('Channel Z','Channel 1','Channel 2')

index=abs(cal_data)>=max_amp;
above_max_amp_time=time(index);
percentage_time_above_max_amp=(length(above_max_amp_time)/length(time))*100

cal_data_update=cal_data;
outlier=abs(cal_data_update) > max_amp;
cal_data_update(~outlier)=0;                    % Sets entire signal below max amp to zero
cal_data_update(outlier)=sign(cal_data_update(outlier)); % This sets all magnitudes above max
amp to 1 (builds a square wave)

W=pulsewidth(abs(cal_data_update),Fs); % stores times of pulses above max amp

[S,INITCROSS]=pulsesep(abs(cal_data_update),Fs);
S=[INITCROSS(1); S];
```

```
figure
histogram(W)
set(gca,'Yscale','log')  % this gives you average time of pulses above max amp
title({'Histogram of Length of Continuous Time Signal Exceeding Maximum','Channel
Z'},'Fontsize',16)
xlabel('Time (s)','Fontsize',12)

figure
histogram(W)
ylim([0 50])
xlabel('Time (s)','Fontsize',12)
title({'Histogram of Length of Continuous Time Signal Exceeding Maximum','Channel
Z'},'Fontsize',16)

figure
histogram(S)
set(gca,'Yscale','log')
xlabel('Time (s)','Fontsize',12)
title({'Histogram of Length of Time Between Signals that Exceed Max Amplitude','Channel
Z'},'Fontsize',16)

figure
histogram(S)
ylim([0 50])
xlabel('Time (s)','Fontsize',12)
title({'Histogram of Length of Time Between Signals that Exceed Max Amplitude','Channel
Z'},'Fontsize',16)

figure
histogram(cal_data,400)
set(gca,'Yscale','log')
xlabel('Velocity Amplitudes (m/s)')
ylabel('Number of Occurrences')
title('Histogram of Channel Z Amplitudes')

figure
histogram(cal_data,400)
xlabel('Velocity Amplitudes (m/s)')
ylabel('Number of Occurrences maxed at 20')
ylim([0 20])
title('Histogram of Channel Z Amplitudes')

std_z=std(cal_data)
```

C. LOW AMPLITUDE VIBRATION ANALYSIS CODE

```
function
low_amp_vibration_analysis(rsac_channel_Z,max_amp,Fs,rsac_channel_1,rsac_channel_2)
%  OBS, ocean bottom seismometer, maximum amplitude, BHZ, sampling frequency
%
%  Purpose:  Run this function if the sample day does not exceed max
%  amplitude with vibration_analysis.m (does not cross max amplitude at
%  all).  Takes three calibrated channels of OBS data, OBS sampling
%  frequency, and maximum desired amplitude. Function outputs an
%  amplitude (m/s) vs time plot (for all three channels), the mean and
%  standard deviation of entire sample amplitude, power spectral densities
%  of entire day, and a histogram of amplitudes.
%
%  Sample needs to be at least 15 hours long for this function to work
%  properly.
%
%  Output Variables:
%     avg_z = mean of absolute value of channel z amplitude
%     std_z = standard deviation of absolute value of channel z amplitude
%     percentage_time_above_max_amp = percentage of time above max amp
%           (should be zero)
%
%  Input Variables:
%     rsac_channel_Z = vertical .sac file after it has been read through
%     rsac.m
%     max_amp = desired maximum amplitude (m/s)
%     Fs = sampling frequency of OBS (Hz)
%     rsac_channel_1 = channel 1 .sac file after it has been read through
%     rsac.m
%     rsac_channel_2 = channel 2 .sac file after it has been read through
%     rsac.m
%
%  Local Variables:
%     cal_data = calibrated vertical channel amplitude (m/s)
%     time = time (seconds)
%     length_z = length of cal_data (vector length), channel Z
%     taperz = amount to subtract from beginning/end of sample to get rid
%     of taper, channel Z
%     length_1 = vector length of channel 1 amplitude vector
%     taper1 = amount to subtract from beginning/end of sample to get rid
%     of taper, channel 1
%     length_2 = vector length of channel 2 amplitude vector
%     taper2 = amount to subtract from beginning/end of sample to get rid
%     of taper, channel 2
%     rsac_channel_1 = amplitude vector channel 1
%     rsac_channel_2 = amplitdue vector channel 2
%     N = FFT length
%     overlap = pwelch overlap value
%     Pxx = channel Z distribution of power per unit of freq, but in this
%           application units of [m/s/sqrt(Hz)]
%     F, F1, F2 = Frequency (Hz)
%     Pxx1 = channel 1 distribution of power per unit of freq, but in this
```

```
%           application units of [m/s/sqrt(Hz)]
%       Pxx2 = channel 2 distribution of power per unit of freq, but in this
%           application units of [m/s/sqrt(Hz)]
%       index = index locating where cal_data is greater than the maximum
%           amplitude
%       above_max_amp_time = time where cal_data is greater than maximum
%           amplitude (s)
%
%       Functions Called:  None.
%
%       Filename: low_amp_vibration_analysis.m
%       Written by: Jeremy R. Hankins

cal_data=rsac_channel_Z(:,2);
time=rsac_channel_Z(:,1);

length_z=length(cal_data);
taperz=floor(.05*length_z);

length_1=length(rsac_channel_1(:,2));
taper1=floor(.05*length_1);

length_2=length(rsac_channel_2(:,2));
taper2=floor(.05*length_2);

rsac_channel_1=rsac_channel_1(:,2);
rsac_channel_2=rsac_channel_2(:,2);

figure
plot(time,cal_data)
hold on
plot([time(1) time(length(time))],[max_amp max_amp],'r-')
hold on
plot([time(1) time(length(time))],[-max_amp -max_amp],'r-')
ylabel('Velocity (m/s)','Fontsize',12)
xlabel('Time (s)','Fontsize',12)
title('Entire Day of Data with Desired Maximum Amplitude Displayed, Vertical Velocity (Channel
Z)','Fontsize',16)
legend('Calibrated amplitude','+/- max amplitude')

figure
plot(time,rsac_channel_1)
hold on
plot([time(1) time(length(time))],[max_amp max_amp],'r-')
hold on
plot([time(1) time(length(time))],[-max_amp -max_amp],'r-')
ylabel('Velocity (m/s)','Fontsize',12)
xlabel('Time (s)','Fontsize',12)
title('Entire Day of Data with Desired Maximum Amplitude Displayed, Horizontal Velocity
(Channel 1)','Fontsize',16)
legend('Calibrated amplitude','+/- max amplitude')

figure
plot(time,rsac_channel_2)
hold on
```

```
plot([time(1) time(length(time))],[max_amp max_amp],'r-')
hold on
plot([time(1) time(length(time))],[-max_amp -max_amp],'r-')
ylabel('Velocity (m/s)','Fontsize',12)
xlabel('Time (s)','Fontsize',12)
title('Entire Day of Data with Desired Maximum Amplitude Displayed, Horizontal Velocity
(Channel 2)','Fontsize',16)
legend('Calibrated amplitude','+/- max amplitude')

% get rid of tapers

cal_data=cal_data(taperz:length_z-taperz);
rsac_channel_1=rsac_channel_1(taper1:length_1-taper1);
rsac_channel_2=rsac_channel_2(taper2:length_2-taper2);
time=time(taperz:length_z-taperz);

N=2^12;
overlap=N/2;

figure
[Pxx,F]=pwelch(cal_data,hamming(N),overlap,N,Fs);
[Pxx1,F1]=pwelch(rsac_channel_1,hamming(N),overlap,N,Fs);
[Pxx2,F2]=pwelch(rsac_channel_2,hamming(N),overlap,N,Fs);
plot(F,10*log10(Pxx),'r')
hold on
plot(F1,10*log10(Pxx1),'b')
hold on
plot(F2,10*log10(Pxx2),'m')
ylabel('dB re m/s/$$\sqrt{Hz}$$','Interpreter','Latex','Fontsize',14)
xlabel('Frequency (Hz)','Fontsize',12)
title({'Power Spectral Density Estimate'},'Fontsize',16)
grid on
legend('Channel Z','Channel 1','Channel 2')

figure
plot(F,10*log10(Pxx),'r')
hold on
plot(F1,10*log10(Pxx1),'b')
hold on
plot(F2,10*log10(Pxx2),'m')
ylabel('dB re m/s/$$\sqrt{Hz}$$','Interpreter','Latex','Fontsize',14)
xlabel('Frequency (Hz)','Fontsize',12)
xlim([0 2])
title({'Power Spectral Density Estimate','0 to 2 Hz'},'Fontsize',16)
grid on
legend('Channel Z','Channel 1','Channel 2')

index=abs(cal_data)>=max_amp;
above_max_amp_time=time(index);
percentage_above_max_amp_time=(length(above_max_amp_time)/length(time))*100  % will be
zero with this function

figure
histogram(cal_data,400)
set(gca,'Yscale','log')
```

THIS PAGE INTENTIONALLY LEFT BLANK

APPENDIX B. DATA TABLES

Table 3. YM 39 and YM 38 Standard Deviation and Percentage of Time Spent Above Maximum Amplitude Threshold.

YM 39				YM38			
Date	Standard deviation (μm/s)	RMS acceleration ($\mu m/s^2$)	Percentage above max amplitude	Date	Standard deviation (μm/s)	RMS acceleration ($\mu m/s^2$)	Percentage above max amplitude
13-Jun-08	191	155	17	13-Jun-08	0.23	2.7	0.00
14-Jun-08	143	65.8	10	14-Jun-08	0.40	3.6	0.00
1-Jul-09	112	57.0	36	1-Jul-09	0.45	3.6	0.00
15-Jul-08	604	919	83	15-Jul-08	1.9	9.5	0.03
1-Aug-08	395	355	86	1-Aug-08	7.3	8.1	0.16
15-Aug-08	324	403	83	15-Aug-08	1.2	3.7	0.00
1-Sep-08	662	574	91	1-Sep-08	0.57	3.8	0.00
15-Sep-08	350	392	86	15-Sep-08	0.70	6.1	0.00
1-Oct-08	365	364	83	1-Oct-08	0.56	3.9	0.00
15-Oct-08	375	303	77	15-Oct-08	0.44	4.8	0.00
1-Nov-08	399	358	80	1-Nov-08	1.1	3.8	0.01
15-Nov-08	219	279	74	15-Nov-08	1.2	12.7	0.00
13-Dec-08	200	489	42	13-Dec-08	1.3	4.1	0.01
14-Dec-08	277	303	33	14-Dec-08	1.9	4.3	0.04
1-Jan-09	727	185	84	1-Jan-09	0.55	4.6	0.00
15-Jan-09	366	323	68	15-Jan-09	1.3	3.9	0.02
1-Feb-09	46.4	128	10	1-Feb-09	0.42	3.4	0.00
15-Feb-09	150	33.0	30	15-Feb-09	0.43	3.9	0.00
1-Mar-09	309	48.4	57	1-Mar-09	1.3	5.1	0.00
15-Mar-09	119	74.6	54	15-Mar-09	0.57	4.7	0.00
1-Apr-09	96.9	19.0	34	1-Apr-09	2.9	13.3	0.03
15-Apr-09	88.0	71.9	8	15-Apr-09	1.3	8.8	0.01
1-May-09	63.9	86.3	25	1-May-09	0.56	4.7	0.00
15-May-09	16.1	28.9	1	15-May-09	0.31	3.4	0.00

Table 4. 7D J65A and 7D J73A Standard Deviation and Percentage of Time Spent Above Maximum Amplitude Threshold.

7D J65A				7D J73A			
Date	Standard deviation (μm/s)	RMS acceleration ($\mu m/s^2$)	Percentage above max amplitude	Date	Standard deviation (μm/s)	RMS acceleration ($\mu m/s^2$)	Percentage above max amplitude
1-Nov-11	30.5	51.7	9.8	1-Nov-11	28.7	33.0	8
15-Nov-11	26.8	38.5	6.6	15-Nov-11	24.4	25.2	5
1-Dec-11	117	378	1.6	1-Dec-11	17.2	33.9	1
15-Dec-11	15.3	38.8	0.2	15-Dec-11	16.4	44.0	0
1-Jan-12	29.2	76.0	8.8	1-Jan-12	166	391	2
15-Jan-12	31.2	50.3	11	15-Jan-12	31.5	40.0	11
1-Feb-12	42.4	56.9	24	1-Feb-12	39.9	46.0	21
15-Feb-12	30.5	48.7	10	15-Feb-12	29.7	39.4	9
1-Mar-12	40.4	61.9	20.0	1-Mar-12	34.5	50.6	14
15-Mar-12	33.3	73.7	13.0	15-Mar-12	33.4	74.6	13
1-Apr-12	32.2	59.3	12	1-Apr-12	38.2	78.2	16
15-Apr-12	10.0	25.2	0.00	15-Apr-12	9.2	21.1	0
1-May-12	25.7	57.7	5.2	1-May-12	20.8	51.9	2
15-May-12	14.7	45.3	0.1	15-May-12	12.2	31.7	0
1-Jun-12	18.1	29.4	1.1	1-Jun-12	22.3	41.3	3
15-Jun-12	11.0	18.6	0.00	15-Jun-12	10.7	25.4	0
1-Jul-12	7.2	29.5	0.00	1-Jul-12	7.6	31.5	0
15-Jul-12	10	37	2.6	15-Jul-12	12.5	35.6	0

Table 5. YM 39 and YM 38 Decibel Values Used in Figure 51. .

YM 39			YM 38		
Date	dB at 1 Hz	dB at 5 Hz	Date	dB at 1 Hz	dB at 5 Hz
13-Jun-08	-135	-154	13-Jun-08	-147	-154
14-Jun-08	-134	-158	14-Jun-08	-141	-153
1-Jul-09	-119	-131	1-Jul-09	-146	-152
15-Jul-08	-86	-103	15-Jul-08	-143	-153
1-Aug-08	-97	-113	1-Aug-08	-144	-148
15-Aug-08	-96	-110	15-Aug-08	-144	-154
1-Sep-08	-93	-108	1-Sep-08	-145	-153
15-Sep-08	-95	-111	15-Sep-08	-138	-149
1-Oct-08	-93	-111	1-Oct-08	-141	-151
15-Oct-08	-100	-116	15-Oct-08	-143	-152
1-Nov-08	-96	-111	1-Nov-08	-143	-151
15-Nov-08	-99	-113	15-Nov-08	-141	-149
13-Dec-08	-122	-137	13-Dec-08	-143	-152
14-Dec-08	-122	-126	14-Dec-08	-143	-150
1-Jan-09	-109	-119	1-Jan-09	-143	-150
15-Jan-09	-115	-114	15-Jan-09	-145	-151
1-Feb-09	-128	-151	1-Feb-09	-146	-154
15-Feb-09	-126	-143	15-Feb-09	-143	-152
1-Mar-09	-122	-135	1-Mar-09	-140	-151
15-Mar-09	-122	-141	15-Mar-09	-139	-148
1-Apr-09	-123	-143	1-Apr-09	-143	-150
15-Apr-09	-130	-132	15-Apr-09	-140	-148
1-May-09	-125	-133	1-May-09	-146	-152
15-May-09	-133	-148	15-May-09	-143	-153

Table 6. 7D J65A and 7D J73A Used in Figure 52.

7D J65A			7D J73A		
Date	dB at 1 Hz	dB at 5 Hz	Date	dB at 1 Hz	dB at 5 Hz
1-Nov-11	-116	-151	1-Nov-11	-116	-155
15-Nov-11	-118	-154	15-Nov-11	-118	-156
1-Dec-11	-117	-147	1-Dec-11	-118	-155
15-Dec-11	-112	-154	15-Dec-11	-114	-155
1-Jan-12	-114	-152	1-Jan-12	-108	-153
15-Jan-12	-115	-152	15-Jan-12	-113	-149
1-Feb-12	-115	-148	1-Feb-12	-114	-149
15-Feb-12	-118	-150	15-Feb-12	-111	-150
1-Mar-12	-114	-153	1-Mar-12	-112	-146
15-Mar-12	-118	-150	15-Mar-12	-109	-149
1-Apr-12	-112	-147	1-Apr-12	-109	-150
15-Apr-12	-121	-148	15-Apr-12	-115	-156
1-May-12	-114	-153	1-May-12	-110	-150
15-May-12	-118	-150	15-May-12	-114	-153
1-Jun-12	-124	-153	1-Jun-12	-117	-148
15-Jun-12	-128	-152	15-Jun-12	-123	-150
1-Jul-12	-121	-149	1-Jul-12	-116	-149
15-Jul-12	-119	-148	15-Jul-12	-108	-152

LIST OF REFERENCES

[1] J. P. Scobo, “Ocean observing systems,” M.S. thesis, Dept. Eng. & Applied Science, Naval Postgraduate School, Monterey, CA, 2012.

[2] Network map for _OBSIP (2015, Dec. 17). IRIS. [Online]. Available: http://ds.iris.edu./gmap/_OBSIP

[3] About IRIS. (n.d.). IRIS. [Online]. Available: http://www.iris.edu/hq/about_iris#vision. Accessed Oct. 25, 2016.

[4] OBSIP—Ocean Bottom Seismograph Instrument Pool (2016, Oct. 25). OBSIP. [Online]. Available: http://www.obsip.org/

[5] IRIS Webinar. (2013, Mar. 14). Under the sea: ocean bottom seismology for landlubbers. [YouTube video]. Available: https://www.youtube.com/watch?v=ZnQZ5npNm1M&feature=youtu.be. Accessed Oct. 31, 2016.

[6] Taiwan integrated geodynamics research (TAIGER) (2016, Sep. 20). OBSIP. [Online]. Available: http://www.obsip.org/experiments/experiment-table/2007/taiger

[7] OBSIP—Ocean Bottom Seismograph Instrument Pool - Specifications (2014, Feb. 20). OBSIP. [Online]. Available: http://www.obsip.org/instruments/long-period/ldeo/specifications/

[8] OBSIP—Ocean Bottom Seismograph Instrument Pool—LDEO (2015, Oct. 13). OBSIP. [Online]. Available: http://www.obsip.org/instruments/long-period/ldeo/.

[9] G. B. Bowden, Calibration of geophone microseismic sensors, 2003. [Online]. Available: http://www-ssrl.slac.stanford.edu/lcls/technotes/lcls-tn-03-6.pdf

[10] OBSIP—Ocean Bottom Seismograph Instrument Pool—Cascadia Instruments (2015, Oct. 13). OBSIP. [Online]. Available: http://www.obsip.org/instruments/cascadia-instruments/

[11] OBSIP—Ocean Bottom Seismograph Instrument Pool—Specifications (2014, Dec. 9). OBSIP. [Online]. Available: http://www.obsip.org/instruments/cascadia-instruments/sio-abalone/specifications/

[12] G. H. Sutton, F. K. Duennebier, and B. Iwatake, “Coupling of ocean bottom seismometer to soft bottom,” *Marine Geophys. Res.*, vol. 5, no. 1172, pp. 35–51, May 1981.

[13] F. K. Duennebier and G. H. Sutton, “Why bury ocean bottom seismometers?” *Geochem. Geophys. Geosyst., Electon. J. Earth Sci.*, vol. 8, no. 2, pp. 1-13, Feb. 2007.

[14] F. K. Duennebier and G. H. Sutton, “Fidelity of ocean bottom seismic observations,” *Marine Geophys. Res.*, vol. 17, no. 6, pp. 535-555, Dec. 1995.

[15] UPSeis: An educational site for budding seismologists (2007, Apr. 16). Michigan Technological University. [Online]. Available: http://www.geo.mtu.edu/UPSeis/waves.html

[16] K. E. Bullen and B. A. Bolt, *An introduction to the theory of seismology*, 4th ed. New York, Press Synd. of the Univ. of Cambridge, 1985, pp. 25–26, 87–89,108-114.

[17] J. Salencon, *Handbook of Continuum Mechanics: General Concepts—Thermoelasticity*, 1st ed. Berlin, Germany, Springer-Verlag, 2001, p. 333.

[18] D. Rauch, “On the role of bottom interface waves in ocean seismo-acoustics: A review,” in *SACLANT ASW Research Center Symp*., La Spezia, Italy, 1985, p. 623.

[19] GeoScienceWorld. (n.d.). Society of Exploration Geophysicists. [Online]. Available: http://geophysics.geoscienceworld.org/content/gsgpy/69/2/330/F1.large.jpg. Accessed Oct. 25, 2016.

[20] IRIS DMC MetaData Aggregator (n.d.). IRIS. [Online]. Available: http://ds.iris.edu/mda/YM/39. Accessed Sep. 1, 2016.

[21] IRIS Data Management Center (n.d.). IRIS. [Online]. Available: http://ds.iris.edu/ds/nodes/dmc/. Accessed Sep. 1, 2016.

[22] IRIS BREQ_FAST Request Form (n.d.). IRIS. [Online]. Available: http://ds.iris.edu/SeismiQuery/breq_fast.phtml?net=YM&sta=39&yyyymmdd=2009/05/30&hhmmss=212011. Accessed Sep. 1, 2016.

[23] Notice (BREQ_FAST Request) (n.d.). IRIS. [Online]. Available: http://ds.iris.edu/cgi-bin/seismiquery/bin/breq_fast.pl. Accessed Sep. 1, 2016.

[24] Seismic analysis code users manual. (2013, Nov.). IRIS. [Online]. Available: http://ds.iris.edu/files/sac-manual/commands/transfer.html.

[25] IRIS—Manuals: EVALRESP. (2014, Jul.). IRIS. [Online]. Available: http://ds.iris.edu/ds/nodes/dmc/manuals/evalresp/

[26] IRIS DMC MetaData Aggregator—Channel summary (1 time span) (n.d.). IRIS. [Online]. Available: http://ds.iris.edu/mda/YM/39/--/BHZ?timewindow=2008/05/11 21:25:51-2009/05/30 21:20:11. Accessed Sep. 1, 2016.

[27] IRIS DMC MetaData Aggregator—Channel summary (1 time span) (n.d.). IRIS. [Online]. Available: http://ds.iris.edu/mda/7D/J65A/--/BHZ?timewindow=2011/10/17 22:31:00-2012/07/16 07:21:00. Accessed Sep. 1, 2016.

[28] IRIS—URL Builder: Timeseries v.1 (n.d.). IRIS. [Online]. Available: http://service.iris.edu/irisws/timeseries/docs/1/builder/. Accessed Sep 1, 2016.

THIS PAGE INTENTIONALLY LEFT BLANK

INITIAL DISTRIBUTION LIST

1. Defense Technical Information Center
   Ft. Belvoir, Virginia

2. Dudley Knox Library
   Naval Postgraduate School
   Monterey, California